UNIVERSIDADE FEDERAL DE MINAS GERAIS

INSTITUTO DE GEOCIÊNCIAS

PROGRAMA DE PÓS-GRADUAÇÃO EM GEOLOGIA

Ana Carolina Liberal Fonseca

EVALUATION OF THE TECTONIC RESPONSES TO THE PHANEROZOIC STRESSES IN OROGENIC AND CRATONIC LANDS OF SOUTHEAST BRAZIL: INSIGHTS FROM APATITE FISSION-TRACK THERMOCHRONOLOGY

AVALIAÇÃO DAS RESPOSTAS TECTÔNICAS AOS ESFORÇOS FANEROZÓICOS EM TERRENOS OROGÉNICOS E CRATÔNICO DO SUDESTE BRASILEIRO: ABORDAGEM EM TERMOCRONOLOGIA EM TRAÇOS DE FISSÃO EM APATITA

Nº 212

BELO HORIZONTE

DATA (21/02/2020)

Ana Carolina Liberal Fonseca

EVALUATION OF THE TECTONIC RESPONSES TO THE PHANEROZOIC STRESSES IN OROGENIC AND CRATONIC LANDS OF SOUTHEAST BRAZIL: INSIGHTS FROM APATITE FISSION-TRACK THERMOCHRONOLOGY

AVALIAÇÃO DAS RESPOSTAS TECTÔNICAS AOS ESFORÇOS FANEROZÓICOS EM TERRENOS OROGÉNICOS E CRATÔNICO DO SUDESTE BRASILEIRO: ABORDAGEM EM TERMOCRONOLOGIA EM TRAÇOS DE FISSÃO EM APATITA

Versão Final

Dissertação apresentada ao programa de Pós-Graduação em Geologia do Instituto de Geociências da Universidade Federal de Minas Gerais como requisito para obtenção do título de mestre em Geologia.

Área de Concentração: Geologia Regional

Orientador: Prof. Dr. Tiago Amâncio Novo

Coorientador: Prof. Dr. Johan De Grave

Belo Horizonte

2020

FOLHA DE APROVAÇÃO

Evaluation of the tectonic responses to Phanerozoic stresses in orogenic and cratonic lands of Southeast Brazil: insights from Apatite Fission-Track thermochronology

ANA CAROLINA LIBERAL FONSECA

Dissertação submetida à Banca Examinadora designada pelo Colegiado do Programa de Pós-Graduação em GEOLOGIA, como requisito para obtenção do grau de Mestre em GEOLOGIA, área de concentração GEOLOGIA REGIONAL.

Aprovada em 21 de fevereiro de 2020, pela banca constituída pelos membros:

Prof. Tiago Amâncio Novo - Orientador
UFMG

Prof. Pedro Fonseca de Almeida e Val
UFOP

Profa. Eliza Inez Nunes Peixoto
UnB

Belo Horizonte, 21 de fevereiro de 2020.

ACKNOWLEDGMENT

During these two years of research I received a lot of support to accomplish this study. I know this acknowledgement will be insufficient to show my gratitude. However, I hope everyone who contributed to this achievement knows that I am sincerely grateful.

Firstly, this master's project was only possible due to the fruitful co-operation between the Geology Department of the Universidade Federal de Minas Gerais (UFMG) and the Laboratory of Mineralogy and Petrology of Ghent University. This co-operation was brilliantly coordinated by the professors Tiago Amâncio Novo and Johan De Grave, who became my mentors. I wish to thank both for their assistance, the constructive discussions and the motivating enthusiasm. I especially thank Tiago for being present on every step of this journey and Johan for having kindly received me in Gent.

My colleague Gabriella Vago Piffer was essential during the fieldwork that was carried out on Minas Gerais and Góias states as well as during the fission-track analyses, which started in Gent and proceed in Belo Horizonte.

The mineral separation was made possible owing to the partnership with SEPURA lab at Centro de Pesquisas Professor Manoel Teixeira da Costa (CPMTC/IGC/UFMG).

I thank Simon Nachtergaele and Gerben Van Ranst for sharing their knowledge in thermochronology and patiently clarify my doubts.

I sincerely acknowledge Professor Mahyra Ferreira Tedeschi for the discussions on Brasília Belt tectonic evolution.

I would also like to thank my colleagues very much for the countless discussions on the office of the graduate students at the Geosciences Institute that undoubtedly improved this work, especially Tobias Fonte Boa, Fernando Pacheco and Samuel Amaral.

Finally, my research would have been impossible without the aid and emocional support of parents, family and friends. There are no words capable of demonstrating my grateful to them.

DAS INDAGAÇÕES

A resposta certa, não importa nada: o essencial é que
as perguntas estejam certas.

Mário Quintana. Caderno H. p.54

DAS RESPOSTAS

Não deves acreditar nas respostas. As repostas são muitas
e a tua pergunta é única e insubstituível.

Mário Quintana. Caderno H. p.81

RESUMO

O arcabouço geológico do sudeste do Brasil é formado pelo Cráton São Francisco (CSF) e seus órogenos marginais. Essas províncias tectônicas foram constituídas e moldadas durante o ciclo orogênico Neoproterozóico-Cambriano, que resultou na amalgamação do Gondwana Ocidental. Durante o Cretáceo, a abertura do Oceano Atlântico Sul separou cinturões orogênicos (e.g. Orógeno Araçuaí) e cratons (e.g. porção nordeste do CSF) de suas contrapartes africanas. Por outro lado, alguns orógenos foram poupados da abertura (e.g. Orógeno Brasília). Uma vez que o CSF e seus cinturões marginais fazem parte de uma região continental considerada estável desde o Cambriano, a evolução tectônica Fanerozóica dessa área é raramente investigada, especialmente as porções distantes da costa. Neste trabalho, um total de quatorze amostras do Orógeno Brasília, doze amostras do CSF e vinte e quatro amostars do Orógeno Araçuaí são analisadas por meio de termocronologia, utilizando traço de fissão em apatita (TFA). O método de TFA é adequado para definir as trajetórias de temperatura-tempo (t-T) das rochas na crosta rasa (2 a 4 km), permitindo a determinação de fases de resfriamento que podem estar relacionadas a eventos de reativação tectônica. No Orógeno Brasília, as idades centrais de TFA das amostras analisadas variaram de 386 a 106 Ma e os comprimentos médios dos traços (CMT) variaram entre 10,8 e 13,5 μm. No CSF, as idades centrais de TFA variaram de 160 a 344 Ma e o CMT variaram de 11,2 a 12,7 μm. No Orógeno Araçuaí, as amostras apresentaram as idades centrais de TFA entre 210 a 53 Ma e o CMT variando de 11,5 a 13,5 μm. A partir do conjunto de dados termocronológicos foi possível executar a inversão de Markov Chain Monte Carlo e determinar modelos térmicos (t-T). Foram identificados três períodos principais de exumação do embasamento dessas províncias tectônicas: (i) Paleozóico, registrado por amostras do CSF e do Orógeno Brasília; (ii) Aptiano a Cenomaniano, registrado por amostras do Orógeno Araçuaí; e (iii) Cretáceo tardio ao Paleoceno, inferido em amostras de todos os domínios. A fase Paleozóica parece ter sido desencadeada por uma erosão extensa que provavelmente foi induzida pela extensão tectônica durante o fraturamento da crosta continental no contexto de subsidência das bacias intracontinentais, principalmente as bacias do Paraná e Sanfranciscana. O resfriamento do Aptiano ao Cenomaniano foi relacionado ao soerguimento desencadeado pela abertura do Oceano Atlântico Sul durante a fase sin-rifte. Por fim, o evento erosivo generalizado durante o Cretáceo tardio ao Paleoceno, foi conectado às reativações tectônicas induzidas pela interação entre a flexão da margem continental e os esforços compressivos intraplaca, transmitidos a partir dos limites da placa Sul-Americana. Nos eventos Fanerozóicos, o papel da herança litosférica parece ter sido decisiva nos processos de exumação diferencial. A litosfera rígida do CSF provavelmente concentrou as reativações Meso-Cenozóicas em zonas de fraqueza estreitas (e.g. rift Recôncavo-Tucano-Jatobá) enquanto que o Orógeno Araçuaí exibiu uma extensa deformação Meso-Cenozóica. No Orógeno Brasília não foram encontradas evidências de forte atividade tectônica Meso-Cenozóica, corroborando hipóteses anteriores de que esse orógeno apresenta uma litosfera orogênica enrigecida que inibe o retrabalhamento.

Palavras Chave: Orógeno Brasília. Orógeno Araçuaí. Exumação. Gondwana Ocidental. Herança litosférica.

ABSTRACT

The geological setting of Southeast Brazil comprises the São Francisco Craton (SFC) and its marginal belts. These tectonic provinces were shaped during the Neoproterozoic–Cambrian orogenic cycle which resulted in the West Gondwana amalgamation. During the Cretaceous, the opening of the South Atlantic Ocean separated orogenic (e.g. Araçuaí Orogen) and cratonic (e.g. Northeast SFC) lands from their African counterparts, whereas some mobile belts were spared from this disruption (e.g. Brasília Belt). The Phanerozoic tectonic evolution of this area is rarely investigated, especially the portions far from the coast, since the SFC and its marginal belts have been part of a fairly stable continental region since the Cambrian. Here, fifty apatite fission-track (AFT) analyzes of samples from the Brasília Belt, the SFC, and the Araçuaí Orogen were reported. The AFT method is suitable to constrain time-temperature (t-T) paths of the rocks in the shallow crust (2 to 4 km), allowing the determination of cooling phases that may be related to tectonic reactivations. In the Brasília Belt, fourteen samples display the AFT central age ranging from 386 to 106 Ma and the mean track lengths (MTL) ranging between 10.8 to 13.5 μm. In the SFC, twelve samples yield the AFT central age ranging from 160 to 344 Ma and the MTL ranging from 11.2 to 12.7 μm. In the Araçuaí Orogen, twenty-four samples present the AFT central age ranging from 210 to 53 Ma and the MTL ranging from 11.5 to 13.5 μm. Thermal models were performed from the dataset using the Markov Chain Monte Carlo inversion. Three main periods of basement exhumation were identified: (i) Paleozoic, recorded by samples from the SFC and the Brasília Belt; (ii) Aptian to Cenomanian, recorded by samples from the Araçuaí Orogen; and (iii) Late Cretaceous to Paleocene, inferred in some samples from all domains. The Paleozoic phase seems to be triggered by extensive erosion that was probably induced by the tectonic extension during the rifting of continental crust in the context of tectonic subsidence of the intracontinental basins, mainly Paraná and Sanfranciscana basins. The Aptian to Cenomanian cooling was linked with the uplift triggered by the opening of the South Atlantic Ocean during the syn-rift phase. Finally, the widespread post-rift erosional event, i.e. Late Cretaceous to Paleocene, was connected with reactivations prompted by the interplay between flexural bending of the margin and the intraplate compressive stress transmitted from the plate boundaries. Over Phanerozoic events, the role of the lithosphere inheritance seems to be decisive to the processes of differential exhumation. The stiff lithosphere of SFC likely concentrated the Meso-Cenozoic reactivations in narrow weak zones (e.g. Recôncavo-Tucano-Jatobá rift) while the Araçuaí Orogen displayed a far-reaching Meso-Cenozoic deformation. The Brasília Orogen seems to be an example of a stronger orogenic lithosphere, inhibiting reworking, since it was not found evidence of strong Meso-Cenozoic tectonic activity in this belt.

Keywords: Brasília Orogen. Araçuaí Orogen. Exhumation. West Gondwana. Lithospheric inheritance.

CONTENTS:

INTRODUCTION

In Southeast Brazil, Cambrian to Precambrian basement rocks from the São Francisco Craton and its marginal orogens are the dominant outcrop lithology. These cratonic and orogenic lands were shaped during the amalgamation of the supercontinent West Gondwana between 640 and 500 Ma (Almeida et al., 2000; Campos Neto, 2000). The orogenic systems encompass plate margins, micro-continents and intra-ocean magmatic arcs involved in the collision processes (Almeida et al., 2000), also known as the Brasiliano orogenic cycle. The São Francisco Craton basement was spared of the major tectonic effects of the Brasiliano orogeny (Almeida et al., 1981). During the Phanerozoic, these terrains were part of the West Gondwana hinterland until the onset of extensional processes that resulted in the break-up of the paleocontinent and the opening of the South Atlantic Ocean.

During the Phanerozoic, the West Gondwana basement seems to have experienced reactivations of pre-existing zones of lithospheric weakness during the subsidence of intracontinental basins and the break-up taphrogenic efforts (Carneiro et al., 2012; Zalán, 2004). On the Brazilian passive margin, a number of works have been constraining the time of exhumation episodes using low-temperature thermochronology that revealed important post-rift uplift events (e.g. Hackspacher et al., 2007; Japsen et al., 2012; Jelinek et al., 2014). However, in the hinterland, the Phanerozoic tectonic activity of São Francisco Craton and its orogenic belts still poorly constrained.

Therefore, it is the aim of this study to contribute to the understanding of the Phanerozoic tectonic evolution of São Francisco Craton and two of its marginal belts, i.e. Araçuaí and Brasília orogens, in the Brazilian hinterland. The apatite fission-track (AFT) method is one of the most successful applied tools to identify time-temperature paths of cooling events in the shallow crust (2-4 km). Here, the AFT method is used in samples from these provinces to produce a regional scenario of the basement thermal evolution, giving special attention to (i) possible episodes of reactivation and (ii) the role of structural and lithospheric inheritance.

The first chapter introduces the localization of the samples, the AFT method, and the geological background of the Phanerozoic events that are recorded in the study area. The second chapter presents two manuscripts that deal with the AFT results, the discussions as well as the conclusions provided by the acquired data set combined with the previous works. Finally, in the third chapter, suggestions for future works are outlined.

CHAPTER I

1.1 – Localization, access and sampling

The study area includes the Minas Gerais and the Goiás states of Brazil. Three sampling transects (southern, central and northern), approximately E-W oriented, were collected along the roadside (Fig. 1). Table I presents the samples localization and the rock types. The access was carried out by the major highways, leaving from Belo Horizonte. Where possible, the distance between the outcrops was 20 to 30 km. This rule was not obeyed in occasions where there were no suitable outcrops, especially in the portions dominated by Phanerozoic basins.
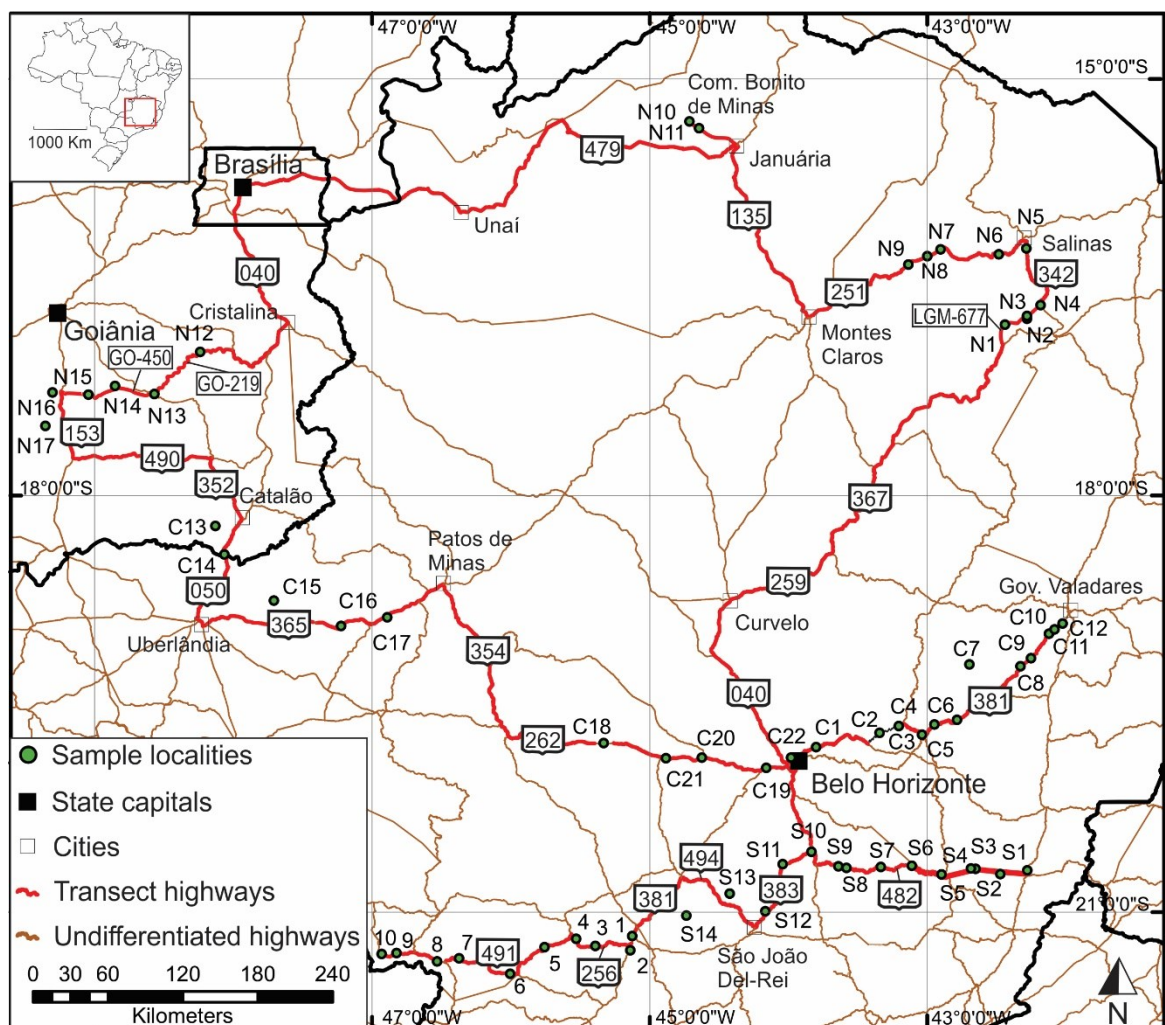

Figure 1- Road map of the study area, northwestern portion of Minas Gerais and eastern portion of Goiás states. Sample settings and access highways are highlighted.

Table 1- Sample settings: localization, height (m), lithology and access road.

Sample	Zone	UTM E	UTM N	Height (m)	Lithology	Road
1	23K	487041	7658633	786	migmatitic hornblende gneiss	BR381
2	23K	485651	7647333	870	granite	BR381
3	23K	459456	7650665	919	biotite gneiss	BR256
4	23K	445115	7656370	805	hornblende granite	BR256
5	23K	421654	7649513	893	biotite gneiss	BR491
6	23K	396015	7628074	793	pyroxene gneiss	BR491
7	23K	357746	7640276	883	pyroxene gneiss	BR491
8	23K	341333	7637703	972	pyroxene gneiss	BR491
9	23K	311031	7643824	777	pyroxene gneiss	BR491
10	23K	300002	7643042	791	granite	BR491
S1	23K	783649	7708551	718	gneiss	BR482
S2	23K	763340	7705845	1192	pyroxene granite	BR482
S3	23K	744688	7710388	651	pyroxene granite	BR482
S4	23K	741204	7710778	614	biotite gneiss	BR482
S5	23K	719099	7706238	619	biotite gneiss	BR482
S6	23K	696895	7713612	615	biotite gneiss	BR482
S7	23K	673748	7712850	663	biotite gneiss	BR482
S8	23K	647881	7712193	722	biotite gneiss	BR482
S9	23K	641770	7713499	738	biotite gneiss	BR482
S10	23K	621654	7725349	926	biotite granite	BR482
S11	23K	599879	7715475	878	biotite gneiss	BR383
S12	23K	586740	7678105	1084	biotite granite	BR383
S13	23K	560053	7692337	992	biotite granite	BR494
S14	23K	527604	7674832	997	porphyritic basalt	BR381
C1	23K	625776	7808729	855	migmatitic biotite gneiss	BR381
C2	23K	673812	7819627	720	biotite gneiss	BR381
C3	23K	688418	7825005	735	biotite granite	BR381
C4	23K	705754	7817909	558	biotite gneiss	BR381
C5	23K	715274	7825804	723	pyroxene gneiss	BR381
C6	23K	732416	7829342	262	biotite gneiss	BR381
C7	23K	742405	7873447	242	biotite gneiss	BR381
C8	23K	780959	7871563	197	amphibolite	BR381
C9	23K	789129	7877833	208	biotite gneiss	BR381
C10	23K	803151	7897111	204	porphyritic basalt	BR381
C11	23K	807314	7900436	177	biotite gneiss	BR381
C12	23K	813633	7905037	188	biotite gneiss	BR381
C13	22K	803889	7982928	740	biotite gneiss	BR050
C14	22K	810265	7960084	748	migmatite	BR050
C15	23K	214728	7923680	856	biotite granite	BR356
C16	23K	266200	7904132	884	biotite granite	BR356
C17	23K	301046	7911513	1061	metaconglomerate	BR356
C18	23K	465543	7812418	614	migmatite	BR262
C19	23 K	588101	7792332	851	biotite gneiss	BR262
C20	23 K	539596	7800683	850	biotite granite	BR262
C21	23 K	512529	7800315	682	biotite gneiss	BR262
C22	23 K	606835	7800359	859	biotite gneiss	BR262
N1	23 K	773043	8144123	703	weathered gneiss	LGM677
N2	23 K	790025	8148567	631	biotite schist and pegmatite vein	LGM677
N3	23 K	790054	8150858	557	tourmaline pegmatite	LGM677
N4	23 K	800576	8159265	310	biotite granite	BR342
N5	23 K	790290	8204597	445	greywacke	BR342
N6	23 K	768893	8200254	751	greywacke	BR251
N7	23 K	724118	8204759	832	weathered gneiss	BR251
N8	23 K	713917	8199207	831	weathered gneiss	BR251
N9	23 K	699219	8192887	915	weathered granite	BR251
N10	23 L	538487	8302281	602	granite	road to Bonito de Minas Community
N11	23 L	530911	8307635	620	granite	road to Bonito de Minas Community
N12	22 K	794404	8122052	898	gneiss	GO219
N13	22 K	758747	8088995	758	milonitic granite	GO450
N14	22 K	728683	8095737	761	migmatite	GO450
N15	22 K	708259	8089088	705	migmatite	GO450
N16	22 K	680652	8091096	631	milonitic granite	GO450
N17	22 K	675023	8064481	666	ultramafic rock	BR153

1.2 – Method

Apatite Fission-Track (AFT) thermochronology fundamentals

Fission Tracks

Fission tracks are linear crystalline defects, resulted of nuclear fission process that form amorphous channel in some insulating solid (detector). The fission can be spontaneous or induced by neutron bombardment. Heavy atoms (Z>92) are susceptible to the spontaneous fission process, occurring naturally in the isotopes of uranium and thorium. The majority of observed tracks in natural materials are generated by U^{238} decay, because the other uranium isotopes are in order of 10^3 to 10^5 times less abundant than U^{238}, and Th^{232} is a monoisotope with half-life 10^{21} times longer.
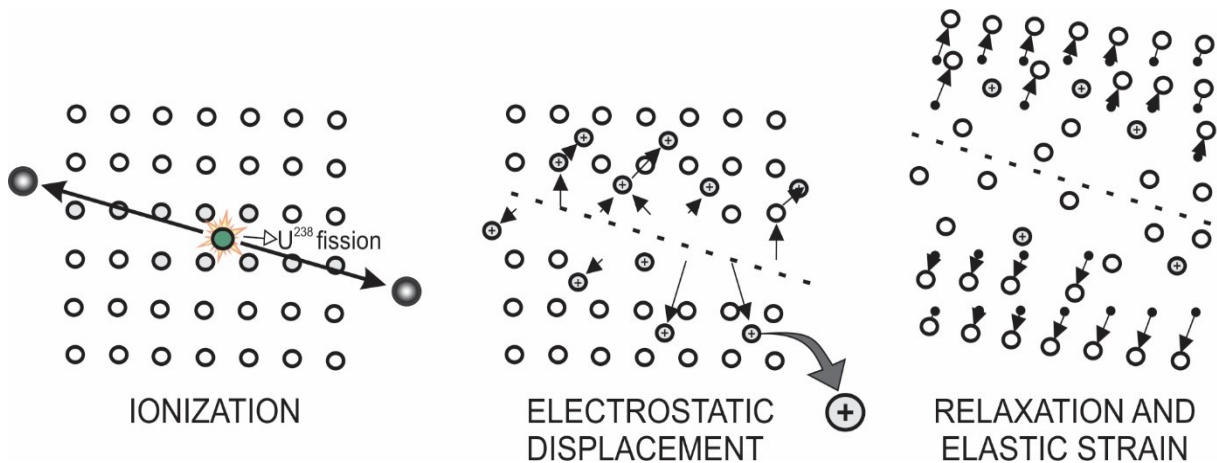

Figure 2- The three stages of track formation according to 'ion explosion spike' theory. Ionization of the atoms through the projection of two high-energy fission fragments. Electrostatic displacement due to Coulomb repulsion. Relaxion and elastic strain create a permanent trail of the lattice damage, the fission track. (After Fleisher et al., 1975).

The mechanism by the tracks are registered in crystals stills aim of debate (Chadderton, 2003; Durrani and Bull, 1987; Fleisher et al., 1975; Gleadow et al., 2002; Wagner and Van den haute, 1992). The most widely accepted theory is the "ion explosion spike" mechanism (Fig. 2), proposed by Fleisher et al., (1975). The model assumes that the tracks are narrow (radius <50 A), stable and have chemically reactive centers that are formed by displaced atoms. It postulated that the passage of a heavy-ion at high velocity in the crystallographic array of a dielectric solid is capable to ionize particles immediately next to the trajectory of this ion. The ionization generates a positively charged center that automatically repels itself. Then the elastic relaxation phenomenon decreases the local stresses, spreading the tension more widely. The disorganization in the crystalline structure generated in this process is presented as heterogeneities in the crystal. Eventually, the particles are decelerated by interaction with the

solid. The distance traveled by the particle is called the range. The vectors of the ranges, coming from the same fission, form a linear trait that is called fission track.

Dating

Each spontaneous fission-track is created by one atomic fission event, thus the track density depends on the rate of fission decay (λsf $\cong 8.46 \times 10^{-17}$ year^{-1}), the U^{238} concentration and time. If is viable to determine the ratio between the daughter product (fission track) and the parent (U^{238}), it is possible to calculate the age from which the tracks were preserved (fission-track age).
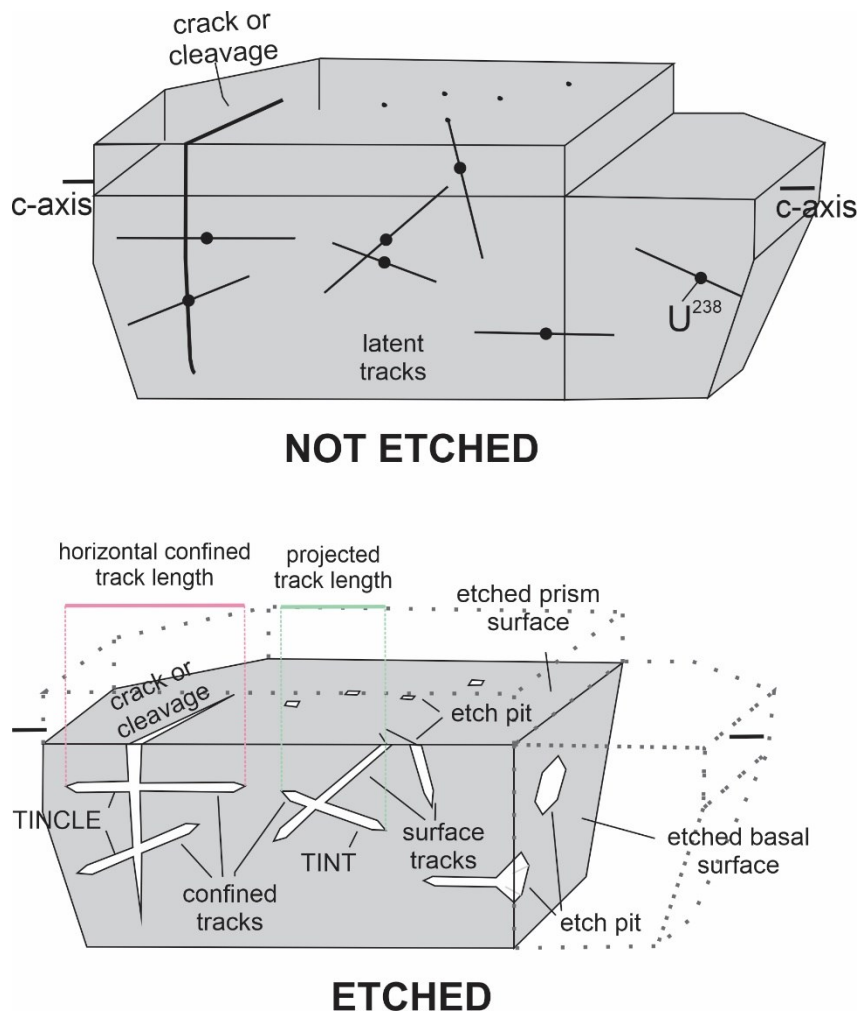

Figure 3- Schematic diagram comparing apatite crystal not etched and etched. The fission tracks on the crystals are widened by etching. Surface track intersect the etched prism surface, not preserving its length completely. Confined tracks are etched tracks which don't intersect the etched prism surface, preserving its length completely. TICLE is a confined track which intersects a crack or cleavage. TINT is a confined track which intersects a surface track. (Adapted from Hurford, 2019).

The spontaneous track density is the record of the U^{238} nuclides decayed through spontaneous fission, thus it can be considered the daughter product. In apatite, a fission track is originally 16 μm long and, in natural state (latent tracks), only can be visualized with a

transmission electron microscope (TEM), or an atomic-force microscopy (AFM), or a scanning-electron microscope (SEM). Polishing and chemical etching (using HNO_3 for apatite) procedures are required to widen the tracks and enable the observation in an optical microscope. The chemical etching acts in the latent tracks that intersect the polished surface (surface tracks) and the ones that intersect channels connected with the surface (confined tracks) (Fig. 3). The channels that connect the confined track with the surface can be other tracks, forming the tracks-in-track (TINT), or discontinuities, forming tracks-in-cleavage (TICLE) (Fig. 3). To dating, only surface tracks must be counted.
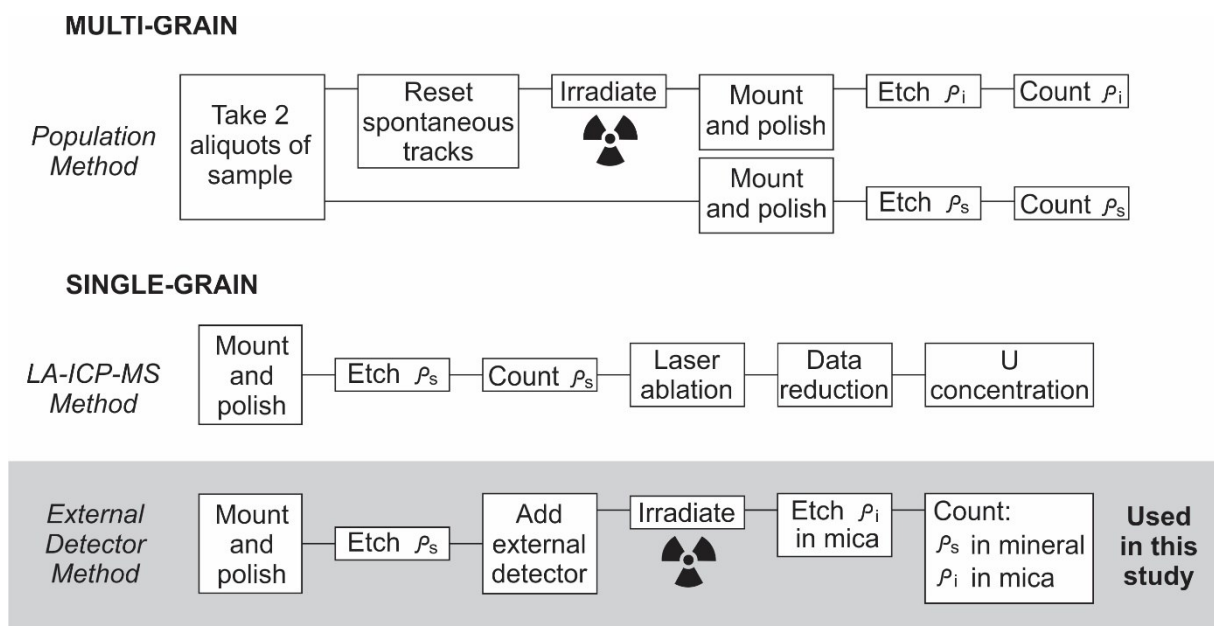
MULTI-GRAIN

SINGLE-GRAIN

Figure 4- Experimental strategies employed for AFT method. (After Hurford and Green, 1982).

Regarding the parent factor, the U^{238} current concentration needs to be obtained. There are direct and indirect methods to acquire this data (Fig. 4). The Laser Ablation-Inductively Coupled Plasma-Mass Spectrometry (LA-ICP-MS) is the fastiest way to determine uranium concentration directly (Hasebe et al., 2004) (Fig. 4). However, it is a very new technique that still faces challenges to present precise results. The indirect path, presupposes that the natural ratio between the two isotopes of uranium is known (I= $^{235}N/^{238}N$ = 7.2527x10^{-3}, Cowan and Adler, 1976; Steiger and Jager, 1977), so the U^{238} concentration can be acquired inducing a proportion of less abundant U^{235} isotope to fission. The irradiation is realized in nuclear reactors with low to moderated thermal energy. How and where count the induced tracks depends on which experimental strategy the analyst use. Population method is a multi-grain strategy that uses different apatite aliquots to determine spontaneous and induced tracks (Fig. 4). The irradiation is conducted in thermal reset apatites, with no spontaneous tracks. Then, the two

groups of grains (one with spontaneous and other with induced tracks) are processed and counted (Fig. 4). This method supposes a homogeneous uranium distribution in the grains and between the aliquots, however it is frequently not true.

Here, the external detector method (EDM) (Naeser and Dodge, 1969) is used. The EDM is a single-grain strategy such as the LA-ICP-MS approach, so the same grain gives information about spontaneous and induced tracks. The apatite grains are polished, etched, and then they go to the reactor with an external detector (industrial low-uranium muscovite) fixed against the polished surface of the grains (Fig. 5). In the reactor, the ^{235}U fission is induced and tracks are registered in the detector, as a carbon paper. Tracks in the detector are etched with HF. The track density is counted in the mica (induced track density - σ_i), as well as in the grains (spontaneous track density - σ_s) (Fig. 5).

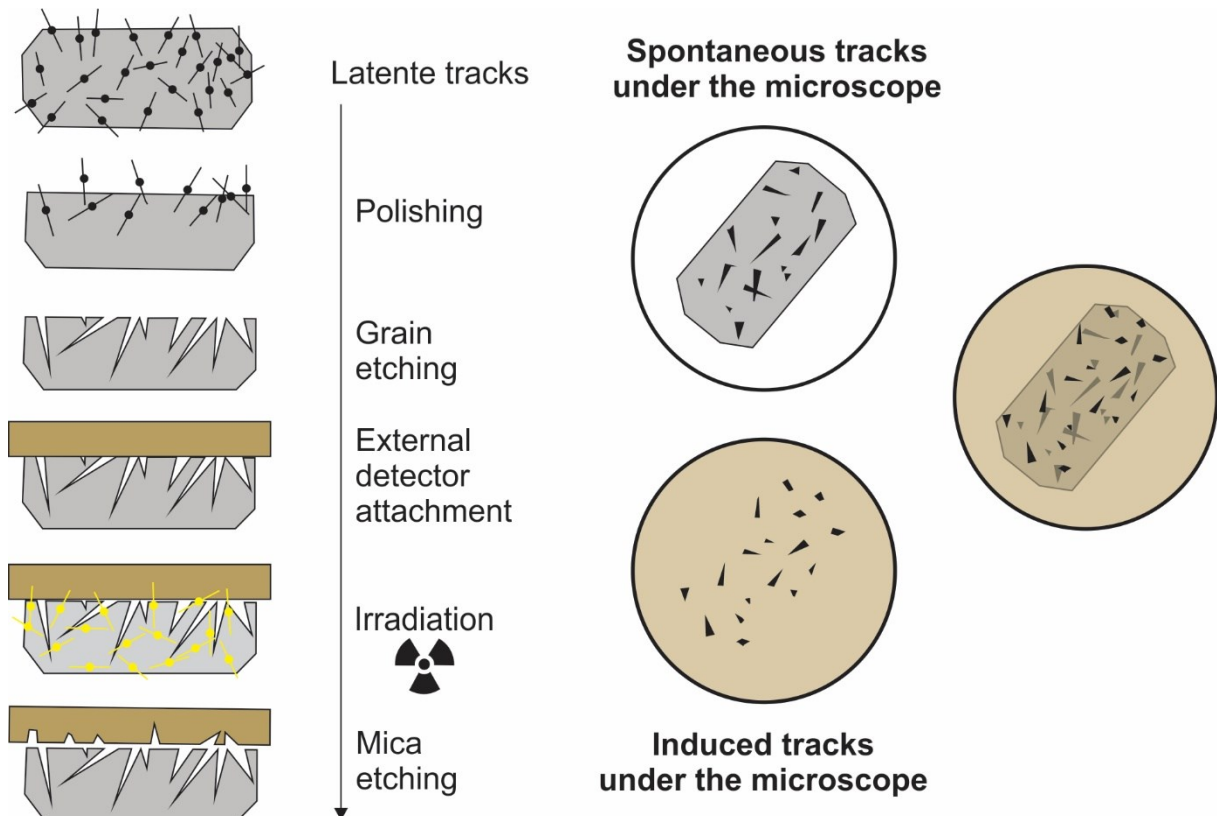*Figure 5- Schematic diagram of the procedures adopted in the EDM method.*

Dating Equation

The AFT age, as in any isotopic dating method, can be calculated by the abundance of the daughter product (N_d), the current abundance of the parent isotope (N_p), the decay rate constant (λ) and time (t), by the equation:

$$N_d = N_p(e^{\lambda t} - 1) - eq. 1$$

As stated earlier, one fission track is the product of one fission event, thus the N_d corresponds to the number of spontaneous fission tracks per unit volume ($N_d = N_s$) in the AFT dating equation. The N_p is the number of remaining U^{238} per unit volume ($N_p = N^{238}$). The uranium decay (λ_U) is the sum of alpha decay and fission decay ($\lambda_U = \lambda_\alpha + \lambda_f$). Therefore, we can reconstruct eq.1 as:

$$N_s = \left(\frac{\lambda_F}{\lambda_U}\right) N^{238}\left(e^{\lambda_U t} - 1\right) - eq.\,2$$

However, fission decay constant is much smaller than alpha decay constant ($\lambda_\alpha \gg \lambda_f$), so it is possible to consider $\lambda_U = \lambda_\alpha$:

$$N_s = \left(\frac{\lambda_F}{\lambda_\alpha}\right) N^{238}\left(e^{\lambda_\alpha t} - 1\right) - eq.\,2$$

In function of time, the equation becomes:

$$t = \lambda_\alpha^{-1} \ln\left[(\lambda_\alpha/\lambda_f)(N_s/N^{238}) + 1\right] - eq.\,3$$

The EDM uses the induction of nuclear fission reaction in U^{235} to indirectly measure N^{238}. The number of induced fission tracks per unit volume (N_i), is given by:

$$N_i = N^{235}\sigma\phi_{th}$$

where N^{235} is the number of U^{235} per unit volume, σ is the cross section for induced nuclear fission of U^{235} by thermal neutrons (580.2 x 10^{-24}cm^2) and ϕ_{th} is the thermal neutron fluence.

Considering the ratio: ($U^{235}/U^{238} = I = cte$), it is possible to write

$$N_i = N^{238}I\sigma\phi_{th}$$

and replace in eq.3:

$$t = \lambda_\alpha^{-1} \ln\left[(\lambda_\alpha/\lambda_f)(N_s/N_i)I\sigma\phi_{th} + 1\right] - eq.\,4$$

Note that the eq.4 is in terms of the volumetric parameters N (tracks/cm^3). Instead, the data is acquired in areal density (ρ; tracks/cm^2). Therefore, Fleisher et al., (1975) and Wagner and Van den haute, (1992) derived the mathematical relationship between N and ρ, assuming U homogeneous fashion in the detector, no preferential track orientation and constant track length. The Figure 6 presents an O position, where the isotope suffers fission and create a latent track of length $l = 2R_l$. Thus, the possible tracks define a sphere with radius R_l and center O.
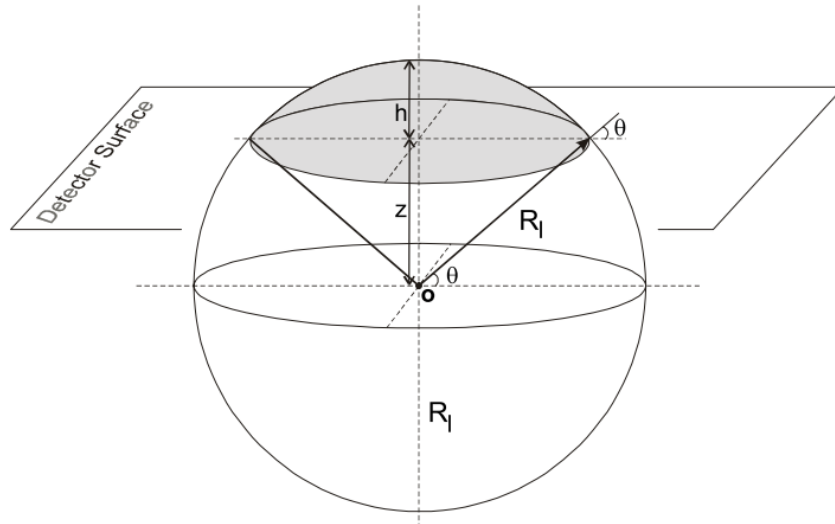
Figure 6- Schematic model to a uranium atom at point O within a crystal lattice, situated at depth z beneath the detector surface. A fission track with length $l = 2R_l$ is created, only tracks with upper ends in the gray zone of the sphere cut the detector surface.

The number of nuclei situated within a layer of unit area and infinitesimal thickness dz at distance z $(\leq R_l)$ below the considered surface is given by $N_f$dz. Z is the distance beneath the detector surface until the center O. The track angle with detector surface (θ) needs to be equal or greater than arcsin (z/R_l) to a track intersect a detector surface. The probability $(P(z))$ of one track be under this condition is given by the ratio of the area of the sphere above the considered detector surface to the area of the semi-sphere above the position O.

$$P(z) = 2\pi R_l h / 2\pi R_l^2 = R_l(R_l - R_l sin\theta)/R_l^2 = (1 - sin\theta)$$

Thereafter, $(1 - sin\theta)N_f$dz is the number of tracks intersecting one surface and the areal latent track density ρ_l is:

$$\rho_l = \int_0^{R_l} (1 - \sin\theta)N_f dz = \int_0^{R_l} N_f(1 - z/R_l)dz = N_f R_l/2 \ or \ N_f l/4$$

In this case, it is considered tracks intersecting the surface that come from both sides of the detector (4π-geometry). In EDM, induced tracks only result from one side (2π-geometry), so:

$$\rho_l = gN_f R_l \ or \ gN_f l/2$$

where g is a geometry factor that is 0.5 to EDM.

It is important to note that, on the procedures, the analyst counts the etched track and not the latent tracks. The etching effects are corrected by the etching efficiency factor $(\eta =$

revealed tracks/latent surface tracks). Another point to be considered is the observation parameter (q), that is dependent of the researcher and the observation equipment (Wagner and Van den haute, 1992). So, the areal density of revealed tracks is given by:

$$\rho_e = \eta q \rho_l = g N_f R_e \eta q \ or \ g N_f l_e \eta q / 2$$

N_s/N_i can be now written as:

$$\frac{N_s}{N_i} = \frac{\rho_s}{\rho_i} \frac{g_i R_{e,i} \eta_i q_i}{g_s R_{e,s} \eta_s q_s}$$

Then, the geometry factor (G) and procedure factor (Q) are defined:

$$G = g_i/g_s = 0.5 \ to \ EDM$$

$$Q = \frac{R_{e,i} \eta_i q_i}{R_{e,s} \eta_s q_s}$$

Finally, it is possible to rewrite eq.4 as:

$$t = \lambda_\alpha^{-1} \ln\left[(\lambda_\alpha/\lambda_f)(\rho_s/\rho_i) Q G I \sigma \phi_{th} + 1\right] - eq.5$$

Zeta Calibration

After all rearrangements that lead to eq.5, the parameters can be divided as the defined constants: $\lambda_\alpha, \lambda_f, G$, I, σ or the experimental determined/measured properties: ρ_s, ρ_i, Q, ϕ_{th}. Amongst them, λ_f is not well determined (Bigazzi, 1981; Van den haute et al., 1998) and Q and ϕ_{th} are very difficult to calculate accurately (Van den haute et al., 1998). In this scenario, the empirical zeta calibration, based on analysis of age standards (Hurford and Green, 1983, 1982) is recommended (Hurford, 1990). ϕ_{th} is calculated by etched induced fission-track density on U-doped standard glass (ρ_d), irradiated on the same irradiation package.

$$\phi_{th} = B\rho_d$$

where B is an empirical calibration constant.

Standards samples of known age (t_s) are also irradiated with the glasses and samples with unknow age (t_u). The age equations are given by:

$$t_s = \lambda_\alpha^{-1} \ln\left[(\lambda_\alpha/\lambda_f)(\rho_s/\rho_i)_s Q G I \sigma B (\rho_d)_s + 1\right]$$

$$t_u = \lambda_\alpha^{-1} \ln\left[(\lambda_\alpha/\lambda_f)(\rho_s/\rho_i)_u QGI\sigma B(\rho_d)_i + 1\right]$$

The zeta age calibration factor (ζ) includes the indeterminade paramaters:

$$\zeta = \frac{QI\sigma B}{\lambda_f}$$

giving the following equation:

$$t_s = \lambda_\alpha^{-1} \ln[\lambda_\alpha(\rho_s/\rho_i)_s G\zeta(\rho_d)_s + 1]$$

that can be rearranged as:

$$\zeta = \frac{e^{\lambda_\alpha t_s} - 1}{\lambda_\alpha(\rho_s/\rho_i)_s G(\rho_d)_s}$$

All the parameters can be determinate or are known, thus the zeta can be calculated. Note that on zeta definition, some of the components are dependent of the researcher and equipment. So, it just can be used for the same researcher using the same equipment. Several ages standards are used to do an averaged and generate an *overall weighted mean zeta* (OWMZ) (Hurford and Green, 1983).

After the zeta determination, it is possible to calculate the unknow age:

$$t_u = \lambda_\alpha^{-1} \ln[\lambda_\alpha(\rho_s/\rho_i)_u G\zeta(\rho_d)_u + 1]$$

Where λ_α is the alpha decay constant of U^{238} (λ_α=1.55125x10^{-10} a^{-1}, from Jaffey et al., 1971; Steiger and Jager, 1977); ρ_s and ρ_i are superficial density of spontaneous and induced tracks, respectively; G is geometry factor (G=0.5, for external detector method); ζ is the OWMZ and ρ_d is an interpolated value from the superficial density of tracks on the glasses after irradiation.

In EDM around 20 grains are dated per sample. To crystalline rocks, it is expected that all grain resided in same temperature conditions, experimenting same cooling rate. Thus, one population age is also expected and can be reported as:

a) *Central age:* is the weighted mean of all grains log-normal distribution (Galbraith and Laslett, 1993). The deviation of ages, confirming the unique population and the analytical precision is quantified with chi-square statistic test.

b) *Pooled age:* The densities of spontaneous (ρ_s) and induced (ρ_i) tracks are acquired with the sum of all spontaneous and induced tracks and areas in the grains, as they work as a single grain (e.g. $\rho_s = (N_{sg1} + \cdots + N_{sg19} + N_{sg20}) / (A_{sg1} + \cdots + A_{sg19} + A_{sg20})$).

c) *Mean age:* The densities of spontaneous (ρ_s) and induced (ρ_i) tracks are acquired with the average ratio of all grains individual ratio (e.g. $\rho_s/\rho_i = (\rho_{sg1}/\rho_{ig1} + \cdots + \rho_{sg19}/\rho_{ig19} + \rho_{sg20}/\rho_{ig20})$ /20).

Track Stability and the Annealing

Since the beginning of fission tracks studies, the track stability was recognizing as extremally sensitive with temperature. Processes of fading, shortening, and erasure of tracks occur at certain temperatures and in a transition zone (Carlson, 1990; Donelick, 1991; Green et al., 1986). In a smaller scale, other factors can influence the annealing, in particular, the chemical composition (Ketcham et al., 2007a) and the crystallographic orientation (Donelick, 2005; Donelick et al., 1999). Annealing prevents the recovery of the daughter product above ~120ºC in apatites, this zone is called total annealing zone (Fig. 7). Between ~120ºC and 60ºC the shortening process is partial and not erases totally the tracks, so it is called apatite partial annealing zone (APAZ) (Fig. 7). Below ~60ºC all tracks are maintained and the zone is called total stability zone (Fig. 7).

Dodson, (1979, 1973) defined the closure temperature (t_c) in fission-track dating as the temperature at the given time by its AFT age. After decades of researches, t_c is considered within the transition zone (i.e. APAZ) and it varies in function of several factors, such as the cooling rate and the apatite composition. Even though t_c is variable, it is always very low under geological conditions and is achieved at the shallow crust (2 to 4 km). Thus, AFT age is also reported as a cooling age and the method becomes a robust tool to low temperature thermochronology.

Length Measurement and Thermal History

A rock can go through many paths after cross the total annealing zone in direction to the surface (Fig. 7). During this time, fission processes generate tracks that can be annealed. One track retained in the APAZ for a long time must be shorter than one track generated close to the surface. If the rock resided more time on annealing conditions, more tracks will be shortening. It implies directly on the cooling rate. For examples, a volcanic rock pass very fast through the APAZ, resulting in long track lengths distribution (Fig. 7). Based on this principle, the track lengths histograms and AFT age are used to model the low thermal history of the rocks

(Gallagher, 2012; Ketcham et al., 2007a). The measurements of tracks need to be in confined tracks because they present the totally length preserved (Fig. 3). Horizontal tracks are preferably chosen, otherwise, the slope needs to be determined. Approximately 100 tracks are statistically necessary to reproduce a reliable thermal history. Attention is necessary to measure track that were totally etched (rounded tips). Additional constrains, as geological data or multi-method approach, are also important to make the truthful models.
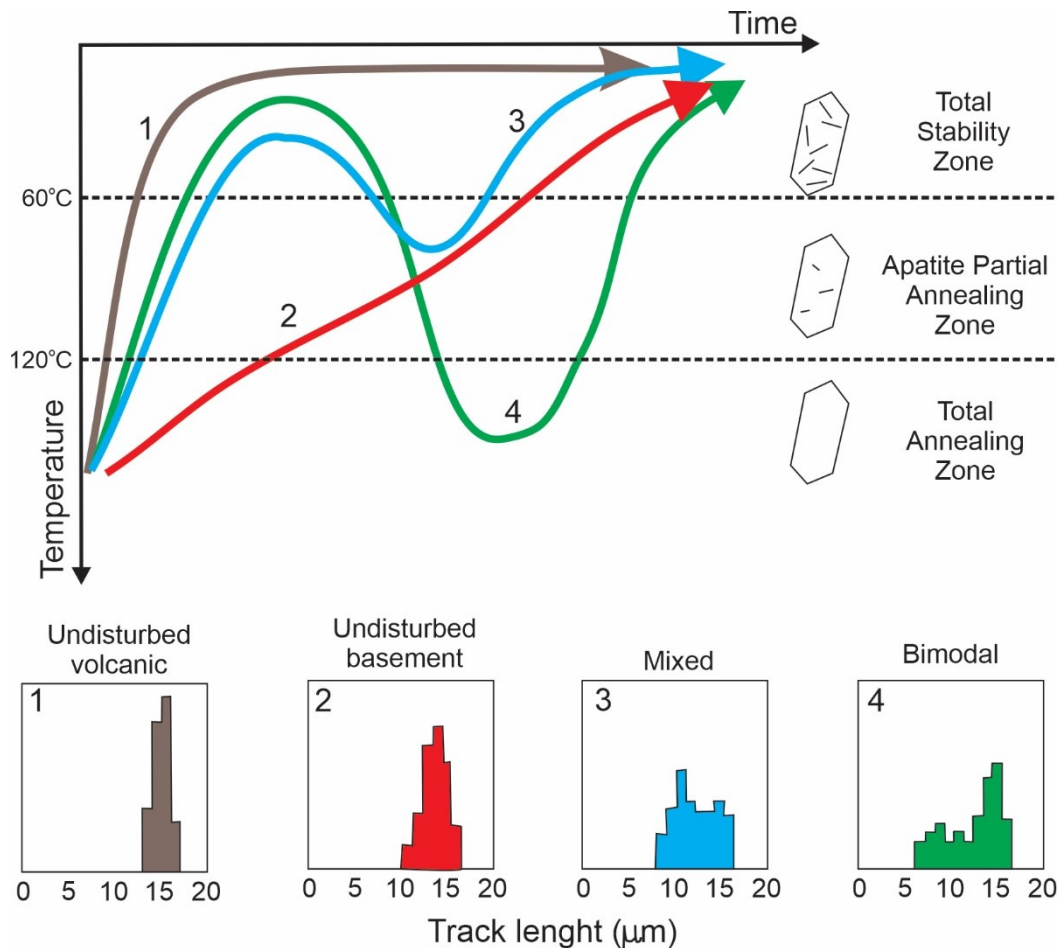

Figure 7- Schematic cooling curves and fission tracks length distribution. Curve 1 represents rapid cooling rock, resulting in unimodal distribution with long fission tracks and low standard deviation. Curve 2 represents slow cooling rock, tracks formed during residence in APAZ are partially annealed, the distribution is unimodal with medium track lengths. Curve 3 represents a rock which was reheated, giving a mixed age and track-length mixed distribution. Curve 4 represents a reset age, reheating of already cooled samples, giving bimodal length distribution. (Hurford, 2019).

1.3 – Phanerozoic geological overview of São Francisco Craton and its marginal orogens

São Francisco Craton and its marginal orogens are located on the South American Platform (Fig. 8), a stable continental region of South America not affected by Phanerozoic orogenic events (Almeida, 1967). The stabilization occurred after Brasiliano/Neoproterozoic

orogenic cycles, that resulted in the formation of West Gondwana (Fig.8). The oldest collage event took place in the southwest margin of São Francisco/Congo Craton, around 630 Ma, creating the southern of Brasília Belt (Alkmim and Martins-Neto, 2001; Pimentel et al., 2004; Valeriano et al., 2004). On the other side, around 580 to 540 Ma, the gulf between São Francisco peninsula and Congo continent was closed, developing Araçuaí-West Congo Belt (Alkmim et al., 2006; Pedrosa-Soares et al., 2001, 2007).

The Phanerozoic geological history of this region was pioneer defined and divided by Almeida, (1969, 1967) and after updated by Zalán, (2004). The major phases described by Zalán, (2004) – Transitional Platform, Stable Platform and Reactive Platform (Fig. 8) - are briefly presented here in time: Paleozoic and Mesozoic-Cenozoic.

Paleozoic

The Paleozoic Era started with the decrease and end of the tectonic pulses within the marginal belts. During the Cambrian until the middle Ordovician, the Transitional Platform phase was characterized by the end of the folding processes and predominance of brittle structures, promoting, in this region, the platform stabilization and consolidation of West Gondwana.

Afterward, two almost simultaneous events marked the onset of relative tectonic quietness in Stable Platform phase: Paraná Basin subsidence, next to Brasília Belt, and collisions on orogenic fronts on the south of the paleocontinent. Milani and Ramos, (1998) suggested that the Paraná Basin subsidence was influenced by these geodynamics cycles (Events 1-4 on Fig. 8). They considered that the intraplate stress on the platform, generated by the orogeneses on the southern border of Gondwana, caused reactivations of basement weakness zones. During the basin sinking, Brasília Belt worked as highland, limiting Paraná Basin and Sanfranciscana Basin, operating as source area.

Large Paleozoic Syneclises sub-phase is recorded by the Santa Fé glaciogenic sediments in Sanfranciscana Basin (Event 17 on Fig. 8) (Campos and Dardenne, 1997; Sgarbi et al., 2001) and by three supersequences deposited in the Paraná Basin (Events 10-12 on Fig. 8). Both basins present pieces of evidence of an important glacial event that affected the southern South America during the Carboniferous to the Permian (Limarino et al., 2014). The glaciogenic fronts occupied the sedimentary rocks as well as the highland (see Buso et al., 2017; Caputo and Crowell, 1985; Eyles et al., 1993; Griffis et al., 2018; Limarino et al., 2014; Montañez and Poulsen, 2013). South of Brasília Belt was probably covered by some ice caps, however, there are no strong evidence of ice caps in São Francisco Craton basement.
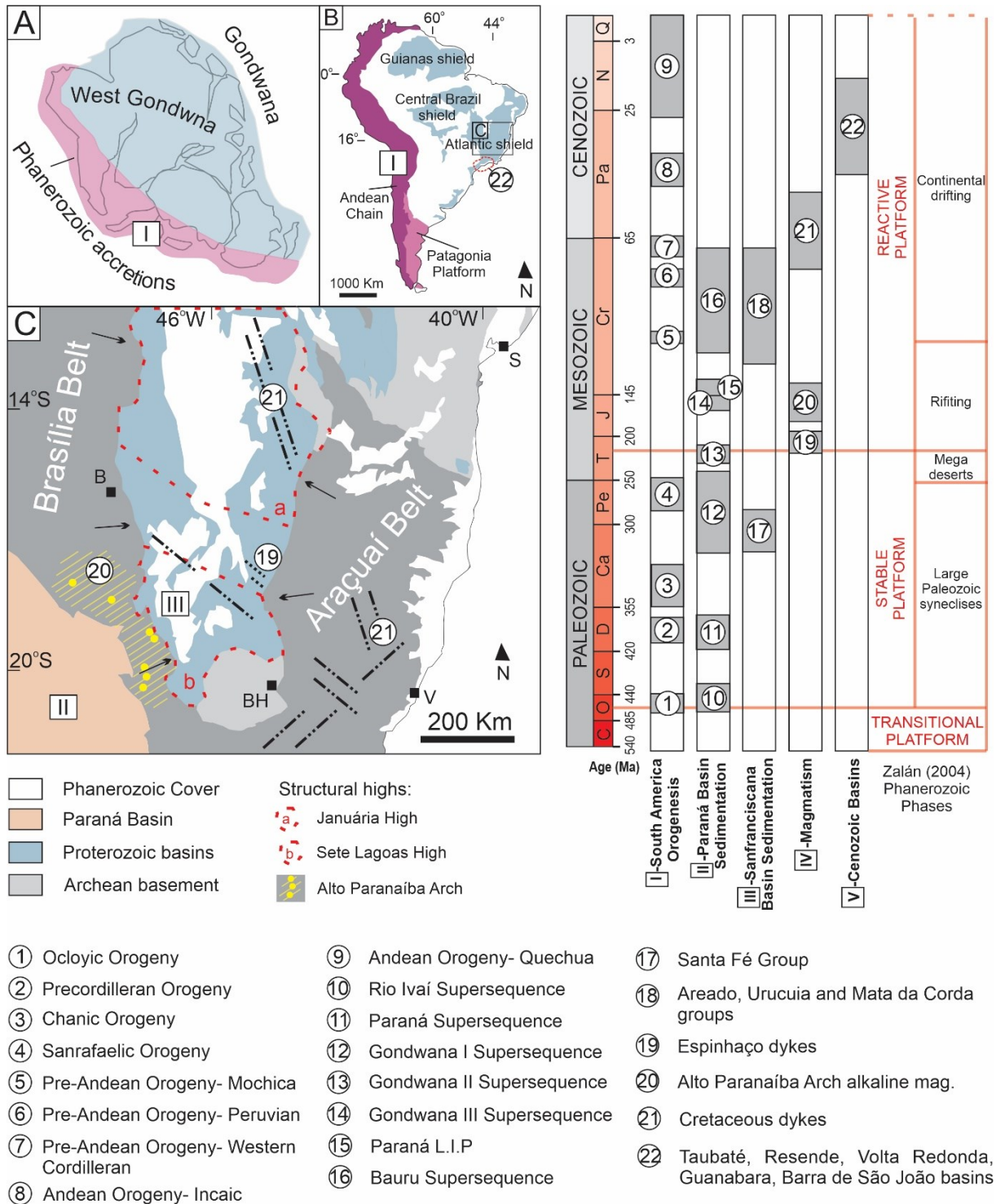
Figure 8- Phanerozoic evolution of São Francisco Craton and its marginal orogens connected with South America tectonic history. Mainly events are presented chronologically numbered. (after Almeida, 1967). A) Schematically characterization of Gondwana Supercontinent and the region of Phanerozoic accretions. B) Geological configuration of South America continent. C) Schematically geological map of the São Francisco Craton and adjacent areas.

Mesozoic and Cenozoic

The glacial period was followed by an increase in arid condition, in the end of the Paleozoic. During the Triassic, extreme greenhouse conditions took place and marked the

Mega-deserts sub-phase. In Paraná Basin, Gondwana II Supersequence (Event 13 on Fig. 8) records semi-arid conditions in a fluvial environment (Zerfass et al., 2003). In general, it is possible to point out that this entire period between the Ordovician and the Triassic was tectonically stable, with no magmatism and pervasive deformational processes. Just some weak deformation is found on Paraná sedimentary layers, concentrated on zones above ancient basement faults.

The Reactive Platform phase was more tectonically active and is defined with the beginning of taphrogenic processes (rift systems, gulfs), that culminated in the total disruption between South America and Africa in the Lower Cretaceous, resulting in the opening of the South Atlantic Ocean. The São Francisco Craton and the Araçuaí Belt was completely individualized from its African counterparts. All events displayed in the Fig. 8 between 14-20 (after 220 Ma) were connected with the break-up. This phase is divided in Rifting and Continental Drifting sub-phases.

In the São Francisco Craton, a stable behavior was prevalent. Restricted rifting and sedimentation processes occurred in the western part and along costal area. During the Cretaceous, the Abaeté graben opened through extensional reactivations following Precambrian structures (Reis et al., 2017; Sawasato, 1995). The Areado, Urucuia and Mata da Corda groups (Event 18, on Fig. 8) filled the depocenter. Magmatism was rare on the cratonic area and only a few Jurassic diabase dikes intrude the Serra do Espinhaço rocks (Proterozoic).

Next to the south of Brasília Belt, Jurassic widespread aeolian sedimentation (Event 14, on Fig. 8) was partially covered and intertrapped by basalts of the Paraná Large Igneous Province (L.I.P) at 135 Ma (Event 15, on Fig. 8), in the face of the continental crust cracking (Thiede and Vasconcelos, 2010). To the northeast of the basin, Brasília Belt limited the flood dispersion and remained in a steady condition until experience rearrangements during the Cretaceous, that caused the reactivation of the Alto Paranaíba Arch. The region is an NW-SE trend of structural high, where several alkaline magmatism intruded (Event 19, on Fig. 8). The Alto Paranaíba Arch seems to have been reactivated afterward, mainly in the Upper Cretaceous associated with dike's intrusions, alkaline bodies, and kamafugitic lavas. The eruptions were genetically related to the deposition of pyroclastic rocks of the Mata da Corda Group in the Sanfranciscana Basin. Coeval sedimentation took place filling the Bauru Supersequence in Paraná Basin (Event 16, on Fig. 8). Batezelli and Ladeira, (2016) suggest a main role of the Alto Paranaíba Arch reactivations to the sedimentation of both the Sanfrancisca Basin and the Bauru Supersequence. However, Menegazzo et al., (2016) correlates the tectonic pulses and

depocenter migration observed in Bauru deposits with the Andean tectonism (Events 5-7, on Fig. 8).

In the Araçuaí Belt, NW-SE trending basement lineaments of the Brazilian coast were reactive at least two times in the Lower Cretaceous. Firstly, when they hosted tholeiitic dykes, and secondely promoting rearrangements of normal brittle faults (Event 20, on Fig. 8) (Santiago et al., 2019). The moviments are also connected with the sedimentation of the offshore basins on Brazil eartern margin with sediments supply generation (Calegari et al., 2016; Lourenço et al., 2016). Cenozoic onshore rifting basins occur next to the Araçuaí Belt (Event 21, on Fig. 8). They are: Gandarela and Fonseca basins, to the east of the Quadrilátero Ferrífero (Iron Quadrangle); and basins that compose the Continental Rift of Southeastern Brazil (CRSB), to the south. The CRSB presents multiples signs of Cenozoic reactivations in a transpression regime (Riccomini et al., 2004).

2.4 - São Francisco Craton and marginal orogens AFT thermochronology
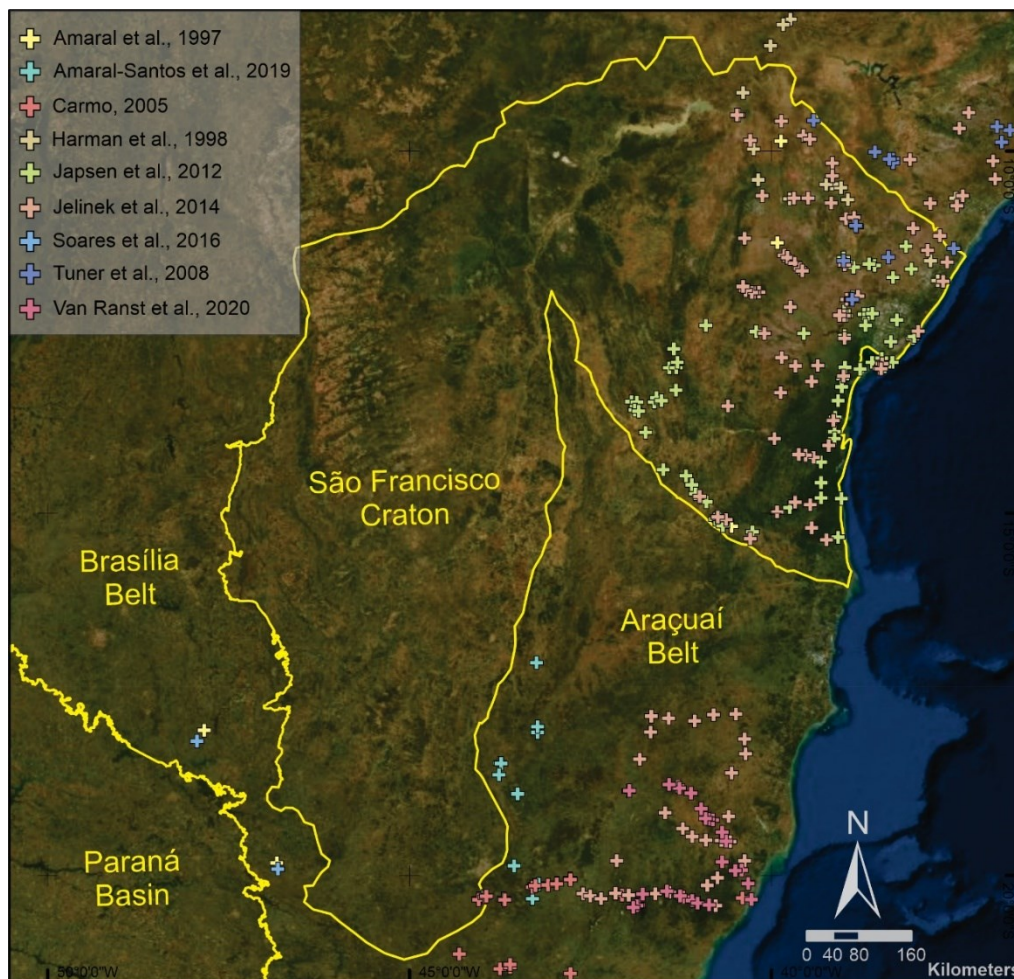

Figure 9- Location map of the published AFT data in the São Francisco Craton and marginal orogens. (São Francisco Craton limits by Heilbron et al., 2017).

Previous works using AFT thermochronology in the São Francisco Craton and marginal orogens are presented in the Figure 9 and the AFT central ages calculated by them in the Figure 10. The majority of the studies were concerned with understanding the Brazilian continental margin (Amaral-Santos et al., 2019; Amaral et al., 1997; Carmo, 2005; Harman et al., 1998; Japsen et al., 2012; Jelinek et al., 2014; Turner et al., 2008; Van Ranst et al., 2020). Alkaline intrusions were also target of Amaral et al., (1997) and Soares et al., (2016) studies.
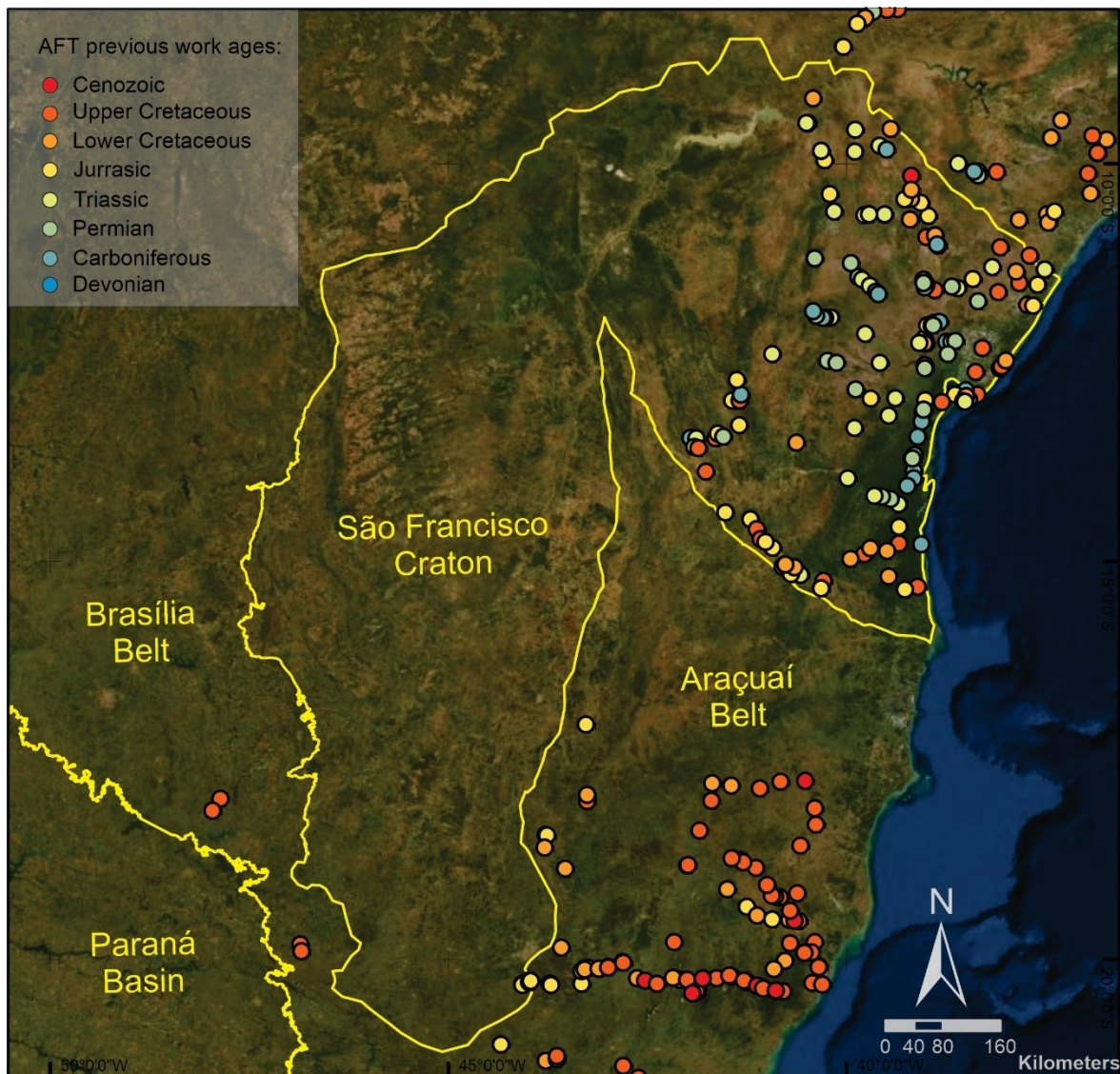
Figure 10- AFT central age map of the published AFT data in the São Francisco Craton and marginal orogens. (São Francisco Craton limits by Heilbron et al., 2017).

The AFT central ages in the coast range from Ordovician to Neogene. The data shows that the response to the extension efforts of the opening of the South Atlantic Ocean during Lower Cretaceous was not homogeneous (Fig. 10). The orogenic area of Araçuaí Belt registers three thermal events: Lower Cretaceous, Upper Cretaceous and Paleogene-Neogene (Carmo, 2005; Jelinek et al., 2014; Van Ranst et al., 2020). In general, this region follows the expected

model for passive margins in which there is an increase of the AFT ages from 30-90 Ma, in the margin, to 200 Ma, in the continental hinterland (Carmo, 2005). The range of AFT young ages shows that the sensu stricto rifting process is not the only responsible for the configuration of the relief on the coast, thus post-rift reactivations events must have took place. The authors suggest that the post-breakup reactivations can be explained by: (i) compression between Andean subduction zone and the mid-Atlantic ridge (Jelinek et al., 2014; Van Ranst et al., 2020), (ii) Extensive reburial and uplifts events (Japsen et al., 2012), and/or (iii) Isostatic uplift caused by the sedimentation on offshore basins (Jelinek et al., 2014).

On the northeast coast, constituted by the lithosphere of the São Francisco Craton, the cooling ages are older, ranging from Carboniferous to Lower Jurassic. According to Jelinek et al., (2014), older events are related to the erosion of topography built during the Gondwanide Orogeny during the late Paleozoic. The change in the value of the AFT ages for the cratonic coast is evidence that the extensive efforts of the generation of the opening of the Atlantic Ocean did not act in this region in a pervading way (Jelinek et al., 2014).

CHAPTER II

This chapter presents the two research papers produced from the acquired AFT dataset. After the mineral separation, among the 63 samples colleted, 50 samples were selected to proceed to the irradiation and following steps. The 13 discarded samples (2, 3, C5, C10, C13, N1, N2, N6, N8, N9, N14, N15, N17) did not present apatite grains of adequate quality and quantity for the AFT analysis. The "Article I" present and discuss the results of 7 samples from the Brasília Belt (8, 9, C17, C16, C15, C14, N13), focusing in constrain the hitherto not investigated exhumation history of this terrain. The "Article II" is based on the entire dataset (50 samples) to discuss the main phases of Phanerozoic cooling in the São Francisco Craton and its marginal orogens.

2.1 − Article I: Paleozoic post-orogenic denudation of the Brasília Belt of West Gondwana: insights from apatite fission track thermochronology

Authors: Ana Carolina Liberal Fonseca[a1], Gabriella Vago Piffer[a], Simon Nachtergaele[b], Gerben Van Ranst[b], Johan De Grave[b], Tiago Amâncio Novo[a]

[a]*Universidade Federal de Minas Gerais, Programa de Pós-Graduação em Geologia, CPMTC-IGC, Campus Pampulha, Belo Horizonte, MG, Brazil*

[b]*Laboratory for Mineralogy and Petrology, Department of Geology, Ghent University, Ghent, Belgium*

Abstract:

The Brasília Belt in southern Brazil is a Neoproterozoic orogenic belt that represents the northern border of the Paraná Basin, a long-lived early Paleozoic intracratonic basin. The belt is surrounded by cratonic domains and were modestly affected and reactivated by the opening of the South Atlantic Ocean during the Cretaceous. Here we present new apatite fission track data from crystalline rocks of the Brasília Belt. The apatite fission track central ages range from 386 to 243 Ma and the mean track lengths range between 11.4 and 13.7 μm. Thermal history modeling reveals Paleozoic cooling, which we interpret as the main final exhumation of the Brasília Belt, implying that indeed the influence of posterior Mesozoic and Cenozoic geodynamic history on the belt is limited. The Paraná Basin and surrounding elevated terranes therefore provide a time window to study the tectonic history of Gondwana and the effect of far-field intraplate stresses on the interior of West Gondwana. Rapid basement exhumation of

the Brasília Belt is coeval with extension and tectonic subsidence in the Paraná Basin as a result of continent-scale tectonic forces occurring over entire West Gondwana.

Keywords: Low-temperature thermochronology, Erosional denudation, West Gondwana basement, Pre-Andean orogenies, Paraná Basin

1.Introduction

The West Gondwana paleocontinental basement was composed of Archean cratons and Proterozoic lithospheric blocks, welded along Neoproterozoic – early Paleozoic orogenic belts (Fig. 1). After its Paleozoic amalgamation, the basement experienced a transition to a stable platform, where several large intraplate basins or syneclises, surrounded by elevated areas, developed (de Wit et al., 2008). The subsidence of the syneclise depocenters was contemporaneous with Pre-Andean southward-direct subduction of oceanic lithosphere of Panthalassa and associated collision-accretion events, during the entire Paleozoic (Fig.1) (Du Toit, 1937, 1927; Keidel, 1916). In the late Cretaceous, West Gondwana was affected by progressing fragmentation, and eventually the South American and African continents were separated due to the opening of the South Atlantic Ocean.

The basement cooling of the West Gondwana orogenic belts leading to the post orogenic stability can be understood as the result of interplay between rock-uplift and tectonic forces with erosional processes (e.g. Braun et al., 2006; Braun and Robert, 2005; Pazzaglia and Kelley, 1998; Reiners and Brandon, 2006; Spotila, 2005; Whipple and Meade, 2006). Erosive denudation and sediment production pulses can be periodically renewed by tectonic reactivation, drainage reorganization or climate changes (Fitzgerald et al., 1999; Zhang et al., 2001). Isotopic chronometers, sedimentary record and tectonic evolution of adjacent depocenters are fundamental tools to clearly understand how high-temperature rocks from the crustal roots of orogenic belts are exhumed to the surface (Enkelmann et al., 2014; Fan and Carrapa, 2014; Kasanzu et al., 2016; Tinker et al., 2008; Weber et al., 2004).

Geothermochronometric techniques, such $^{40}Ar/^{39}Ar$ in potassium bearing minerals, or U/Pb dating on zircon, titanite, and monazite are commonly applied to understand the long-term bedrock tectonic evolution, providing time constraints in the medium to high temperature window (e.g. Babinski et al., 2013; D'Agrella-Filho et al., 2011; Danderfer et al., 2009; Gresse and Scheepers, 1993; Manhica et al., 2001; Nonnotte et al., 2008; Oliveira et al., 2010; Sims et al., 1998; Tohver et al., 2010). Few researches have however investigated the further evolution

of the basement rocks in our study area towards ambient temperature. The difficulties lie in the fact that data from low-temperature thermochronometers are very sensitive to reheating and ancient orogenic belts are commonly thermally reset over time (Enkelmann and Garver, 2016; Spotila, 2005). Besides, the erosional product information of ancient processes is highly dependent on the preservation of the sedimentary record. The opening of the Atlantic Ocean was responsible for the overprint of previous thermal history information embedded in the West Gondwana bedrock. The Atlantic passive margin of South America and Africa was the subject of a series of thermochronological works that highlight its post-rift thermal evolution (e.g. Cogné et al., 2011; Oliveira et al., 2016; Gallagher et al., 1994; Green et al., 2018; Hueck et al., 2017; Japsen et al., 2012; Jelinek et al., 2014; Krob et al., 2019; Van Ranst et al., 2020; Wildman et al., 2015).

In the hinterland, restricted areas are able to retain their former cooling signals associated with the evolution of the West Gondwana basement and add relevant data for understanding long-term landscape dynamics (Reiners and Brandon, 2006; Spotila, 2005). The Brasília Belt (Fig.1) is such an example and was spared of major Phanerozoic tectonic events, remaining confined between large cratonic blocks, mainly the São Francisco and Amazonia cratons (Valeriano et al., 2008). This belt is a remnant of the Neoproterozoic orogen formed during the amalgamation cycle that culminated in the ultimate formation of the Gondwana Supercontinent (Pimentel, 2016; Valeriano et al., 2008). After amalgamation, it worked as a paleohigh and source of sediments for its intracratonic sedimentary basins that developed during the Phanerozoic, i.e. mainly the Paraná Basin in this case. This basin preserves seven-kilometer-thick of sedimentary sequences (Milani et al., 2007). The post-orogenic cooling history of the belt is hitherto not constrained by low temperature thermochronometers.

This paper presents results of low temperature thermochronometry, in particular Apatite Fission Track (AFT) analysis, performed on seven basement samples from the Brasília Belt, and will be linked to the sedimentary basin evolution of the adjacent Paraná Basin. With the new apatite fission track data, it is attempted to further solve the outstanding research questions on the Phanerozoic evolution of the region and the effects of the opening of the South Atlantic Ocean on the Neoproterozoic orogenic lithosphere of the continental interior of South America.
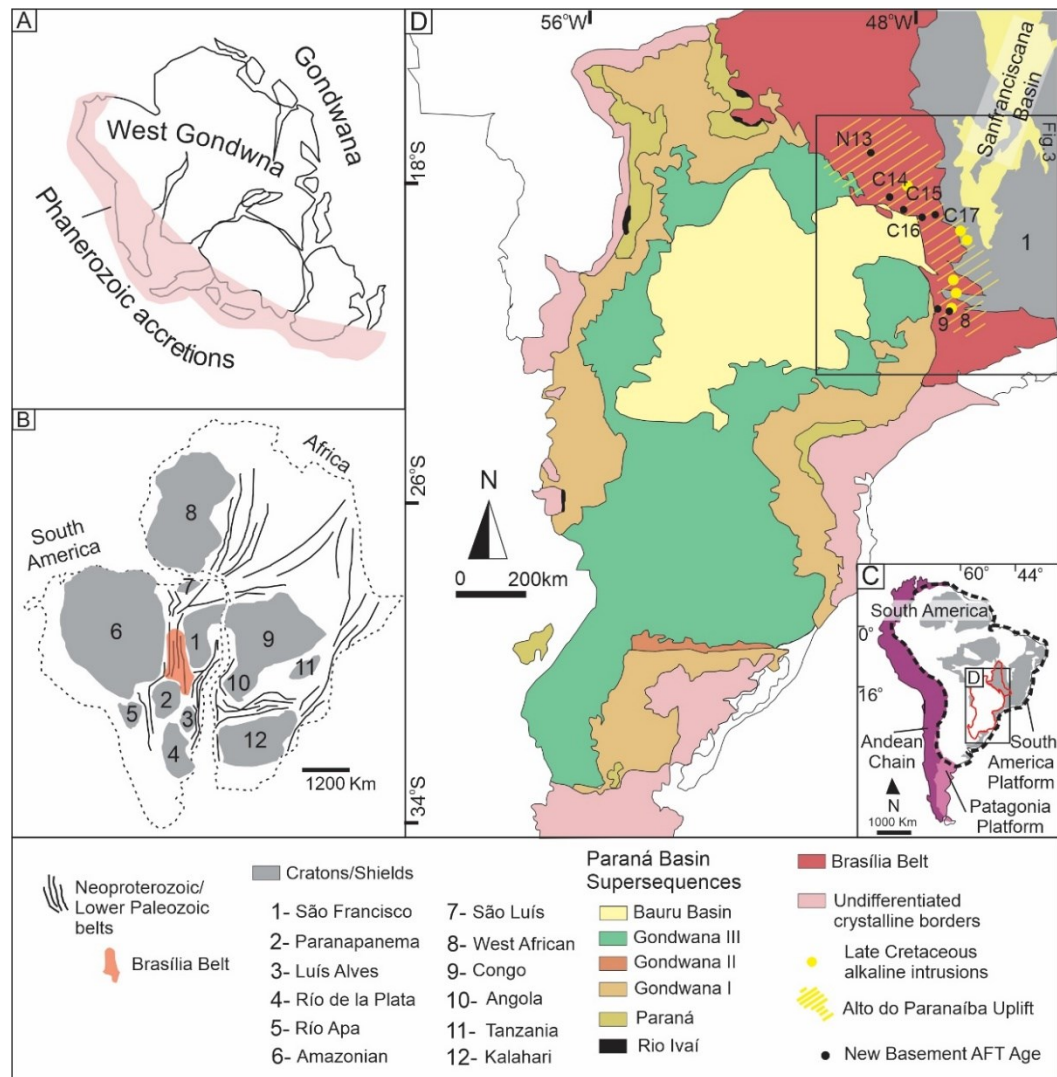
Figure 1: Geological context of the study area. A) Gondwana Supercontinent and the Phanerozoic accretions (after Almeida et al., 1981). B) Schematic representation of West Gondwana basement, with the shields, cratonic continental masses and Neoproterozoic-Late Paleozoic orogenic belts (after Tohver et al., 2006; Vaughan and Pankhurst, 2008). C) Schematic representation of current tectonic subdivision of South America (after Almeida et al., 1981). D) Geological regional map showing the location of analyzed samples in the Neoproterozoic Brasília Belt, the Alto do Paranaíba Uplift with the major alkaline intrusions (adapted from Gibson et al., 1995), the Paraná Basin supersequences (adapted from Milani and Ramos, 1998), the Sanfranciscana Basin (adapted from Heilbron et al., 2017) and surrounding basement units.

2.Geological Setting

2.1 - Brasília Belt

The Brasília Belt comprises an Archean to Paleoproterozoic basement which, together with Proterozoic metasedimentary rocks, a Paleoproterozoic juvenile magmatic arc (Goiás arc), and Neoproterozoic granitic intrusions, is folded and thrusted toward the São Francisco Craton (Fig.1B) (Pimentel et al., 2000). This tectonic unit is the result of the Neoproterozoic orogeny during an early phase of the Gondwana Supercontinent amalgamation that consumed the large

Goiás-Pharusian ocean crust over a long time of between ca. 900 and 600 Ma (Brito Neves, 1999; Pimentel, 2016). It was formed due to the convergence of the Amazonia, São Francisco-Congo and Paranapanema paleocontinents (Pimentel et al., 2004). After the orogenic construction the relaxation of the geothermal gradient took place during Cambrian to Ordovician (Valeriano et al., 2008).

The transition through a relatively stable platform lasted until the Silurian-Devonian and was characterized by the development of the large Paleozoic syneclises (Brito Neves, 2002; Milani and Thomas, 2000), such as the Paraná and Sanfranciscana basins (Fig. 1D). During the Phanerozoic, the southern portion of the belt worked as a structural high that limited the extension of the aforementioned basins (Sgarbi and Dardenne, 1996). The area was affected by a glaciation and glacio-isostatic forces during the Carboniferous - early Permian. Paleocurrents and paleo slope analysis on Paraná Basin glacial sediments point to influx coming from the Brasília Belt (Eyles et al., 1993; Mottin et al., 2018). Moreover, in the Sanfranciscana Basin, Carboniferous glaciogenic facies are located approximately 400 km northeast of the study area with the Brasília Belt as a possible source area as well (Mottin et al., 2018). In the Cretaceous, the belt worked as a barrier to the advance of the Serra Geral volcanism in the Paraná Basin, also known as the Paraná Large Igneous Province (L.I.P) (Sgarbi and Dardenne, 1996). Finally, in the Late Cretaceous, the southern portion of the belt hosted alkaline magmatism related to the breakup of West Gondwana (Riccomini et al., 2005). The region of magma emplacement occurs in a positive tectonic feature known as Alto Paranaíba Uplift and covers our study area (Fig.1D) (Hasui et al., 1975b).

2.2 - Paraná Basin

2.2.1 -Sedimentary record

The Paraná Basin is an intracratonic sedimentary basin (Fig. 1) developed during the late Ordovician to Late Cretaceous. It covers an area of 1,500,000 km^2 and preserved sedimentary sections up to 7 km (Milani et al., 2007). Milani et al., (1994) recognize six supersequences, mainly composed of siliciclastic and volcanic rocks: with at the base the Rio Ivaí (Ordovician-Silurian), Paraná (Devonian) and Gondwana I (Carboniferous - Late Permian) supersequences representing major Paleozoic transgressive-regressive cycles, whereas, on the top, Gondwana II (Triassic), Gondwana III (Early Cretaceous) and the Bauru (Late Cretaceous) supersequences are fully continental packages (Fig. 2).

The Rio Ivaí and Paraná supersequences correspond to a succession of sandstones, conglomerates and black shales, recording marine sedimentation (Fig. 2). They are truncated by a regional unconformity marked by glacial pavements, that indicates advances and retreats of Gondwana ice caps during the Carboniferous (Linol et al., 2015). The accumulation of the Gondwana I Supersequence started during de-glaciation episodes. The thick glaciogenic package (1.5 km) is composed of diamictites intercalated with sandstones and shales, sedimented in both glacio-terrestrial and glacio-marine environments (Milani and De Wit, 2008). The marine nature of the sediments is supported by the overall presence of *Tasmanites* and acritarchs (Daemon and Quadros, 1970).

The continued deposition of the Gondwana I Supersequence registers a progressive and irreversible closure of the Paraná Basin. The onset of the closure, forming a restricted water circulation between the basin and the Panthalassa Ocean, is evidenced by the presence of evaporites and carbonates to the north of the basin and bituminous shales to the south (Milani et al., 2007). Successively, the upper portion of the supersequence, the late Permian sedimentary record (Rio do Rastro Formation), represents the first part of entirely intracratonic terrigenous sedimentation in the Paraná Basin (Fig. 2), in a deltaic environment.

Triassic, and Jurassic deposits from Gondwana II and Gondwana III supersequences show increasingly hotter and more arid conditions in a paleo-desert environment near the center of West Gondwana (Milani and De Wit, 2008). During the Early Cretaceous, the basin was overlain by a large flood basalt (Paraná L.I.P) (Renne et al., 1992; Thiede and Vasconcelos, 2010) related to the opening of South Atlantic Ocean and break-up of the supercontinent. Finally, in the Late Cretaceous, the sedimentation of the Bauru Supersequence changed to a semi-arid setting (Fig. 2).

2.2.2 -Subsidence

The development of the Paraná Basin above a cratonic nucleus was only better understood after drill core analyses and geophysics studies, since the cratonic basement only occurs in the subsurface. The basin sediments are underlain by the Paranapanema block, characterized by a fragmented cratonic root (Julià et al., 2008; Milani and Ramos, 1998). Several studies have focused on presenting models for subsidence of the basin. Zalán et al., (1990) and Milani and De Wit, (2008) describe tectonic subsidence curves that highlight the highest rates between the Ordovician to Devonian and late Carboniferous to Early Triassic (Fig. 2).

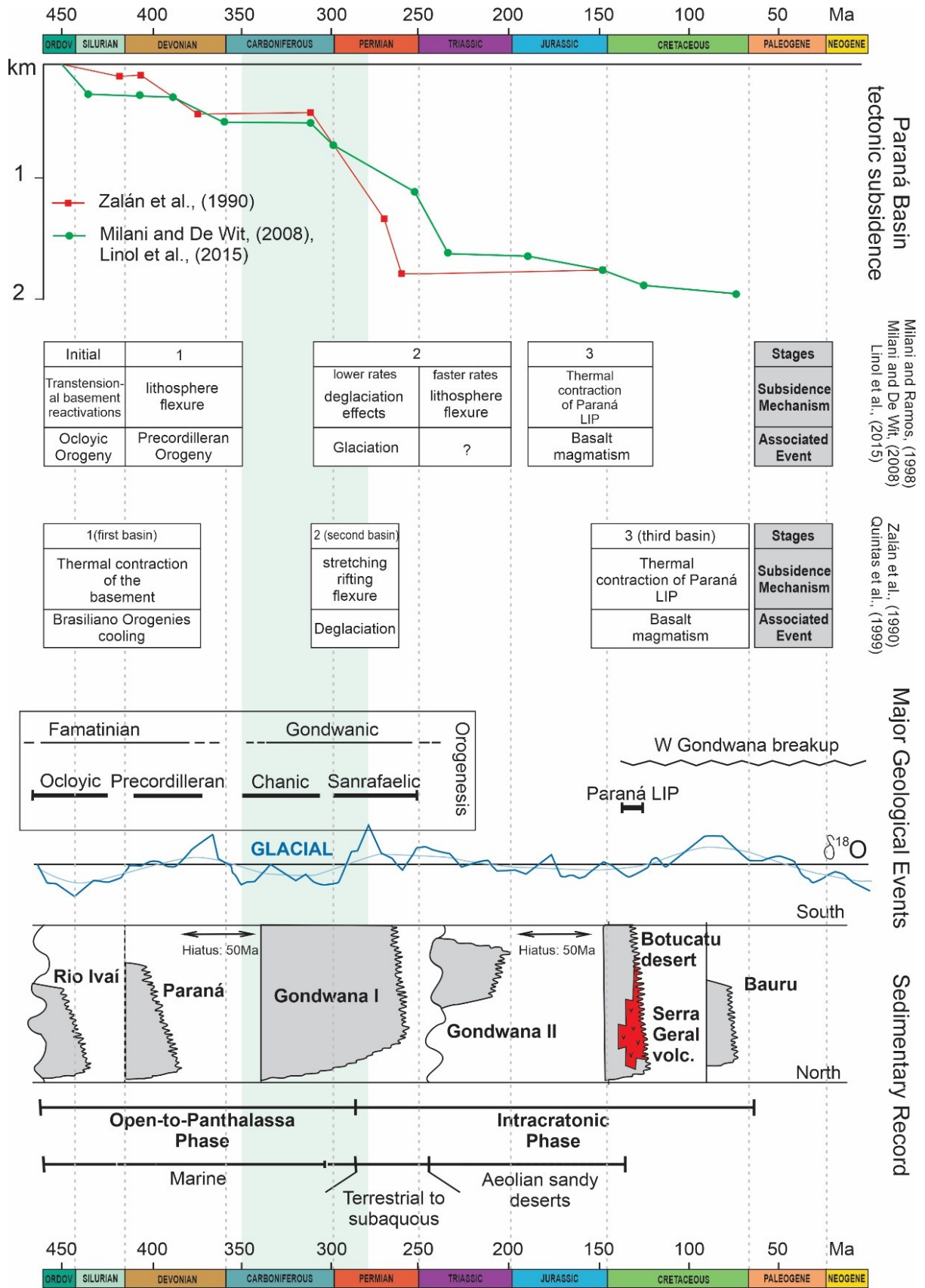*Figure 2: Paraná Basin development from the Ordovician to the Cretaceous. Subsidence rates from* Linol et al., (2015); Milani and De Wit, (2008); Zalán et al., (1990). *Major geological events and sedimentary record from* (Milani et al., 2007). *Subsidence history proposed by* Linol et al., (2015); Milani and De Wit, (2008); Milani and Ramos, (1998); Quintas et al., (1999); Zalán et al., (1990).

Zalán et al., (1990) in the first efforts to understand the Paraná Basin subsidence, pointed out three majors phases: Silurian - Devonian, Permian - Carboniferous, and Late Jurassic - Early Cretaceous, which define three different basins. The authors propose that the initial depression started in response to the cooling of the Gondwana shield after the Neoproterozoic orogeny by regional thermal subsidence. The second phase was triggered in response to a large glaciation event by a combination of stretching and rifting of the crust with associated flexure. The third phase coincides with cooling of the Paraná L.I.P. (Oliveira, 1989; Quintas et al., 1999; Zalán et al., 1990).

On the other hand, Milani and Ramos, (1998) from the analyses of tectonic subsidence curves (Fig.2) and the Phanerozoic geodynamics cycles of southwestern Gondwana (Fig. 1A), revealed a close relationship between the subsidence episodes and the orogenic efforts. In this model, the basin was affected by persistently active convergence between the Gondwana Supercontinent and the oceanic lithosphere of Panthalassa, in the Famatinian and Gondwanic cycles (Linol et al., 2015; Milani et al., 2007; Milani and De Wit, 2008). In the Ordovician, transtensional basement reactivation in response to the Oclóyica Orogeny led to the initial subsidence (Milani and Ramos, 1998). Analysis of seismic reflection and other geophysical studies show that the first depressions occurred along a NE-SW trend along weakened zones in the cratonic roots (Julià et al., 2008; Milani et al., 2007). In the Devonian until the late Carboniferous, an accelerated subsidence in the foreland domain took place, and is related to lithospheric flexure by the onset of the Precordilleran Orogeny. Lower subsidence rates (5-10 m/Ma) during the Carboniferous to Triassic occurred in response to the aforementioned deglaciation event. Then a new period of accelerated subsidence (10-20 m/Ma) started in the late Permian and is coeval with the Chanic and Sanrafaelic orogenies. In the Mesozoic the subsidence rates are considerably lower. The Gondwanic Orogeny was over and the basin found itself trapped inside the continent.

3. Analytical procedures

Seven samples for Apatite Fission Track (AFT) analysis were acquired from the Precambrian crystalline rocks from the Brasília Belt at the northeastern border of Paraná Basin (Fig. 1). Details of sample lithology and geographical locations are provided in Table 1. The samples were crushed and sieved to retain the sand fraction. Apatite grains were separated by conventional panning, magnetic separation, heavy-liquid and hand-picking protocols. They

were mounted in Struers CaldoFix-2 epoxy resin (~200 grains per sample mount). The mounts were polished using diamond suspension (6 μm, 3 μm and 1 μm). Apatite grains were etched for 20 s in 5.5 M(mol/L) HNO_3 solution at 21°C to reveal the spontaneous fission tracks (Donelick, 1991). All mineral preparation procedures described above were performed in Centro de Pesquisas Professor Manoel Teixeira da Costa (CPMTC), at the Federal University of Minas Gerais, and the Laboratory for Mineralogy and Petrology (Department of Geology) at Ghent University (e.g. Van Ranst et al., 2020).

Table 1: Sample locations (in World Geodetic System – WGS84) and rock types.

SAMPLE	GENERAL FEATURES			
Code	Long (W)	Lat (S)	Elevation (m)	Rock type
8	46.5302	21.3558	972	coarse grained pyroxene gneiss
9	46.8217	21.2976	777	coarse grained pyroxene gneiss
C14	48.0631	18.4268	748	biotite bearing migmatite
C15	47.7057	18.7589	856	biotite granite
C16	47.2202	18.9419	884	biotite granite
C17	46.8889	18.8789	1061	metaconglomerate
N13	48.5663	17.2696	758	mylonitic granite

All samples were analyzed with the external detector (ED) method (Hurford, 1990) using thermal neutron irradiation and following the standard procedure used at Ghent University (e.g. described by De Grave et al., 2011; De Pelsmaeker et al., 2015; Glorie et al., 2010; Nachtergaele et al., 2019). Irradiation was performed at the Belgian Reactor 1 (BR1) facility of the Belgian Nuclear Research Centre in Mol. The IRMM-540 dosimeter glass (de Corte et al., 1998) was used to monitor the thermal neutron fluence. Durango and Fish Canyon Tuff apatite age standards were also irradiated and stacked in between the samples at regular distances, to be used for zeta-calibration method (Hurford and Green, 1983). After irradiation, induced tracks were revealed in the muscovite ED with 40% HF for 40 min at 20°C.

Fission track density was obtained by counting tracks of 20 or more apatite grains for each sample using the motorized Nikon Eclipse Ni-E microscope with a DS-Ri2 camera attached, at a 1000x magnification (Van Ranst et al., 2020). Calculations used the overall weighted mean zeta (OWMZ) value of 249.1 ± 5.5 a·cm² (Analyst Gabriella Piffer) and 254.6 ± 8.8 a·cm² (Analyst Tiago Novo) based on multiple Durango and Fish Canyon Tuff apatite age standards.

The ages are reported as central ages and pooled ages in Table 2. Central ages were obtained using "IsoplotR" software (Vermeesch, 2018). Chi-squared test (χ^2) was used as a homogeneity test (Galbraith, 2005, 1981; Galbraith and Laslett, 1993; Green, 1981).

Table 2: Basement apatite fission track analysis results; n is the number of analyzed grains. ρ_s and ρ_i are the densities of spontaneous (apatite) and induced tracks (in muscovite external detector), respectively. ρ_d are interpolated values of the density of induced tracks in the external detector irradiated against regularly spaced Uranium-doped glass dosimeters (IRMM-540) in the radiation package. All densities expressed in 10^5 tracks/cm². N_s and N_i are the number of spontaneous and induced tracks, respectively. N_d is the interpolated value of number of induced tracks in the external detector stemming from co-irradiated glass dosimeters (IRMM-540). $P(\chi^2)$ is the chi-squared probability that the dated grains have a constant ρ_s/ρ_i ratio. $t(\zeta)$ is the apatite fission track central age (Ma) and $t_p(\zeta)$ is the fission track pooled age. l_m is the mean track length, σ is the standard deviation of the track length distribution, obtained by measurements of the number (n) of limited natural horizontal tracks; A is the analyst (G- Gabriella Piffer ζ =249.09±5.53 a.cm², T- Tiago Novo ζ =254.63±8.81 a.cm²).

SAMPLE														
Code	n	ρ_s (±1σ)	N_s	ρ_i (±1σ)	N_i	ρ_d (±1σ)	N_d	P(χ2)	t(ζ)	t_p(ζ)	lm	n	σ	Dpar	A
8	25	15.481(0.308)	2524	3.250(0.140)	542	5.818 (0.075)	5957	0.20	337 ± 21	391± 23	12.2	80	1.3	1.50	T
9	20	5.780(0.170)	1156	1.070(0.073)	214	5.807 (0.075)	5967	0.91	386 ± 31	421 ± 33	13.5	100	1.2	1.70	G
C14	20	23.620(0.473)	2491	5.419(0.225)	579	5.764 (0.106)	2953	0.48	302 ± 16	337 ± 18	12.1	105	1.2	1.95	G
C15	3	28.298(1.636)	299	7.245(0.820)	78	5.766 (0.106)	2954	0.25	269 ± 37	274 ± 36					G
C16	20	28.350(0.493)	3302	6.230(0.231)	729	5.769 (0.106)	2940	0.36	318 ± 17	326 ± 16	12.0	105	1.2	1.91	G
C17	7	14.702(0.798)	340	3.203(0.367)	76	5.781 (0.106)	2955	0.24	314 ± 41	335 ± 44					G
N13	20	30.056(0.679)	2024	9.005(0.370)	592	5.827 (0.107)	2985	0.50	243 ± 13	258 ± 14	11.4	100	1.8	2.07	G

Where possible, confined track lengths and the angle between the track and the crystallographic c-axis were measured. Approximately 50 to 100 confined (sub)horizontal tracks in each sample were measured to construct an AFT length-frequency distribution. Thermal history modelling was performed using QTQt software (Gallagher, 2012) on samples with sufficient number of lengths (more than 50). The Markov Chain Monte Carlo search method for inverse modeling with 10^5 post-burn in iterations was used. The time-temperature (t-T) prior was set to the (oldest age ± oldest age) to time, $70 \pm 70\,^{\circ}C$ to temperature and $25 \pm 20^{\circ}C$ as present-day temperature. D_{par} values were determined as the mean of 100-200 etch pit diameter per sample using a custom-made image recognition protocol within NIS Elements (Van Ranst et al., submitted) and was used in the multi-kinetic annealing model (Ketcham et al., 2007b) by QTQt.

4.Results

The results of seven apatite fission track (AFT) analyses are shown in Table 2 and geographically displayed in Fig.3. All samples pass the chi^2 test of homogeneity. The AFT central ages range from Devonian, 386 ± 31 Ma (sample 8) to Triassic 243 ± 13 Ma (sample C15). Samples C15 and C17 contained less than 20 analyzable apatite grains, therefore they are not used for in depth discussion, although they corroborate the results of the other samples. In the age-elevation plot (Fig. 4), in general, a clear normal trend, i.e. older ages at higher elevations, is found, although one or two outliers are present. Fragmentation of the profile due to the intricate local fault network is probably responsible for the latter. The track-length distribution is unimodal and quasi symmetrical for all samples (Fig. 5), except for sample N13 that shows a broad slightly asymmetric distribution. The mean track length (MTL) ranges from 11.4 µm (sample N13) to 13.7 µm (sample 9) and standard deviation from 1.2 (sample C14) to 1.8 (sample N13). While for example sample 9 shows rather long track lengths, typical of rapid basement cooling, in most cases clear thermally induced track length reduction associated with prolonged residence time in Apatite Partial Annealing Zone (APAZ). APAZ is the temperature window between 60-120ºC in which tracks accumulate but progressively shortened (e.g. Ketcham et al., 2007a; Wagner and Van den haute, 1992).

It is possible to see a relationship between the AFT central age and MTL as the half part of a boomerang trend (Fig. 6, Green et al., 1986). Sample 9 would represent the exhumation peak in the Devonian with longer track lengths, indicative of fast cooling through the APAZ (Carlson et al., 1999; Gleadow and Duddy, 1981; Green et al., 1989, 1986; Wagner and Van den haute, 1992). The other samples tail mixed signature with shorter track lengths and Carboniferous to Early Triassic ages and represent part of an exhumed APAZ.

Five thermal history models were generated by using the QTQt software (Gallagher, 2012)(Fig. 5). D$_{par}$ measurements range from 1.5 to 2.1 µm. The angle measurements of confined fission tracks and the apatite c-axis (Ketcham et al., 2007b) was also applied. Sample 9 shows the fastest Paleozoic cooling, starting around ~500 Ma and remaining stable in the Mesozoic and Cenozoic. Sample 8 initially cooled to ~50ºC around 400 Ma and after that maintained the same almost constant cooling rate (0.1ºC/Ma) up to present surface temperatures. The model for sample N13, the northernmost sample from Paraná Basin, shows a Paleozoic cooling until 250 Ma when the rock went from ~110 ºC to ~70 ºC. During the Mesozoic it remained in the temperature below 85 ºC until ~100 Ma, when it underwent the final main cooling event until reaching present ambient temperatures. Models from samples C14 and C16 present similar

results, both experienced relatively fast cooling, ~120ºC to 40ºC between ~420 Ma to ~250 Ma, and afterward a relative stability in 50ºC to 30ºC. Both models display a Neogene-Quaternary rapid cooling. Most likely, this episode is a well-known artefact (Jonckheere, 2003). So, we chose to reject it because we have no further arguments from other geological data.
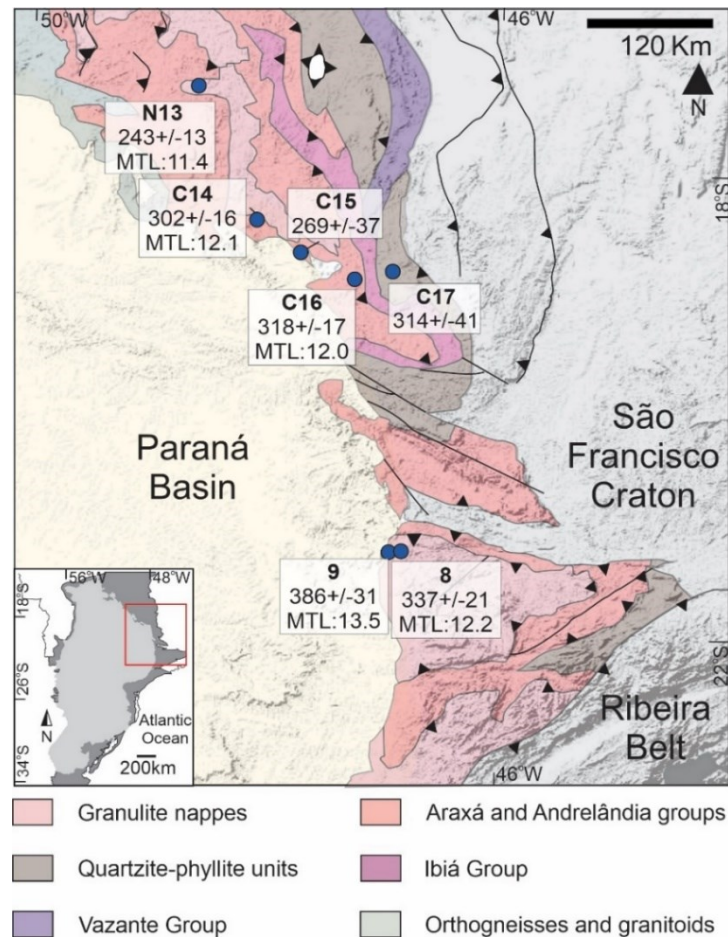

Figure 3: Simplified geological map of the study area with indication of the sample locations, central AFT ages (in Ma), and Mean Track Lengths (MTL) (in µm). (Geological map from Valeriano et al., 2008)*. For general location see box in figure 1D.*
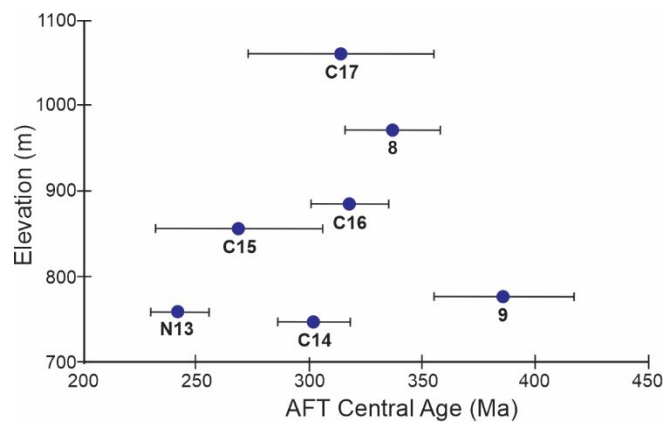

Figure 4: AFT age – elevation plot. See text for details.
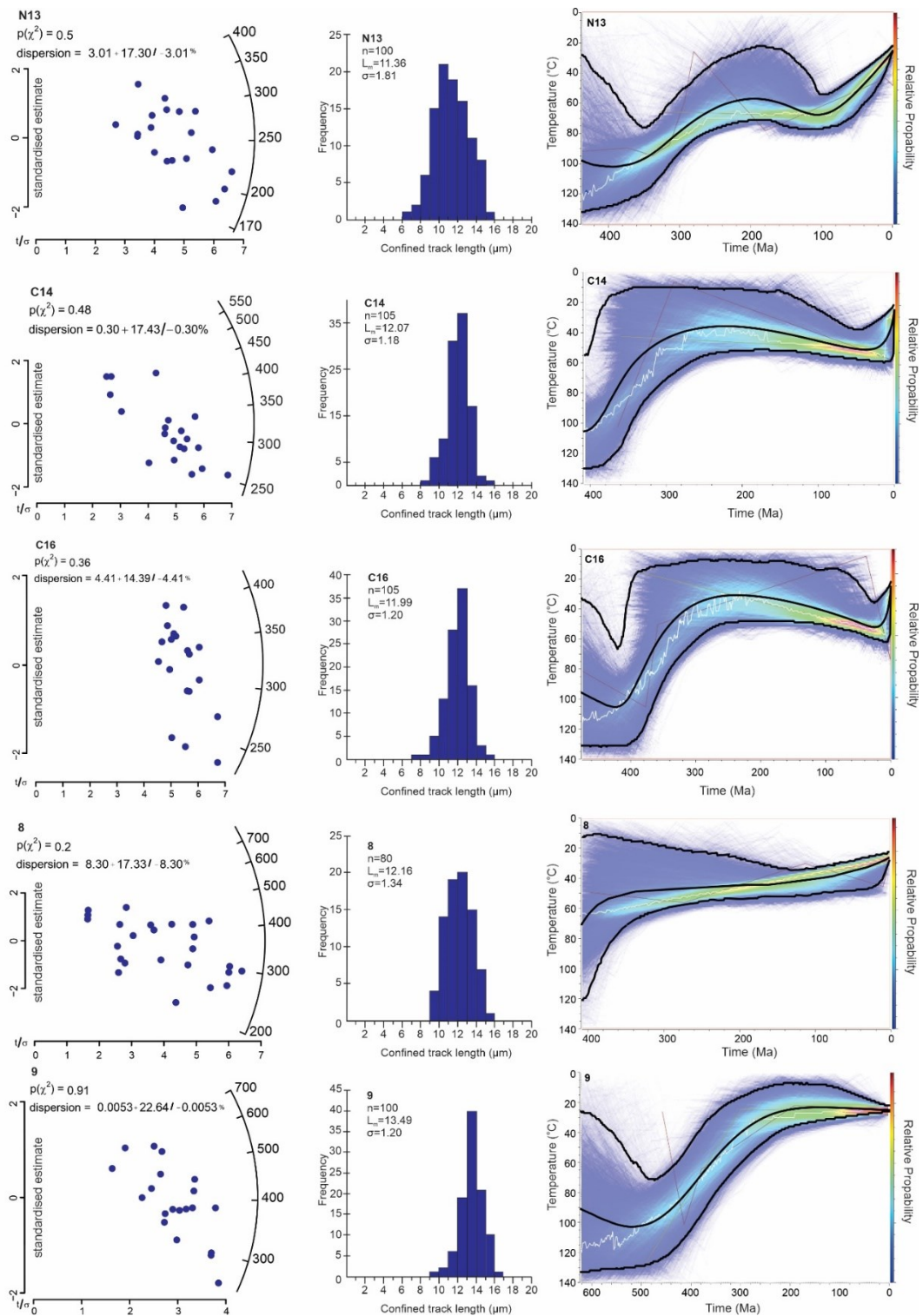
Figure 5: AFT data from samples N13, C14, C16, 8 and 9. Radial plots of AFT central ages, dispersion and the P(χ²) test were calculated with IsoplotR software (Vermeesch, 2018) *and presented in the first column. Track length histograms showing number of measured tracks (n), the MTL (L_m) and standard deviation (σ) are presented in the second column. Thermal history models reconstructed using the QTQt software* (Gallagher, 2012) *and the* (Ketcham et al., 2007b) *algorithm are presented in the third column.*

Figure 6: AFT age vs. MTL or "boomerang" plot (Green et al., 1986) *of the Brasília Belt basement samples. See text for details.*
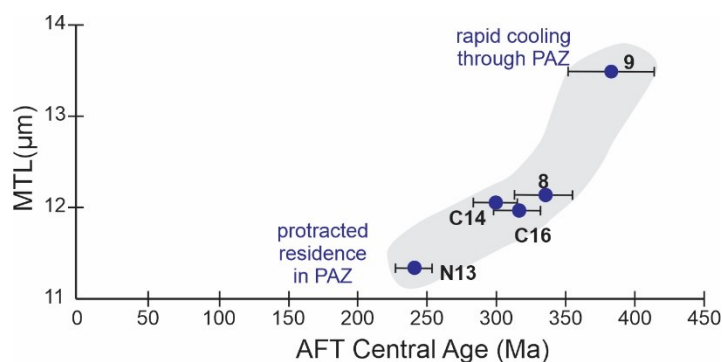
5. Discussion

5.1 - Paleozoic Brasília Belt exhumation and Paraná Basin subsidence

The thermochronological analyses of samples from the Brasília Belt not surprisingly, show cooling ages (central AFT ages) younger than the Neoproterozoic formation of the belt (900-600 Ma) (Pimentel, 2016), but clearly older than the West Gondwana break-up in the early Cretaceous (Mizusaki et al., 1998). The AFT central age versus MTL plot and thermal history models from samples 8, 9, C14, C16 and N13, indicate fairly rapid cooling of the Brasília Belt basement below temperatures of ~120-40°C already during Paleozoic times, mainly around 350-400 Ma (Fig. 6). Samples 8 and 9 show the earliest cooling phase (before 400Ma). This data indicates that exhumation of the current basement was already mostly attained at the end of the Paleozoic and that no or little posterior events have significantly affected the Brasília Belt basement since then. Further, this data also suggests a possible link between the Paleozoic cooling event of the Brasília Belt, its erosion and the influx of sediments into adjacent basins, in this case in particular the Paraná Basin. The Paraná Basin subsidence history was influenced by multiple pulses caused by Gondwana geodynamic cycles (Milani and Ramos, 1998). The tectonic subsidence curves (Fig. 7) show that the phases with the highest rate of accommodation and space generation also occurred in Paleozoic times, between the Ordovician (~450 Ma) and the Early Triassic (~240 Ma), i.e. coeval with basement cooling as indicated in our data. Reactivations and uplift through pre-Paleozoic structures could have been triggered by the tectonic extension generated during the subsidence through rifting processes (e.g. Glorie et al., 2012). Among all tectonic pulses, the MTL versus central age plot (Fig. 6) shows that the highest cooling rate through the APAZ occurred in late Paleozoic times. It suggests that the

Famatinian Orogeny that is deemed responsible for the break-up of the Paranapanema Craton (Fig. 1B) and the Paraná Basin formation, substantially affected the Brasília Belt basement, indeed provoking its rapid exhumation.
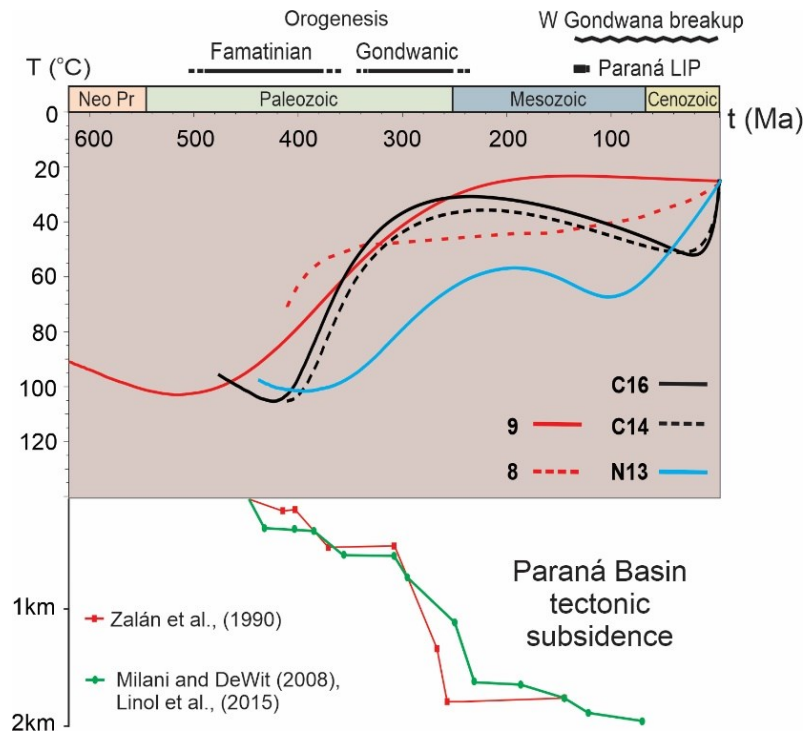

Figure 7: Time relationship between the major Phanerozoic events that affected West Gondwana, our thermal history models obtained by QTQt (Gallagher, 2012) *and the subsidence rates of the Paraná Basin* (Linol et al., 2015; Milani and De Wit, 2008; Zalán et al., 1990). *The thermal histories are shown with their Expected Model line as exhibited in Fig. 4.*

However, uplift alone cannot cause isotherm suppression and basement cooling, and hence denudational processes are evidently required. Erosional denudation is the most probable link between tectonic uplift and other processes, including chemical weathering, sediment production, transportation and deposition in the nearby depocenters (Reiners and Brandon, 2006). The previous paleocurrent data of the first three supersequences (Rio Ivaí, Paraná and Gondwana I) of the Paraná Basin (Alessandretti et al., 2016; Assine, 1999; Assine et al., 1998; Gesicki et al., 2002; Lobato and Borghi, 2005; Mottin et al., 2018; Scherer and Lavina, 2006) points to the Brasília Belt as a possible source area, as well as the fact that U-Pb detrital zircon data of Carboniferous to Triassic sedimentary rocks show significant contributions from the Neoproterozoic belts (Canile et al., 2016). Therefore, the provenance analysis agrees with the proposed hypothesis that the basement denudation in the northern sector of the Paraná Basin has been active since the deposition of the Rio Ivaí Supersequence. Up to the end of the

Paleozoic, erosion processes may have actively contributed to the basement exhumation and the associated deposition of more than 5,000 meters of sediments in the Paraná Basin (Milani et al., 2007).

Furthermore, during the late Paleozoic, West Gondwana was subjected to glaciation and was covered by ice caps (Buso et al., 2017; Caputo and Crowell, 1985; Eyles et al., 1993; Griffis et al., 2018; Montañez and Poulsen, 2013; Mottin et al., 2018; Visser, 1987), which provoke important changes on the nature of the surface processes and tectonic readjustments (Milani et al., 2007). Paleocurrent data and the position of the Brasília Belt between two Carboniferous glacial deposits (in Paraná and Sanfranciscana basins) show that glacial fronts probably resided in our study area (Eyles et al., 1993; Mottin et al., 2018). The glacial erosion can be one or two orders of magnitude higher than its fluvial counterpart (Hallet et al., 1996), substantially increasing the denudation rates. Moreover ice-proximal marine environments, such as the Carboniferous Paraná Basin (Fig.8), are even more susceptible to readjustments and isostatic subsidence promoted by relative sea-level drop and isostatic rebounds induced by glacial retreat (Boulton, 1990; Powell and Cooper, 2002). Reiners and Brandon, (2006) show a clear correlation between low temperature thermochronology signals in bedrock and regional glacial activity.

Thereby, the results suggest that after Paleozoic exhumation episode, samples 8, 9, C14, and C16 were part of a stable continental interior and they were not significantly affected by reburial or tectonic and thermal processes related for example to Gondwana break-up, or Cretaceous alkaline intrusions.

5.2 - Post-Paleozoic stability of the Brasília Belt

AFT thermochronometry from the Brasília Belt basement shows that most of the samples experienced a long period of stability during the Mesozoic and Cenozoic. Thus, we can suggest that from that time, these rocks slowly cooled to ambient temperatures as they were exhumed to near-present surface positions were they still reside today. The post-Paleozoic stability of the study area can be explained by taking into account several factors. During the Mesozoic, the Gondwanic Orogeny ceased and the Paraná Basin subsidence rates became considerably slower (Milani and Ramos, 1998). The Paraná Basin was trapped in the then arid interior of the Gondwana Supercontinent, changing to a continental base level. According to e.g. Bishop, (2007) the arid climate slows the landscape evolution to very low rates of denudation. Thus, the environmental situation and the Mesozoic-Cenozoic shallower depocenters induced

significantly less of erosional forces after the Paleozoic, hence slowing down or halting measurable erosional denudation. The thinner sedimentary packages observed in the adjacent basins during this time (Milani et al., 2007) support this hypothesis.

The modeled t-T path of sample N13 shows a more complex thermal history, which includes a possible reheating during the Mesozoic and a basement cooling episode starting approximately at 100 Ma, until the present surface temperatures. Along the northeast edge of the Paraná Basin, the emplacement of Late Cretaceous alkaline intrusions associated to deep mantle thermal anomalies (Ernesto, 2005) could be invoked as a reheating source. However, it is unlikely that this event affected only sample N13, which is the furthest from these intrusions (see in Gibson et al., 1995). It is also possible to observe that around the well-studied alkaline intrusion of Poços de Caldas, thermochronological analyses do not show evidence of reheating in the country rocks close to the alkaline intrusion (Cogné et al., 2011; Doranti-Tiritan et al., 2014). Thus, it is more reasonable to suggest reburial of these rocks by Paraná Basin sediments, followed by Cretaceous denudation to explain the possible reheating event. The reburial and renewed denudation could then be related to differential reactivation of regional structures as response to the changing stress-field associated with either the emplacement of the alkaline intrusions and/or to the extension accompanying the South Atlantic opening. New incisions and fluvio-alluvial erosion promoted by the adjustments during the Cretaceous possibly generated sediments deposits in the adjacent basins, as suggest by Batezelli, (2017) and Milani et al., (2007) for the Bauru Supersequence of the Paraná Basin or Campos and Dardenne, (1997) and Uhlein et al., (2011) for the Sanfranciscana Basin (Fig. 8).

5.3 - Paleozoic denudation of West Gondwana

Previous thermochronological research on late Paleozoic-Precambrian lithosphere of ancient West Gondwana terrains reveal significant Paleozoic exhumation (Fig.7; Bicca et al., 2013; Borba et al., 2002, 2003; Doranti-Tiritan et al., 2014; Oliveira et al., 2016; Enkelmann et al., 2014; Jelinek et al., 2014; Kasanzu, 2017; Kasanzu et al., 2016; Krob et al., 2019; Ribeiro et al., 2005; Souza et al., 2014). The authors gave similar suggestions to explain this period of cooling, relating their thermochronological results with far-field compressional tectonic processes from the Famatinian and Gondwanic cycles and the generation of adjacent sedimentary basins.
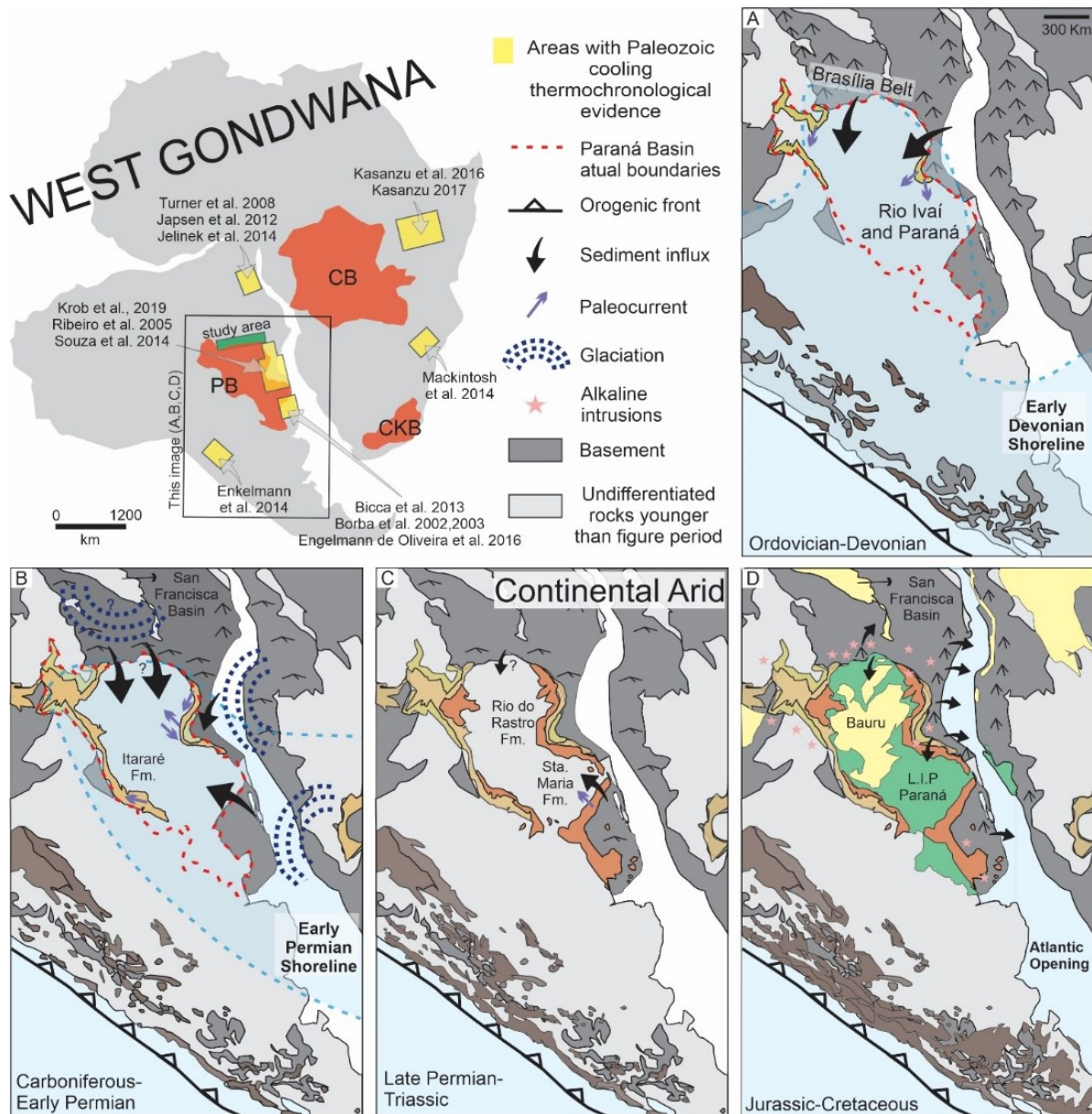
Figure 8: Schematic model for the Paraná Basin sediments, borders, and sediment influx. West Gondwana reconstruction after Tohver et al., (2006) *showing our study area, PB - Paraná Basin, CB -Congo Basin, CKB - Cape-Karoo Basin and previous works presenting Paleozoic cooling as evidenced from thermochronological data. Paleo-maps in A, B, C, and D adapted from* Linol et al., (2015). *A) Ordovician - Devonian: deposition of the Rio Ivaí and Paraná supersequences in the context of basin open-to-sea. Paleocurrent data* (Assine, 1999; Assine et al., 1998) *show the Brasília Belt as probable source area. B) Carboniferous-Early Permian: deposition of the glacial Itararé Formation, first of the Gondwana I Supersequence in the Paraná Basin and the glacial Santa Fé Group in the Sanfraciscana Basin* (Campos and Dardenne, 1997). *Glacial fronts from* Mottin et al., (2018) *and paleocurrent data (from* Carvalho and Vesely, 2017; Mottin et al., 2018; Rosa et al., 2019; Vesely et al., 2015; Vesely and Assine, 2014) *showing probable high erosion rates in the Brasília Belt due to glacial processes. C) Late Permian - Triassic: deposition of the Rio do Rastro Formation, Gondwana I Supersequence, and Santa Maria Formation, Gondwana II Supersequence. Reduction of erosion rates and sediment influx due to deceleration of tectonic subsidence of the Paraná Basin and confinement in an arid environment. D) Jurassic - Cretaceous: Paraná Large Igneous Province (L.I.P) flood basalt (Jurassic) and Bauru Supersequence deposition in the Paraná Basin (Cretaceous), coeval with the Areado Formation deposition in the Sanfranciscana Basin. Opening of the South Atlantic Ocean with emergence of coastal basins and emplacement of alkaline intrusions in the hinterland.*

Tankard et al., (1995), Linol et al., (2015) and Milani and De Wit, (2008) propose a shared genetic history for three of the most extensive West Gondwana basins: Paraná, Congo and, Cape–Karoo basin (Fig. 7), based on regional stratigraphic correlations and their similar subsidence history. The authors suggest that during the Paleozoic the basin subsidence were linked and coupled to the Famatinian and Gondwanic evolution. In the Early Paleozoic, they evolve into a single, truly intracratonic basin until the Early Cretaceous disruption and opening the South Atlantic Ocean (Linol et al., 2015; Milani and De Wit, 2008). This work and previous results indicate that basin basement denudation in surrounding uplifted areas in West Gondwana could be induced by the same geodynamic events.

Thus, the Paleozoic subsidence-exhumation cycle along West Gondwana seems to be driven by Famatian and Gondwanic collisions and their distal effects inside the continent (e.g. depocenter generation). In addition, Late Paleozoic widespread glaciation in Gondwana (López-Gamundí and Buatois, 2010) probably boosted the basement cooling considering the larger glaciogenic erosive potential. It shows that surface processes were intimately connected to tectonic events and, during this time, it could have acted on a broad regional scale. In this sense, the Paleozoic seems to have been an essential period of relief changes with high denudation rates in the entire southern sector of West Gondwana. Moreover, the stability of Precambrian - Late Paleozoic basement since the end of the Gondwanic orogeny is an indicator that the Paleozoic processes have had far more influence on these areas than the Pangea fragmentation.

AFT, and low-temperature thermochronometry in general, applied to stable cratons or platforms such as the Brasília Belt or the Tanzanian Craton for example, shows great potential to gain a better understanding of their tectonic evolution, sediment provenance and topographic development.

6. Conclusions

Our new AFT data in addition with the thermal history modeling of the Neoproterozoic basement of the Brasília Belt allow us to draw the following conclusions:

- Relatively fast post orogenic cooling occurred during the Paleozoic (~400-350 Ma) in the Brasília Belt. The exhumation of the southern portion of the belt was associated with the effect of tectonic extension during the breakup of cratonic lithosphere that generated the subsidence of the Paraná Basin. The Brasília Belt, that worked as a paleo high, was a source of for the clastic sedimentation found in the

Paraná Basin and therefore agrees with our new data on the exhumation history of the Brasília Belt. During the Carboniferous-Early Permian, glacial processes might have contributed to increasing the denudation rates.

- In the Mesozoic, the Gondwanic orogeny ceased, decelerating the tectonic subsidence of the Paraná Basin. The changing arid environment also may have reduced the erosional processes and, as a consequence, the erosional denudation of the basement. The Brasília Belt remained in relative stable conditions from the Mesozoic until the present day as evidenced by our thermal history models.

- Evidence of significant Paleozoic exhumation across the basement of West Gondwana has been progressively revealed through thermochronological studies. It could be interpreted as a regional denudation of the bedrocks induced by the generation of depocenters on the continent during this time. Famatinian and Gondwanic orogenic cycle are pointed as the main responsible for the widespread subsidence, like in the Paraná, Congo and Cape-Karoo basins (Linol et al., 2015; Milani and De Wit, 2008).

- The Brasília Belt is a key region to understand the Pre-Mesozoic tectonic history of West Gondwana, due to the lack of regional reheating events or strong denudation after the Paleozoic. Due to its "protected" position, the basement has retained its Paleozoic exhumation signals.

- Further study using a multi-thermochronological approach is recommended to improve the resolution of the thermal history models.

2.2 – Article II: Differential evolution of cratonic and non-cratonic lithosphere during the Phanerozoic: a case study of the São Francisco Craton and its marginal orogens from a thermochronological perspective, implications for continental reworking

Authors: Ana Carolina Liberal Fonseca[a], Tiago Amâncio Novo[a], Simon Nachtergaele[b], Tobias Fonte-Boa[a], Gerben Van Ranst[b], Johan De Grave[b]

[a]Universidade Federal de Minas Gerais, Programa de Pós-Graduação em Geologia, CPMTC-IGC, Campus Pampulha, Belo Horizonte, MG, Brazil

[b]Department of Geology, Ghent University, Ghent, Belgium

Abstract:

The São Francisco Craton (SFC) and its marginal Araçuaí and Brasília orogens exhibit a significant diversity in their lithospheric architecture. These orogens were shaped during the Neoproterozoic–Cambrian amalgamation of West Gondwana. The rigid cratonic lithosphere of the SFC and the relatively weak lithosphere of the Araçuaí Orogen were disrupted during the Cretaceous opening of the South Atlantic Ocean, whereas the Brasília Orogen remained in the continental hinterland. In earlier research, the thermal effects of the Phanerozoic reactivations in the shallow crust of the Araçuaí Orogen have been revealed by low-temperature thermochronology, mainly by apatite fission track (AFT) analysis. However, analyses from the continental interior are scarce. Here we present new AFT data from 43 samples from the Brasília Orogen, the SFC and the Araçuaí Orogen, far from the passive margin of the Atlantic coast (~150 to 800 km). Three main periods of basement exhumation were identified: (i) Paleozoic, recorded both by samples from the SFC and Brasília Orogen; (ii) Aptian to Cenomanian, recorded by samples from the Araçuaí Orogen; and (iii) Late Cretaceous to Paleocene, inferred in samples from all domains. We compare the differential exhumation pattern of the different geotectonic provinces with their lithospheric strengths. We suggest that the SFC likely concentrated the Meso-Cenozoic reactivations in narrow weak zones while the Araçuaí Orogen displayed a far-reaching Meso-Cenozoic deformation. The Brasília Orogen seems to be an example of a stronger orogenic lithosphere, inhibiting reworking, confirmed by our new AFT data. Understanding the role of the lithosphere rigidity may be decisive to comprehend the processes of differential denudation and the tectonic–morphological evolution over Phanerozoic events.

Keywords: Brasília Orogen; Araçuaí Orogen; exhumation; West Gondwana; continental lithosphere rigidity; lithospheric inheritance; apatite fission track thermochronology

1.Introduction

During the evolution of the continental lithosphere, lithospheric strength plays a significant role in controlling the initiation and character of extensional and compressional deformation (Kusznir and Park, 1984). Rifting, reactivations and reworking are mainly concentrated in pieces of weak lithospheres and pre-existing shear zones (Manatschal et al., 2015; Petersen and Schiffer, 2016; Schiffer et al., 2019; Tommasi and Vauchez, 1997). In contrast, rigid and stiff lithosphere, such as characteristic of cratons, is more resilient to be affected by major tectonic events (Artemieva, 2006). Several main factors contribute strongly to lithosphere rigidity: (i) mantle and crust rheology; (ii) geothermal gradient; (iii) crustal thickness; (iv) lower crustal composition; and (v) tectonic inheritance (Kusznir and Park, 1984). Orogenic lithosphere is usually considered favorable for reworking due to its fertile content, high concentration in radiogenic elements, and its mantle anisotropy array. However, Krabbendam, (2001) highlighted how an orogen can produce strong lithosphere and inhibit deformation. The West Gondwana break-up during the Early Cretaceous seems to have followed the structural lineaments of pre-orogenic mountain belts (e.g. Araçuaí Orogen) (Tommasi and Vauchez, 2001; Autin et al., 2013; Reuber and Mann, 2019; Will and Frimmel, 2018). Although the rifting also broke cratonic areas (e.g. the Bahia cratonic bridge of the São Francisco–Congo Craton) whereas it preserved other orogenic belts (e.g. Brasília Orogen).

Low-temperature thermochronology has been used to constrain the reactivations in different tectonic environments (e.g. Fernie et al., 2018; Gillespie et al., 2017; Mackintosh et al., 2019), due to its ability to identify cooling/heating episodes that affected the shallow crust. Episodes of high cooling rates are usually connected to moments of crustal deformation (i.e. uplift and exhumation, flexural bending) that are determined by reaction of the lithosphere to a stress source. In Brazil, several thermochronological studies have been realized on its passive margin portions (e.g. Cogné et al., 2011; Gallagher et al., 1995; Jelinek et al., 2014; Japsen et al., 2012; Van Ranst et al., 2020; Harman et al., 1998), mainly focused on detecting thermal variations during rift and post-rift events that are pointed out as essential in the formation of the coastal relief and landscape along the Brazilian Atlantic coast. The cooling phases identified by the previous works indicate that uplift must have taken place during Meso–Cenozoic times, inducing the erosion and exhumation of the crystalline basement. However, the hinterland response to these tectonic forces is still poorly understood in South America (Pérez-Díaz and Eagles, 2014).

In south-eastern Brazil, the São Francisco Craton (SFC) and its marginal belts are part of the South American Platform, which consists of portions of the Precambrian terrains that escaped the major effects of the Andean orogenies (Almeida et al., 1981, 2000; Brito Neves, 1999). The cratonic area preserves the Archean nucleus and segments of a Paleoproterozoic orogen, both partially covered by Proterozoic sedimentary successions and few Phanerozoic deposits (Heilbron et al., 2017). During the Neoproterozoic until the early Paleozoic, various continental collision-accretion events shaped the preceding paleocontinent throughout the Brasiliano orogenic cycle that eventually resulted in the amalgamation of West Gondwana. The portion of the Precambrian basement not involved in deformation triggered by the Brasiliano cycle defines the SFC (Almeida, 1981; Alkmim et al., 1993; Alkmim, 2015). To the west, the Brasília Orogen (Fig.1) was assembled in the course of the closure of a wide ocean during the subduction of distal units, tectonic accretion events and associated nappe exhumation (Valeriano, 2017). It was stabilized relatively early (600-560 Ma) when compared with the other orogenic fronts that surrounded the SFC and afterwards it remained confined in the hinterland of continental blocks, i.e. West Gondwana and South America continents (Pimentel, 2016). To the east of the SFC, the Araçuaí-West Congo (AWCO) Orogen (Fig.1) was formed due to the closure of a fairly narrow ocean branch during the onset of the Neoproterozoic up to the Cambrian–Ordovician boundary (Pedrosa-Soares et al., 2008). The AWCO was disrupted and split into two counterparts with the incipient opening of the South Atlantic Ocean. It currently composes a segment of the Brazilian and Congo passive margin.

As the SFC and its marginal belts are composed of a representative diversity of lithosphere architectures, understanding of their thermal evolution after the Phanerozoic stabilization can clarify the role of the lithospheric strength in their exhumation history. Moreover, the Phanerozoic thermal evolution of the SFC hinterland domains and the Brasília Orogen still remains poorly constrained by low temperature thermochronometry. In this study we present the results of apatite fission track (AFT) thermochronometry applied to forty-three samples collected in three transects crossing the structural fabric of the Araçuaí Orogen, SFC and Brasília Orogen. We aim to constrain the exhumation phases of each terrain, investigating the possible relationships of cooling/heating episodes to geodynamic processes and their surface expressions. From these, we can evaluate if there is a differential exhumation pattern between the terrains and if it is related to the lithospheric characteristics of each tectonic province.

2. Geological Setting

The study area comprises the SFC and two of its marginal orogenic belts, i.e. the Araçuaí and Brasília orogens, which surrounded and shaped the craton during the Ediacaran – Cambrian. In the east and west side of the craton, the belt is composed of the Mantiqueira and Tocantins tectonic provinces, respectively (Fig. 1) (Almeida et al., 1981; Brito Neves et al., 2014). To the north, the SFC constitutes a segment of the Brazilian passive margin that is correlated to the Congo Craton in Africa (Fig. 1). These two cratonic domains were connected by a cratonic bridge, the Bahia cratonic bridge, forming the larger São Francisco–Congo Craton (Fig. 1) (Porada, 1989) before Pangea (including West Gondwana) break-up in the Early Cretaceous.

2.1. São Francisco Craton and its adjacent orogenic belts

In the Brazilian counterpart of the São Francisco–Congo Craton, the definition of the boundaries between the SFC and its margin was subject of intense debate since the middle of the 20th century (Almeida,1967, 1969, 1977; Cordani et al. 1968; Cordani 1973; Ebert, 1968; Trompette et al., 1992). This debate also reflected another, more fundamental, parallel discussion: what is the precise definition of a craton? Almeida et al., (1981), using the craton definition of a continental crust stabilized before the late Precambrian orogenies (the Brasiliano cycle), established the SFC limits based on geophysical and structural analysis. The tectonic meaning of Almeida's definition was explored by Alkmim et al., (1993) in the light of new data. These authors revealed that the SFC boundaries are defined by major reverse or thrust faults, which represent the transition from domains deformed by thin-skinned (in the craton interior) to thick-skinned tectonics (in the marginal belts) respectively. In addition, Alkmim et al., (1993) observed that these major faults also represent inverted normal faults inherited from the pre-orogenic extensional phase. Thus, in this work we consider the SFC as defined by Almeida et al., (1981), Alkmim et al., (1993) and Alkmim, (2015), i.e. that the craton is discriminated from its margin by the non-involvement of the basement in the Ediacaran – Cambrian Brasiliano deformation.

2.2. (Pre)Cambrian basement

The SFC basement was formed originally by an Archean nucleus, that is represented by TTG-type granitoids as result of granite-greenstone terrains amalgamation (Heilbron et al., 2017; Alkmim, 2004). The Archean nucleus was attached, on its eastern side (present-day co-ordinates), to Paleoproterozoic orogenic segments: The Eastern Bahia Orogenic Domain, the Mineiro Belt, and the so-called Quadrilátero Ferrífero (Iron Quadrangle) mineral province (Fig.1) (Heilbron et al., 2017; Alkmim and Teixeira, 2017; Barbosa and Barbosa, 2017). The

Paleoproterozoic orogenic system and the Archean nucleus are remnants of the São Francisco-Congo paleo-continent. This paleo-continent was affected by anorogenic magmatism and taphrogenic processes which created intracratonic basins and passive-margin sedimentation at the end of Paleoproterozoic (Martins-Neto et al., 2001). During the Ediacaran – Cambrian, several continental collisions affected the São Francisco–Congo Craton and led to the final configuration of West Gondwana with the inversion of the previous extensional rifts. This process resulted in the Brasiliano – Pan-African orogenic systems that are used to delineate the boundaries of the craton. Due to its long and complex tectonic history, as well as the large area covered by Phanerozoic sediments, the SFC's structural framework is still not completely understood. In SE Brazil, the craton is surrounded by three Brasiliano orogenic fronts, the Araçuaí, Ribeira and Brasília orogens (Fig.1) (Almeida, 1977) in which the first two belong to the Mantiqueira Province (MP) and the latter one to the Tocantins Province (TP).

The MP is formed by several Neoproterozoic – Cambrian orogenic systems which represents a large area parallel to the south(east) Brazilian coast (Fig 1-C). In southeastern Brazil, the Araçuaí and Ribeira orogens, as well as transitional zones between the Brasília and Ribeira orogens, are exposed. As mentioned, the Araçuaí Orogen is the Brazilian fragment of the larger AWCO fold-and-thrust belt which was separated from its African counterpart by the Atlantic opening (Hasui et al., 1975a; Almeida, 1977; Trompette et al., 1992; Pedrosa-Soares et al., 2007; Alkmim et al., 2017). The AWCO was formed due to the closure of the Adamastor ocean during the amalgamation of West Gondwana (Heilbron et al., 2008).

The Araçuaí Belt, is located to the southeast of the SFC (Fig.1-D) where it underlies the Brazilian Atlantic margin. To the south of the Araçuaí Belt, around Lat 21°S, it merges with the Ribeira Belt. The Araçuaí Belt encompasses an entire magmatic arc, an ophiolite sliver, syn- and post-collisional magmatic bodies, and a suture zone (Pedrosa-Soares et al., 2008). The regional structural trend diverts from NNE to NE from north to south (Fig.1). The metamorphic grade from exposed units ranges from greenschist to amphibolite facies, with metamorphic peak ages of 600-580 Ma and final collision at 540 to 530 Ma (Alkmim et al., 2017). The orogenic collapse is considered to be related to post-collisional magmatism and a variety of extensional structures and is dated to have occurred at around 530-490 Ma (Pedrosa-Soares et al., 2001, 2008; Marshak et al. 2006). The AWCO has been coined a hot orogen (e.g. Cavalcante et al., 2018; Fossen et al., 2017; Vauchez et al., 2007, 2019; Richter et al., 2016) as it is characterized by high temperatures, slow cooling and the emplacement of large volumes of magma (Fossen et al., 2017; Vauchez et al., 2007, 2019).
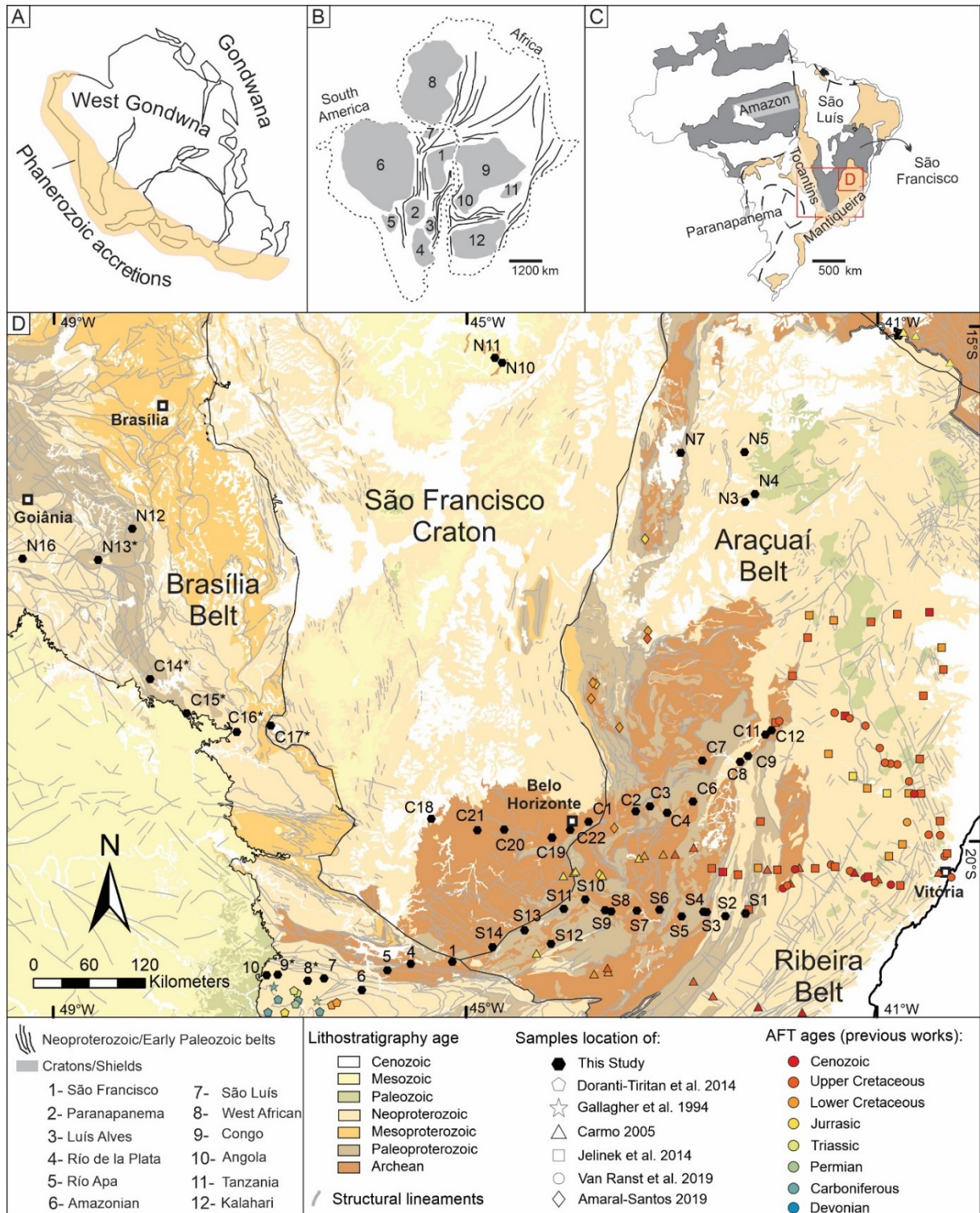
Fig.1 – Geological context of the study area. A) Gondwana Supercontinent and Phanerozoic accretions (after Almeida et al., 1981). B) Schematic representation of West Gondwana basement, with the shields, cratonic continental masses and Neoproterozoic-Late Paleozoic orogenic belts (after Tohver et al., 2006; Vaughan and Pankhurst, 2008). C) Brazilian tectonic provinces (Alkmin, 2015). D) Chronostratigraphic regional map showing the location of analyzed samples with the major structural lineaments and AFT ages from previous works. * indicates samples from Fonseca et al., (SUBMITTED).

On the western side of the SFC, the TP is an orogenic area between the Amazonian and São Francisco cratons (Fig.1-C). It was formed due to the convergence of the Amazonian, São

Francisco-Congo and Paranapanema paleocontinents (Pimentel et al., 2004), that consumed a large oceanic slab (Brito Neves, 1999). The Brasília Belt is one of the three fold belts that belong to the TP. It was developed along the western margin of the São Francisco Craton (Almeida et al., 1981). The fold belt comprises an Archean – Paleoproterozoic basement, which, together with a Proterozoic metasedimentary cover, a juvenile magmatic arc (Goiás arc), and granitic complexes, were folded and thrusted toward the SFC in the Neoproterozoic (Pimentel et al., 2000). In its southern portion, a NW-SE structural trend prevails, while in the southernmost area, the regional trend is overlapped by W-vergent nappes and transitional structures of the Ribeira Belt (Valeriano, 2017). Peak metamorphism is constrained at 650-630 Ma with amphibolite to granulite facies conditions (e.g. Moraes et al., 2002; Piuzana, 2003; Reno et al., 2009; Valeriano et al., 2004). Analysis from medium-temperature thermochronometers (Ar-Ar/K-Ar in biotite and mica) indicates an exhumation and cooling of the Brasília Orogen between 600 to 560 Ma as its orogenic collapse progressed (Hasui and Almeida, 1970; Valeriano et al., 2000, Pimentel et al.,2004).

2.3. Post-Cambrian Evolution and existing thermochronological data

Following the cessation of the Brasiliano orogenic cycle, the West Gondwana continental interior went through a consolidation stage, forming a relatively stable platform during the early Paleozoic (Carneiro et al., 2012; Zálan, 2004). Scarce low-temperature thermochronological data on the SFC and its margins, have revealed a pronounced Paleozoic cooling period in the southern Brasília Orogen (Dorantin-Tiritan et al., 2014; Gallagher et al., 1994; Ribeiro et al., 2005) and in the northeastern SFC (Jelinek et al., 2014; Japsen et al., 2012). These authors tentatively relate the cooling event with far-field effects of the long-lived orogeny at the southern margin of Gondwana, i.e. the Famatian and Gondwanic orogenic cycles (Fig.1, Fig.2: 1 to 4, Jelinek et al., 2014), the deposition of sedimentary sequences in the adjoining Paraná Basin (Fig. 2: 10 to 12, Ribeiro et al., 2005) and widespread Carboniferous glaciation (Doranti-Tiritan et al., 2014).

During the Paleozoic, the Famatian (Early Ordovician to Early Carboniferous) and Gondwanic (Early Carboniferous to middle Permian) orogenic cycles took place in the SW portion of the West Gondwana paleo-continent (Fig.1-A) (Heredia et al., 2018, and references therein) by the docking of continental fragments (collisional type) and by subduction events (non-collisional type). From their analyses of tectonic subsidence curves of the Paraná-Chaco Basin and its sedimentary record, Milani and Ramos, (1998) proposed that these geodynamic cycles were closely related to extensional tectonic subsidence episodes that affected this basin. The

Paleozoic deposits in the Paraná-Chaco Basin preserve marine, fluvial, and coastal sediments, covering a large area (1 500 000 km²) with thicknesses up to 4500 m (Fig. 2: 10 to 12, Milani et al., 2007). The Carboniferous glaciation event is recorded by the Itararé Group in this basin and by striated surfaces in its basement (Fig.2: 12, Buso et al., 2017; Caputo and Crowell, 1985; Eyles et al., 1993; Griffis et al., 2018; Montañez and Poulsen, 2013; Mottin et al., 2018; Visser, 1987). The sedimentary record in the Sanfranciscana Basin of the SFC, initiates with Carboniferous glacial deposits (Santa Fé Group, Fig.2: 17) (Sgarbi et al., 2001; Limarino et al., 2014; Torsvik and Cocks, 2013; Vesely and Assine, 2006; Reis et al., 2017). The Carboniferous glacial period was followed by increasingly arid conditions as reflected in sediments from in the Paleozoic - Mesozoic transition.

During the Mesozoic, the relative stability of the West Gondwana hinterland was disturbed by taphrogenic processes culminating in the complete continental break-up and eventual opening of the South Atlantic Ocean. Preceding the rifting processes, some magmatic events occurred that are mainly well-expressed in the African counterpart. According to Pérez-Diaz and Eagles, (2014), separation started at the latest by 138 Ma in the far south and then it propagated northwards describing a counterclockwise rotation. The onset of the break-up was approximately coeval with the emplacement of the Paraná-Etendeka flood basalts in the Paraná Basin (Fig.2: 15, Hueck et al., 2018). Also, during this time, the Transminas mafic dike swarm (Coelho and Chaves, 2017) intruded the basement of the SFC and the western Araçuaí Orogen (Fig.2: 21, Chaves, 2013; Rosset et al., 2007). Besides this activity, tectonic reactivation and mafic intrusions took place in the Cambrian Colatina Fracture Zone, in the eastern Araçuaí Orogen (Fig.2: 21, Santiago et al., 2019; Mendes, 2017). A reheating effect of these magmatic eventsin the hosting basement has hitherto not been observed (Amaral-Santos et al. 2019; Van Ranst et al. 2020).

Structural inheritance possibly guided the South Atlantic rifting, since it tended to follow the Brasiliano – Pan African structures (e.g. de Wit, et al., 2008; Misra and Mukherjee, 2015; Nemcok, 2016; Tommasi and Vauchez, 2001; Vauchez et al. 1997; Will and Frimmel, 2018). The rheology of the rift-resistant cratonic nucleus led to the development of deep faults and narrow sedimentary basins, in contrast to wide and evaporite-rich basins evolving on the Brasiliano belts (Fig.2, see platform size differences in the map, e.g. Alkmim, 2004; Mohriak et al., 2008). The marginal basins record the tectonic phases of the rifting evolution as syn-rift, transitional and drift phases (Fig. 2 – 21 to 24, e.g. Asmus, 1982). The rifting reached and affected the São Francisco–Congo Craton and AWCO basement at c.a. 120 to 112 Ma (Torsvik

et al., 2009) effectively separating the SFC and Araçuaí Orogen from its African counterparts (Congo craton and West Congo Belt). The uplift and consequential erosion of the rift shoulders are pointed out as the reasons of Early Cretaceous basement cooling inferred by AFT analyses in the Araçuaí Orogen (Jelinek et al., 2014; Van Ranst et al., 2020).

The post-rift evolution is marked by significant volcanic activity, mainly between the Late Cretaceous to Paleogene. In the continental hinterland, series of alkaline intrusions were emplaced in the Alto Paranaíba Arch in the Brasília Orogen (Fig.2: 20, e.g. Riccomini et al., 2005). Several authors suggest a new pulse of sedimentation in the Paraná (Bauru Supersequence, Fig.2: 16, Batezelli, 2017; Milani et al., 2007) and Sanfranciscana Basin (Areado Fm., Fig.2: 18, Campos and Dardenne, 1997; Uhlein et al., 2011) linked to pulses of doming and denudation connected to these intrusions. Offshore Brazil, thre Abrolhos Bank, which forms a remarkable off-shore platform (Fig.2: 19), records a sedimentary-volcanic complex developed during this time (Mohriak and Fainstein, 2012). Furthermore, several seamounts and volcanic islands (e.g. Trindade Island) extend even further eastward, outlining the E-W oriented Vitória-Trindade Chain (Fig.2: 20). Ar/Ar ages of the magmatic rocks in the lineament are 3.90 to 0.25 Ma (Trindade Island; Pires et al., 2016), whereas the majority of the seamounts are lacking age information. The relationship between the Abrolhos Bank and the Vitória-Trindade chain is still unclear as well as the origin of its magmatic activity (e.g. Geraldes et al., 2013, Ernesto et al., 2002).

Late Cretaceous to Paleogene rapid cooling of the regional basement is widely recorded by low-temperature thermochronometry (AFT and U–Th/He) in the Araçuaí Orogen (Carmo, 2005; Jelinek et al., 2014; Van Ranst et al., 2020). The authors interpreted the cooling as the effect of erosion of an uplifted area. This hypothesis is supported by the significant increment of the marginal basin sedimentary thicknesses during this time. Multiple uplift driving forces seem to have acted (e.g. isostasy, basement reactivations and mantle drag), however the distinct role of each one is still unclear. Van Ranst et al., (2020) suggest the influence of a thermal anomaly possible related to the hypothetical Trindade mantle plume and the offshore magmatism (Thompson et al., 1998) which may have weakened the lower crust, and hence making it more susceptible to basement reactivations due to far-field stresses. The stresses may have been triggered by a complex interaction of forces that compress the South American Plate between the Andean collision zone and the ridge-push of the Atlantic Ocean spreading zone. The authors highlighted the synchronism between this Araçuaí Orogen denudation phase and the Peruvian stage of the Andean orogeny (Fig.2- 6) and thus they proposed this collision stage as the main

source of lithospheric stress. Jelinek et al., (2014) also emphasize the role of crustal weakening by mantle heating but pointed at isostasy as main uplift process.
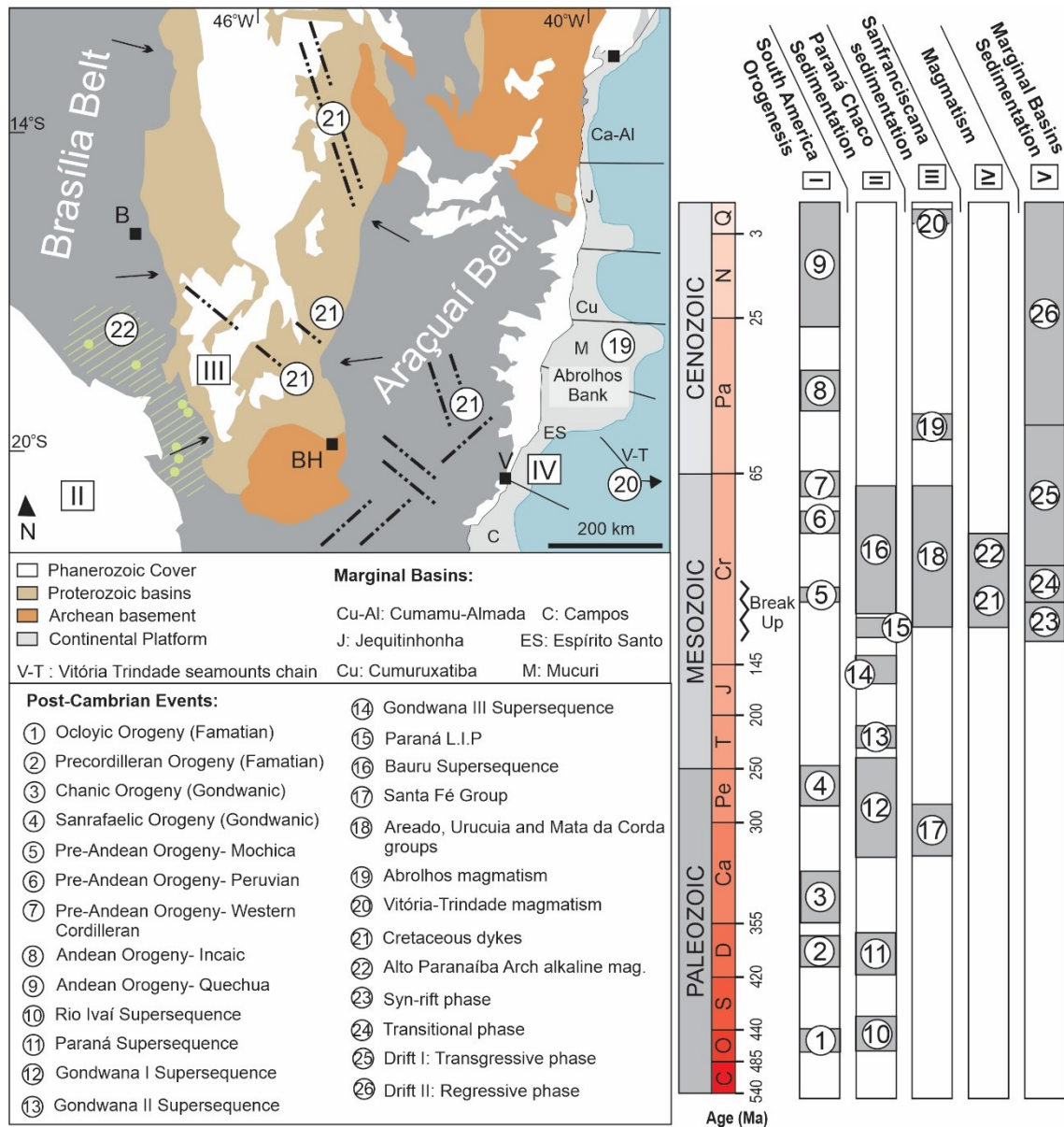

Fig.2 –Main post-Cambrian tectonic, sedimentary and volcanic events (after Zalán, 2004).

3. Samples and Method

In order to investigate the Phanerozoic thermochronological evolution of the SFC and its surrounded mobile belts, this study applied the AFT method on the Precambrian–Cambrian basement. Forty-three samples of granites and gneisses were collected following three approximately E–W oriented transects: S(outh), C(entral) and N(orth) (Fig.1-D). These transects were selected to cross the structural fabric established during the Brasiliano orogeny cycle, and cover the three tectonic provinces (SFC, TP and MP) where only few data, if any,

were previously acquired (Fig.1-D). A lower sampling resolution of basement outcrops in the SFC is due to the extensive Phanerozoic cover which reduces the amount of possible sampling sites. Twenty-four samples are from the Araçuaí Orogen (MP), twelve samples from the SFC and seven samples are from the Brasília Orogen (TP). Details of the lithology, elevation and geographical locations of each sample are provided in Table 1. Apatite grains were concentrated by conventional crushing and magnetic and heavy liquid separation in Centro de Pesquisas professor Manoel Teixeira da Costa (CPMTC), Belo Horizonte (Brazil).

Apatite fission track (AFT) thermochronology is based on the fission decay of ^{238}U and the consequential production of linear damage trails (fission tracks), produced by the ionized fission fragments along their path through the apatite lattice. At low temperatures, these tracks are considered thermally stable on geological time scales, whereas from certain temperatures, diffusion causes shortening and annealing of the tracks until they completely disappear (e.g. Green et al., 1986; Gleadow et al., 1986). The temperature at which the track anneals is affected by many factors such as the detector (mineral, in our case apatite), cooling rate and grain chemistry (Barbarand et al., 2003; Carlson et al., 1999; Green et al., 1986; Tagami et al., 1998). In the mineral apatite fission tracks are retained at temperatures below ~ 60 °C and rapidly anneal in temperatures elevating ~120 °C (e.g. Wagner and Van den haute, 1992). Through the transitional zone between these two conventional thresholds (~60 to ~120 °C), i.e. the apatite partial annealing zone (APAZ) (e.g. Wagner and Van den haute, 1992; Green et al., 1986; Gleadow et al., 1986), tracks can accumulate, but are gradually shortened and eventually removed after prolonged times. Roughly, it can be stated that the AFT age records the time when a sample last cooled through the ~100ºC isotherm (about 2–4 km in crustal depth, depending on the regional geothermal gradient) (Wagner and Van den haute, 1992). Moreover, the track-length analysis provides additional information about the rate and complexity of the cooling or heating path (Gleadow et al., 1986). AFT data can be modelled using empirical annealing equations (e.g. Ketcham et al., 2007a) by inverse modelling (Ketcham, 2005; Gallagher, 2012) to generate a proposed time–temperature path and display a visually comprehensive thermal history.

For this study we applied the AFT external detector method (Hurford and Green, 1982; Fleisher et al., 1975) based on the standard procedures used at the fission track laboratory at Ghent University (described by e.g. De Pelsmaeker et al., 2015; Nachtergaele et al., 2019; Van Ranst et al., 2020). Grains (150–250 per sample) were hand-picked and mounted in Struers CaldoFix-2 epoxy resin, after which they were grinded on SiC paper and polished using diamond

suspension (6 µm, 3 µm and 1 µm). Apatite mounts were etched in 5.5 mol/L HNO^3 solution during 20 s at 21 °C (Donelick, 1991) in order to make the spontaneous fission tracks detectable with optical microscopy. Thermal neutron irradiation was carried out at the Belgian Nuclear Research Centre (SCK, Mol) using the Belgian Reactor 1 (BR1) facility (Channel X26; De Grave et al., 2010). Age standards (Durango and Fish Canyon Tuff) were included in the irradiation package for zeta-calibration (Hurford and Green, 1983). Thermal neutron fluence was monitored by four IRMM-540 dosimeter glasses (De Corte et al., 1998), which were regularly spread over the package. Induced fission tracks were revealed in the irradiated external detectors (ED) (Goodfellow low-U muscovite) using 40 % HF for 40 min at 21 °C.

Age calculations were performed using the overall weighted mean zeta (OWMZ). The majority of the samples were analyzed by one analyst ($\zeta = 313.9 \pm 5.8$, AF) using the Leica DM 2500P microscope equipped with a Leica DFC 295 camera. Using a different microscope and optical set-up, samples S1, S3, S11 and S13 were analyzed by TN ($\zeta = 254.6 \pm 8.8$) and samples 5, 10, C3, S4 and S14 by SN ($\zeta = 286.2 \pm 4.7$), both under the motorized Nikon Eclipse Ni-E microscope with a Nikon DS-Ri2 camera attachment (Van Ranst et al., submitted). To assess the track density, we aimed to count tracks in at least 20 grains for each sample. Central ages and Chi-squared (χ^2) homogeneity test parameters (Galbraith, 2005, 1981; Galbraith and Laslett, 1993) were calculated using "IsoplotR" software (Vermeesch, 2018) and are reported in Table 2.

The length–frequency distributions were acquired by ideally measuring 100 (sub)horizontal confined tracks in each sample. All track lengths and the angles between the track and the crystallographic c-axis were measured with the Nikon Eclipse Ni-E microscope with a DS-Ri2 camera attached at a 1000x magnification. The etch pit diameter parallel to the crystallographic c-axis (Dpar) (Donelick et al., 1999) was measured (100–200 per sample) using a the Dpar module within Nikon NIS-Elements AR (Van Ranst et al., submitted). Data from samples with a sufficient number of track lengths (> 50) were used as input in the QTQt software (Gallagher, 2012) to perform the Markov Chain Monte Carlo (MCMC) inverse modeling with 10^5 pre- and post-burn in iterations. We opted not to use c-axis projection because the anisotropy of our samples is anomalously low, causing c-axis projection to 'overcorrect' and invert anisotropy. (Van Ranst et al. 2020). The present-day temperature was constrained as (25 ± 15) °C. The prior for the MCMC run was set to the (central age ± central age) for time and, (70 ± 70) °C for temperature.

Table.1. Samples location (in World Geodetic System -WGS84), elevation above sea level (a.s.l.), lithology, and tectonic provinces (AB – Araçuaí Belt, SFC. – São Francisco Craton, BB – Brasília Belt). * indicates samples from Fonseca et al., (SUBMITTED).

Sample	X (°)	Y (°)	Elevation (a.s.l) (m)	Lithology	Province
S1	-42.2768	-20.7010	718	banded granulite gneiss	AB
S2	-42.4713	-20.7285	1192	medium grained pyroxene granite	AB
S3	-42.6509	-20.6900	651	medium grained pyroxene granite	AB
S4	-42.6844	-20.6869	614	biotite gneiss	AB
S5	-42.8959	-20.7306	619	medium grained biotite gneiss	AB
S6	-43.1099	-20.6665	615	fine grained biotite gneiss	AB
S7	-43.3320	-20.6757	663	medium grained biotite gneiss	AB
S8	-43.5802	-20.6839	722	fine grained biotite gneiss	AB
S9	-43.6389	-20.6725	738	fine grained biotite gneiss	AB
S10	-43.8328	-20.5669	926	coarse grained biotite granite	AB
S12	-44.1654	-20.9957	1084	medium grained biotite granite	AB
C2	-43.3416	-19.7112	720	coarse grained biotite gneiss	AB
C3	-43.2028	-19.6612	735	biotite granite	AB
C4	-43.0367	-19.7237	558	coarse grained biotite gneiss	AB
C6	-42.7839	-19.6174	262	folded and sheared biotite gneiss	AB
C7	-42.6943	-19.2180	242	biotite gneiss	AB
C8	-42.3276	-19.2300	197	garnet bearing amphibolite	AB
C9	-42.2509	-19.1723	208	fine grained biotite gneiss	AB
C11	-42.0818	-18.9656	177	fine grained biotite gneiss	AB
C12	-42.0225	-18.9231	188	fine grained biotite gneiss	AB
N3	-42.2801	-16.7072	557	tourmaline bearing pegmatite	AB
N4	-42.1826	-16.6299	310	biotite granite	AB
N5	-42.2846	-16.2219	445	metagreywacke	AB
N7	-42.9033	-16.2274	832	gneiss	AB
S11	-44.0412	-20.6574	878	fine grained biotite gneiss	SFC
S13	-44.4227	-20.8681	992	medium grained biotite granite	SFC
S14	-44.7343	-21.0270	997	porphyritic basalt	SFC
1	-45.1248	-21.1736	786	migmatite hornblende gneiss	SFC
C1	-43.7991	-19.8133	855	migmatite biotite gneiss	SFC
C22	-43.9794	-19.8901	859	fine grained biotite gneiss	SFC
C19	-44.1580	-19.9635	851	biotite gneiss	SFC
C20	-44.6217	-19.8897	850	biotite granite	SFC
C21	-44.8803	-19.8934	682	fine grained biotite gneiss	SFC
C18	-45.3290	-19.7837	680	biotite bearing migmatite	SFC
N11	-44.7121	-15.3076	620	granite	SFC
N10	-44.6414	-15.3559	602	granite	SFC
4	-45.5288	-21.1933	805	medium grained hornblende granite	BB
5	-45.7551	-21.2543	893	biotite gneiss	BB
6	-46.0035	-21.4468	793	coarse grained pyroxene gneiss	BB
7	-46.3717	-21.3339	883	coarse grained pyroxene gneiss	BB
8*	-46.5302	-21.3558	972	coarse grained pyroxene gneiss	BB
9*	-46.8217	-21.2976	777	coarse grained pyroxene gneiss	BB
10	-46.9280	-21.3034	791	granite	BB
C17*	-46.8887	-18.8789	1061	metaconglomerate	BB
C16*	-47.2202	-18.9419	884	biotite granite	BB
C15*	-47.7057	-18.7589	856	biotite granite	BB
C14*	-48.0631	-18.4268	577	biotite bearing migmatite	BB
N12	-48.2356	-16.9667	898	garnet bearing gneiss	BB
N13*	-48.5663	-17.2695	758	mylonitic granite	BB
N16	-49.3007	-17.2581	631	mylonitic granite	BB

4. Results

We present a new AFT dataset, which is summarized in Table 2, of 43 analyzed samples from the Araçuaí Orogen, the SFC, and the Brasília Orogen. AFT central ages and confined track

lengths from twelve analyzed samples are geographically displayed in Fig. 3. Swath elevation profiles (north A–B; central C–D; south E–F) with added samples position and AFT central ages are presented in Fig. 4. Supplementary figures on analytical results (amongst others comparative diagrams showing the differential data of the different terrains studied) are to be found in Appendix A. Samples C3 and S4 failed the Chi-squared test (P(χ^2) < 5 %). Samples C8, C11 and N16 yielded insufficient confined tracks (n < 50) to reconstruct thermal history models.
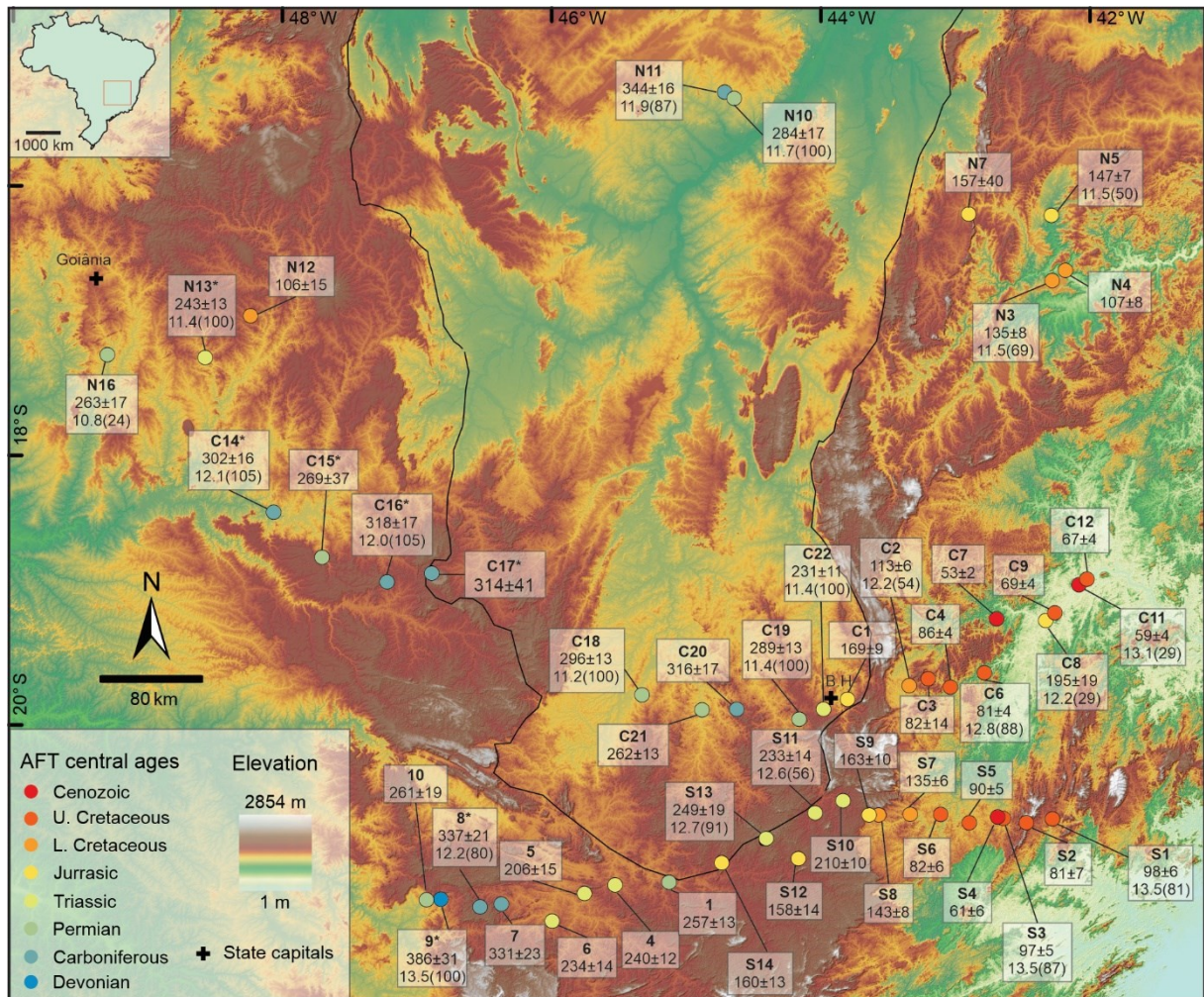

Fig.3 – Digital Elevation Model (DEM) map of the study area with indication of the sample locations, central AFT ages (in Ma), Mean Track Lengths (MTL) (in µm), and number of measured confined track lengths in brackets. For general location see figure 1. * indicates samples from Fonseca et al., (SUBMITTED). BH = Belo Horizonte.
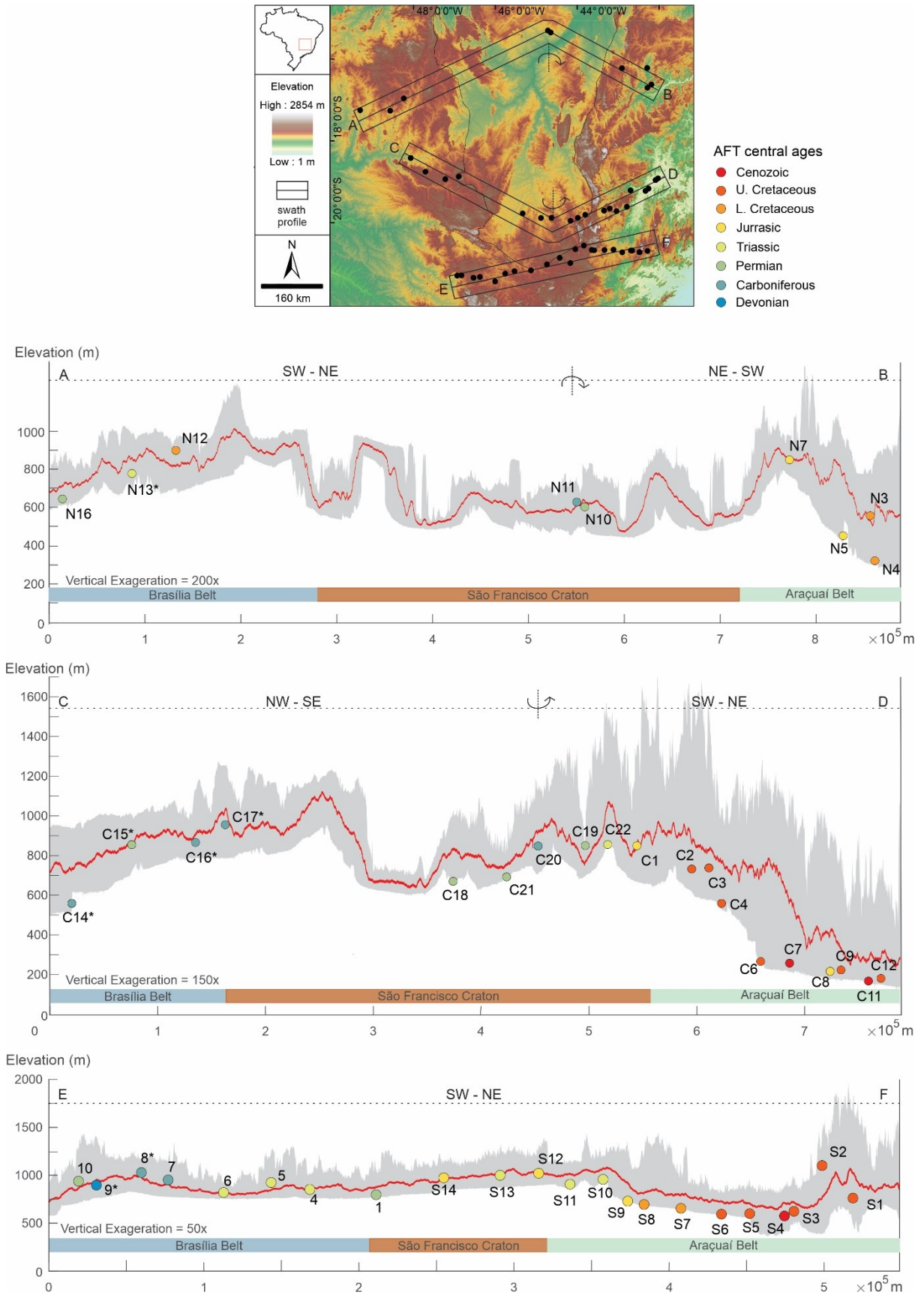
Fig.4 – Swath profile from the three transects: northern (A-B), central (C-D), and southern (E-F). Symbols are color-coded for AFT central age. The red line is the mean elevation profile from the swath profiles. The transition between the tectonic provinces is highlighted. * indicates samples from Fonseca et al., (SUBMITTED).

Table.2. Apatite fission track analysis results; n is the number of analyzed grains. ρ_s and ρ_i are the densities of spontaneous (apatite) and induced tracks (in muscovite external detector), respectively. ρ_d are interpolated values of the density of induced tracks in the external detector irradiated against regularly spaced Uranium-doped glass dosimeters (IRMM-540) in the irradiation package. All densities expressed in 10^5 tracks/cm². Ns and Ni are the number of spontaneous and induced tracks, respectively. N_d is the interpolated value of the number of induced tracks in the external detector stemming from co-irradiated glass dosimeters (IRMM-540). $P(\chi 2)$ is the chi-squared probability that the dated grains have a constant ρ_s/ρ_i ratio. The standard error (s.e.) on the age is given in Ma. Nc is the number of measured confined natural horizontal tracks. MTL is the mean track length, σ is the standard deviation of the track length distribution; A is the analyst (A- Ana Fonseca ζ= 313.9 ± 5.8 a.cm², T- Tiago Novo ζ =254.63±8.81 a.cm², S- Simon Nachtergaele ζ = 286.2 ± 4.7). * indicates samples from Fonseca et al., (SUBMITTED). ** indicates lengths analysis with insufficient measurements to perform inverse thermal history modeling. *** indicates samples that failed in the $P(\chi 2)$ test.

|	Sample	n	ρ_s (±1σ)	N$_s$	ρ_i (±1σ)	N$_i$	ρ_d (±1σ)	N$_d$	P(χ²)	AFT central age (Ma)	1 s.e. (AFT age)	n$_c$	MTL (µm)	σ (MTL) (µm)	Skewness	D$_{par}$	A
ARAÇUAÍ BELT	S1	20	8.051(0.232)	1200	5.859(0.232)	893	5.774(0.075)	5999	0.25	98	6	81	13.5	1.5	-0.6	1.79	T
	S2	11	3.718(0.198)	350	3.455(0.191)	327	4.826(0.098)	2413	0.61	81	7	x	x	x	x	1.69	A
	S3	25	8.512(0.201)	1789	6.338(0.172)	1354	5.716(0.073)	6054	0.43	97	5	87	13.5	1.7	-0.5	1.99	T
	S4***	9	5.691(0.361)	249	5.827(0.361)	261	4.484(0.094)	2255	0.04	61	6	x	x	x	x	x	S
	S5	25	5.464(00.149)	1339	4.498(0.135)	1105	4.750(0.097)	2375	0.18	90	5	x	x	x	x	1.37	A
	S6	22	2.903(0.127)	524	2.580(0.119)	471	4.736(0.097)	2368	0.98	82	6	x	x	x	x	x	A
	S7	20	27.528(0.506)	2963	14.796(0.369)	1606	4.722(0.097)	2361	0.44	135	6	x	x	x	x	1.95	A
	S8	18	3.541(0.211)	281	1.733(0.144)	144	4.708(0.097)	2354	0.97	143	8	x	x	x	x	x	A
	S9	18	22.570(0.696)	1052	9.913(0.457)	470	4.695(0.097)	2347	0.72	163	10	x	x	x	x	1.79	A
	S10	20	34.751(0.704)	2434	12.023(0.416)	836	4.680(0.097)	2340	0.37	210	10	x	x	x	x	1.85	A
	S12	20	7.527(0.303)	616	3.587(0.214)	280	4.650(0.096)	2325	0.12	158	14	x	x	x	x	x	A
	C2	22	8.757(0.244)	1238	5.790(0.201)	831	4.855(0.099)	2427	0.57	113	6	54	12.2	1.6	-0.3	1.74	A
	C3***	16	4.164(0.267)	243	3.160(0.230)	189	4.475(0.095)	2241	0.00	82	14	x	x	x	x	x	S
	C4	20	5.980(0.173)	1196	5.100(0.160)	1020	4.732(0.097)	2366	0.29	86	4	x	x	x	x	1.74	A
	C6	21	14.375(0.263)	2976	13.189(0.252)	2736	4.723(0.097)	2365	0.06	81	4	88	12.8	1.6	-1.1	2.01	A
	C7	21	8.967(0.206)	1888	10.234(0.221)	2154	3.841(0.088)	1920	0.17	53	2	x	x	x	x	x	A
	C8**	8	6.841(0.326)	440	2.536(0.197)	165	4.727(0.097)	2363	0.44	195	19	29**	12.2**	1.5**	0.0	1.71	A
	C9	20	3.508(0.136)	661	3.774(0.142)	709	4.724(0.097)	2362	0.71	69	4	x	x	x	x	1.68	A
	C11**	20	3.872(0.143)	730	4.792(0.159)	905	4.722(0.097)	2361	0.23	59	4	42**	13.1**	1.3**	-0.6	1.83	A
	C12	20	3.592(0.137)	689	3.997(0.145)	762	4.719(0.097)	2360	0.36	67	4	x	x	x	x	2.04	A
	N3	7	31.484(0.912)	1192	16.951(0.670)	642	4.684(0.097)	2342	0.25	135	8	69	11.5	1.8	0.0	1.95	A
	N4	23	3.906(0.149)	687	2.745(0.127)	469	4.681(0.097)	2341	0.09	107	8	x	x	x	x	1.84	A
	N5	23	12.709(0.270)	2214	6.293(0.190)	1093	4.679(0.097)	2340	0.21	147	7	50	11.5	1.9	-0.4	1.78	A
	N7	2	7.016()0.973)	52	3.071(0.627)	24	4.664(0.097)	2332	0.32	157	40	x	x	x	x	x	A
SÃO FRANCISCO CRATON	S11	25	12.780(0.271)	2231	3.920(0.149)	696	5.800(0.074)	6126	0.43	233	14	56	12.6	1.9	-0.3	1.66	T
	S13	21	18.893(0.378)	2500	5.624(0.208)	728	5.795(0.074)	6148	0.12	249	19	91	12.7	1.3	0.3	1.75	T
	S14	20	7.123(0.264)	2018	2.822(0.165)	291	4.514(0.094)	2301	0.77	160	12	x	x	x	x	x	S
	1	23	26.051(0.483)	2908	7.843(0.268)	860	4.954(0.100)	2477	0.22	257	13	x	x	x	x	2.04	A
	C1	25	10.173(0.253)	1615	4.520(0.167)	719	4.870(0.099)	2435	0.53	169	9	x	x	x	x	1.36	A
	C22	20	30.203(0.535)	3191	9.420(0.297)	999	4.687(0.097)	2343	0.26	231	11	x	x	x	x	1.90	A
	C19	22	21.493(0.345)	3881	5.361(0.172)	969	4.694(0.097)	2347	0.34	289	13	100	11.4	1.8	-0.1	1.86	A
	C20	20	25.769(0.438)	3467	5.995(0.214)	785	4.691(0.097)	2346	0.09	316	17	x	x	x	x	1.98	A
	C21	22	17.477(0.304)	3310	4.799(0.160)	904	4.689(0.097)	2344	0.29	262	13	x	x	x	x	1.89	A
	C18	22	28.598(0.363)	6220	7.008(0.179)	1527	4.696(0.097)	2348	0.07	296	13	100	11.2	1.4	0.1	1.98	A
	N11	21	35.810(0.560)	4083	7.523(0.259)	844	4.656(0.097)	2328	0.59	344	16	87	11.9	1.6	0.1	2.02	A
	N10	20	20.383(0.411)	2455	5.054(0.204)	614	4.659(0.097)	2329	0.14	284	17	100	11.7	1.3	-0.2	1.71	A
BRASÍLIA BELT	4	21	25.332(0.529)	2291	7.866(0.292)	726	4.941(0.099)	2470	0.86	240	12	x	x	x	x	2.05	A
	5	20	12.159(0.393)	959	3.659(0.214)	293	4.465(0.095)	2225	0.62	206	15	x	x	x	x	x	S
	6	20	9.860(0.212)	2167	3.205(0.121)	702	4.926(0.099)	2463	0.09	234	14	x	x	x	x	1.67	A
	7	21	12.700(0.355)	1282	2.791(0.164)	291	4.911(0.099)	2456	0.81	331	23	x	x	x	x	1.69	A
	8*	25	15.481(0.308)	2524	3.250 (0.140)	542	5.818(0.075)	5957	0.20	337	21	80	12.2	1.3	0.1	1.50	*
	9*	20	5.780(0.170)	1156	1.070(0.073)	214	5.807(0.075)	5967	0.91	386	31	100	13.5	1.2	-0.4	1.70	*
	10	20	35.992(0.760)	2241	8.844(0.380)	543	4.533(0.094)	2331	0.59	261	19	x	x	x	x	x	S
	C17*	7	14.702(0.798)	340	3.203(0.367)	76	5.769 (0.106)	2940	0.24	314	41	x	x	x	x	x	*
	C16*	20	28.350(0.493)	3302	6.230(0.231)	729	5.766(0.106)	2954	0.36	318	17	105	12.0	1.2	-0.7	1.91	*
	C15*	3	28.298(1.636)	299	7.245(0.820)	78	5.766(0.106)	2954	0.25	269	37	x	x	x	x	x	*
	C14*	20	23.620(0.473)	2491	5.419(0.225)	579	5.764(0.106)	2953	0.48	302	16	105	12.1	1.2	-0.4	1.95	*
	N12	9	4.486(0.382)	138	2.987(0.306)	95	4.654(0.096)	2327	0.48	106	15	x	x	x	x	1.79	A
	N13*	20	30.056(0.679)	2024	9.005(0.370)	592	5.827 (0.107)	2985	0.50	243	13	100	11.4	1.8	0.1	2.07	*
	N16**	23	11.606(0.308)	1423	3.261(0.166)	387	4.646(0.096)	2323	0.23	263	17	24**	10.8**	1.9**	0.3	1.73	A
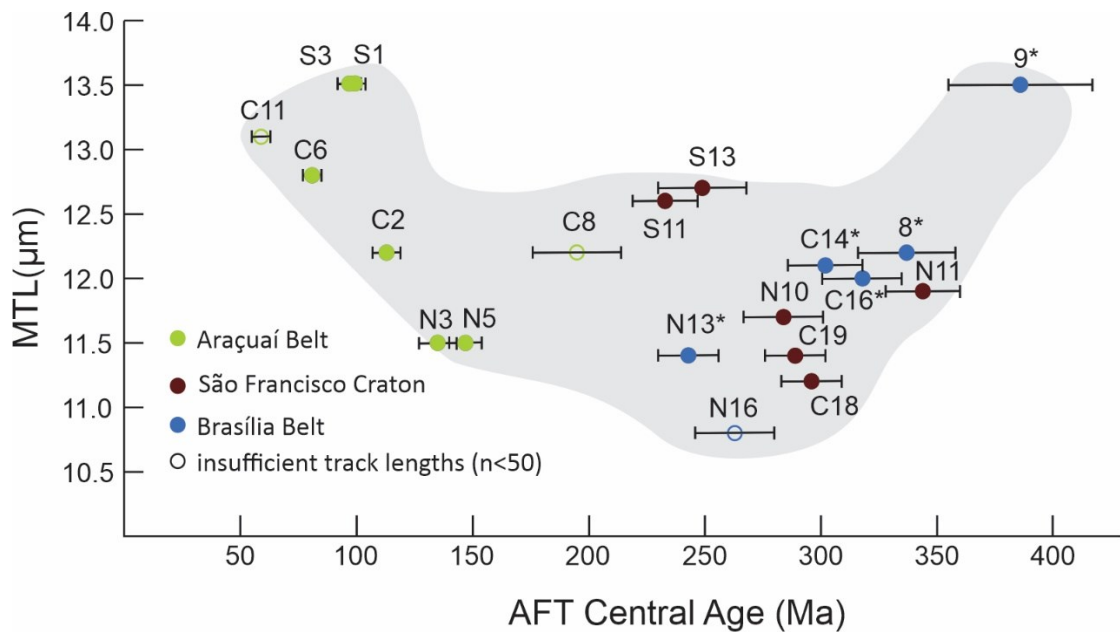
Fig.5 – AFT age vs. MTL or "boomerang" plot (Green et al., 1986) of the Araçuaí Belt, SFC, and Brasília Belt basement samples. See text for details. * indicates samples from Fonseca et al., (SUBMITTED).

Araçuaí Orogen

The twenty-four samples from the Araçuaí Orogen exhibit a wide range of AFT ages, from the late Triassic (210 ± 10 Ma, Sample S10) to the early Paleogene (53 ± 2 Ma, Sample C7). Ages from the Triassic to Early Cretaceous, i.e. pre- to syn-rift, are spatially situated closest to the SFC (samples S10, S8, S7 and C2; Figs. 3, 4) and in the northern transect (samples N3, N4, N5, and N7; Figs. 3, 4). Ages from the Late Cretaceous to early Paleogene, i.e post-rift, are spatially present in samples from the central and southern transects, located closer to the coast (Figure A.1 in Appendix A). On the age–elevation plot (Figure A.2 in Appendix A) the sample set from the Araçuaí Orogen describes a normal trend, in which the older AFT ages tend to be present in the samples collected at higher elevations. Samples C8 and S2 exhibit outlier's behavior, the former being "too old" for its elevation and the latter being "too young". Sample C8 was taken from a river valley at low elevation (197 m) and yields a Jurassic AFT age (195 ± 19 Ma). In the central profile (C–D, Fig.4), it is the only sample with a pre-rift age in close proximity to samples yielding post-rift ages (Figs. 3, 4). Sample S2 is from a site at the highest elevation sampled and gives a Late Cretaceous AFT age (81 ± 7 Ma).

AFT length histograms from the Araçuaí Orogen samples are provided in Figure A.3 in Appendix A. In six samples (S1, S3, C6, C2, N3 and N5) it was possible to measure more than 50 tracks to produce representative length–frequency histograms. Samples from the northern

transect yield the shortest mean track lengths (MTL) (11.5 μm, N3 and N5) and become longer to the south (13.5 μm, S1 and S3). The histograms present a unimodal distribution. Standard deviation varies between 1.5 and 1.9 μm and displays an apparent negative correlation with MTL (Figure A.6 in Appendix A), i.e. the distribution becomes narrower with longer MTL. Skewness values are negative to non-skewed, ranging from -1.1 (Sample C6) to 0.0 (Sample N3), and describe negative correlation with MTL (Figure A.7 in Appendix A), with two outliers (samples S1 and S3). MTL and AFT central ages establish a relationship as the half part of a boomerang trend (Fig. 5, Green et al., 1986). This relationship indicates a fast cooling through the APAZ for samples S1, S3, C11 and C6 (longer MTL), while samples C2, C8, N3 and N5 (shorter MTL) had a protracted residence in the APAZ.

Thermal history modelling was performed for six samples from the Araçuaí Orogen (samples S1, S3, C2, C6, N3 and N5; Figure A.8 in Appendix A). In the southern and central transects, samples S1, S3 and C6 display a similar time–temperature path. For these samples the models show a cooling through the 100 °C isotherm around 120 Ma, followed by a quasi linear, protracted cooling since ca. 110 Ma. Sample C2 displays a residence in the temperature window between ~100 °C to 80 °C between ca. 170 to 140 Ma when it also begins to transfer into a quasi linear, protracted cooling until surface temperature is reached. In the northern transect, samples N3 and N5 show a cooling phase during the Triassic to Early Jurassic (N5 until ca. 200 Ma and N3 until ca. 130 Ma) followed by thermal quiescence (or modest reheating) before a subsequent fast cooling since ca. 50 Ma.

São Francisco Craton

The twelve samples from the SFC exhibit pre-rift AFT central ages ranging from early Carboniferous (344 ± 16 Ma, Sample N11) to Late Jurassic (160 ± 13 Ma, Sample S14). The majority of the samples close to the boundary with the orogenic belts (S11, S13, S14, C1 and C22) present Triassic to Jurassic ages. In the cratonic interior, samples yield ages from Carboniferous to Permian (C18, C21, C20, C19, N10 and N11). These sample were collected from 602 to 997 m elevation above sea level (m.a.s.l.) and their altitudes show no clear relationship with AFT central age (Figure A.2 in Appendix A).

AFT length histograms from the SFC samples are provided in Figure A.4 in Appendix A. In six samples (S11, S13, C18, C19, N10 and N11) it was possible to produce representative length–frequency histograms. Samples from the southern transect display the longest MTL (12.7 and 12.6 μm, samples S13 and S11, respectively) whereas in the others the MTLs range from 11.2

μm (Sample C18) to 11.9 μm (Sample N11). The distributions are unimodal with standard deviations between 1.3 and 1.9 μm, showing no correlation with MTL (Figure A.6 in Appendix A). The histograms are quasi symmetric with skewness varying between -0.3 (Sample S11) to 0.3 (Sample S13). Skewness and MTL describe a negative correlation (Figure A.7 in Appendix A), although one outlier is present (Sample S13). The MTL versus AFT central age plot suggests a half part of a boomerang trend (Fig. 5, Green et al., 1986), however the longest tracks of the SFC samples are relatively short compared to the higher MTLs of the analyzed orogenic belts.

Thermal history modelling was performed on data from six samples from the SFC (samples S11, S13, C18, C19, N10 and N11). Except for the model of sample S11, which predicts a constant slow rate of cooling up to surfaces temperatures since ca. 300 Ma, all samples display a relatively fast cooling during the Paleozoic (N11 until ca. 400 Ma, C18 until ca. 390 Ma N10 and C19 until ca. 350 Ma and S3 until ca. 290 Ma) followed by a long period of thermal stability (60 to 40 °C) in the Mesozoic and afterward a new cooling pulse since ca. 50 Ma.

Brasília Orogen

The majority of the seven samples from Brasília Orogen exhibit AFT ages ranging from the Triassic (206 ± 15 Ma, Sample 5) to the Carboniferous (331 ± 23 Ma, Sample 7). Sample N12 presents a disparate Albian AFT age (106 ± 15 Ma). Even though its grains counting passed in the Chi-squared test (P(χ^2) = 48%), only nine grains could be analyzed. This result thus needs to be regarded with carefulness. The age–elevation plot (Figure A.2 in Appendix A) does not reveal any clear relationship between the variables.

5. Discussion

5.1. Timing and spatial patterns inferred from thermochronology

Low-temperature thermochronology has only seldomly been applied to basement rocks far from the Brazilian coast, thus the majority of our AFT data covers unexplored areas. Our new AFT data can be compared to some other AFT studies (Amaral-Santos et al., 2019; Carmo, 2005; Doranti-Tiritan et al., 2014; Fonseca et al., submitted ; Gallagher et al., 1994; Jelinek et al., 2014; Van Ranst et al., 2020) and apatite (U–Th)/He (AHe) (Van Ranst et al., 2020) from samples from adjacent areas. Our AFT data are in agreement with these previous studies, where they spatially connect. Especially samples from close proximity, such as samples BR-30 and BR-1 from Van Ranst et al. (2020) compared with samples from this study (C12 and S1,

respectively) lie within expected statistical uncertainty. Samples from Fonseca et al., (submitted) complete our dataset on the Brasília Orogen providing additional MTL information (Figure A.5 in Appendix A), and presenting inversion time-temperature models (Figure A.10 in Appendix A), therefore they are combined with our dataset for further discussion.

A clear distinction with respect to the tectonic province can readily be observed in the AFT data set presented here. In general, all AFT central ages range between 386 ± 31 (sample 9) and 59 ± 4 Ma (Sample C11). AFT ages from the Araçuaí Orogen range from 210 ± 10 to 59 ± 4 Ma (Table 2) while ages from the Brasília Orogen and the SFC are generally older, ranging between 386 ± 31 to 160 ± 12 Ma (Table 2) with one outlier (Sample N12, 106 ± 15 Ma). The intermediate ages between these two groups (160 to 210 Ma) predominate in the transition zone between the Araçuaí Orogen and the SFC (Fig. 3 and 4). The relationship between elevation and AFT central age is also distinct. While the Araçuaí Orogen samples show a normal trend, i.e. the older ages at higher elevation, the samples from the Brasília Orogen and the SFC display no clear correlation and suggesting an exhumed APAZ signature (Figure A.6 in Appendix A).

In the AFT samples from the Araçuaí Orogen, the MTL is longer (13.5 μm) in samples with AFT central ages around 95 Ma (sample S1 and S3) and the MTL tends to decrease (with increasing standard deviation) for samples with ages between 110 and 150 Ma (Fig. 5). Hence, it is possible to infer a rapid cooling around 95 Ma (Green et al., 1986). In samples from the Brasília Orogen and the SFC, the longest MTL (13.7 μm) is associated with the oldest AFT age (Sample 9, 386 ± 31 Ma), while younger ages (c.a. 350 to 230 Ma) are derived from samples displaying shorter MTL (12.7–11.2 μm) (Fig. 5). In this case, the fast cooling is associated with a Devonian cooling event and a tail of mixed signatures is showed by samples with AFT ages ranging from Carboniferous to Early Triassic. However, one should be aware of the increased absolute uncertainties on an AFT age when extrapolating further in time and therefore the Devonian basement cooling event is not precisely constrained.

The inverse models also confirm the distinct difference in thermal history between the Araçuaí Orogen and the SFC and Brasília Orogen (Fig. 6). Samples from the latter two display similar time–temperature paths with a fairly rapid cooling between ca. 430 to 350 Ma with a subsequent phase of stability until a last cooling pulse during the Cenozoic. Almost all the modeled samples from Araçuaí Orogen and the SFC had cooled below 70 °C before 250 Ma, and were probably not reheated above this temperature since. In the Araçuaí Orogen, the current surface rocks seem to have cooled through the 100 °C isotherm during the late Mesozoic to the early Cenozoic times, and so therefore the former thermal history is not revealed in the AFT data. The models

suggest the onset of their cooling phase around 120 to 95 Ma, i.e. Aptian to Cenomanian, that indeed is in accordance with their AFT age vs. MTL plot (Fig. 5). Almost all samples describe a modeled late cooling phase that affected all the provinces. In some cases, this cooling phase is inferred during the Late Cretaceous to Paleocene and in others during the Neogene.
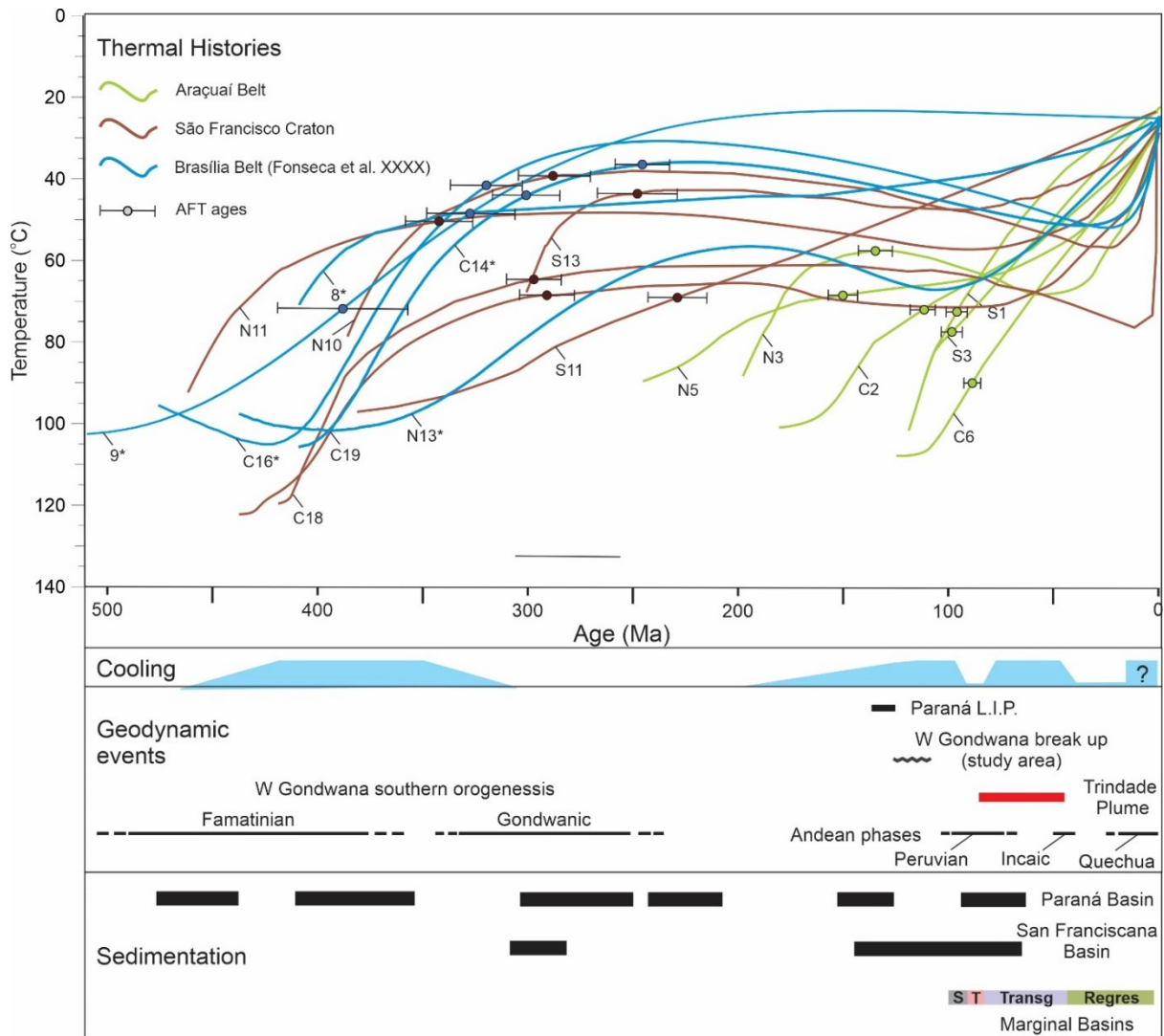

Fig.6 – Summary figure from thermochronology and geological events. Expected t-T paths from models obtained by QTQt (Gallagher, 2012) (see individual thermal history data in Appendix A.8-9-10). Periods of cooling interpreted from the thermal history, geodynamic events and sedimentation events during the Phanerozoic (after Zalán, 2004 and Milani et al., 2007) are added. S = syn-rift and T= transitional phases in the marginal basins.

5.2 Meaning of the cooling phases and depth of exhumation

Paleozoic

A Paleozoic cooling phase is revealed through the thermochronometry and thermal history modelling of samples from the Brasília Orogen and the SFC. The main cooling was constrained between ca. 430 and 350 Ma (Fig. 6) by the inverse modeling (expected model) and corroborated by the relatively high mean track length (MTL) values from sample 9 with a

Devonian AFT age. The cooling phase is however poorly constrained since limited suitable basement outcrops and samples are available and only just one sample (sample 9) yields the long MTL signal. In addition, the absolute uncertainty increases for older ages. Previous AFT data have also revealed a Paleozoic cooling period in the southern Brasília Orogen (Dorantin-Tiritan et al., 2014; Fonseca et al., submitted, Gallagher et al., 1994; Ribeiro et al., 2005) and in the north-eastern SFC (Jelinek et al., 2014; Japsen et al., 2012). Fonseca et al., submitted suggest a close connection between the tectonic subsidence of the Paraná Basin and the coeval cooling of the Brasília Orogen. This is interpreted as a result of exhumation after possible reactivation and basement denudation, in its turn triggered by the tectonic extension during the rifting processes.

In the interior of West Gondwana, the Paleozoic mars the final consolidation of the supercontinent and the collapse of the Brasiliano orogens. The latter was accompanied by the formation of several intracratonic depocenters. The collapse of the Brasília Orogen specifically is constrained by medium-temperature thermochronometers as to have occurred between 600 to 560 Ma (Hasui and Almeida, 1970; Valeriano et al., 2000, Pimentel et al., 2004). Hence this implies termination of the main orogenic activity followed by the relaxation of the upwardly compressed isotherms. Dunlap, (2000) estimates an initial cooling rate driven by isothermal relaxation in excess of 30 °C/Ma using thermomechanical models. Therefore, this initial cooling effect only lasts for about 10 to 20 Ma and thus does not fully explain the reported cooling phase as constrained by our AFT data.

Furthermore, the Brasília Orogen is not the only domain exhibiting this Paleozoic cooling. As mentioned, this signal extends into the SFC and is spread across sampling profiles as far apart as 800 km and hence implies large, regional mechanisms. We suggest that the interplay between intraplate tectonic readjustments followed by erosional processes led to the basement cooling, i.e. Brasília Orogen and SFC. During the Paleozoic both sampled areas were paleohighs that were subjected to erosion, which produced sediments transported to and deposited in the adjacent depocenters of the Paraná and Sanfranciscana basins. Provenance studies of the Paleozoic sediments of the Paraná Basin using paleocurrent data (Alessandretti et al., 2016; Assine, 1999; Assine et al., 1998; Gesicki et al., 2002; Lobato and Borghi, 2005; Mottin et al., 2018; Scherer and Lavina, 2006) and U-Pb detrital zircon analysis (Canile et al., 2016) indeed points to these exhumed northern Precambrian batholiths as possible source areas. Therefore, we link the rapid basement cooling to the significant increase in erosion rates during this period (i.e. Silurian to early Carboniferous). The erosional response of an elevated area (such as the

Brasília Orogen and the SFC during the Paleozoic) depends on an intricate set of variables, such as the subsidence of intra-cratonic depocenters, the local climate, the nature of the main erosional process (e.g. fluvial, glacial, arid processes), and base level drop (Braun and Robert, 2005; Dunlap, 2000). The possible individual influences of these processes and their interaction are discussed in section 5.3.

An approximate depth of exhumation can be calculated through the expected model adopting a simplified assumption of a constant geothermal gradient over time. Following the geothermal gradients defined by Vitorello et al., (1980) for the Precambrian Brazilian interior, we adopted the value of 15 ± 5 °C/km, which is expected to be relative stable (e.g. Stüwe et al., 1994). A removal of 7.0 to 3.5 km of the overlying basement rocks is estimated considering the rapid cooling shown in the data of some of the samples, to 5.0 to 2.5 km in the most protracted cooling samples. Uncertainties regarding modeling and geothermal gradient behavior over time is added in these values, therefore they should be carefully interpreted. A possible re-burial and re-heating episode could possibly be missed in this calculation.

Aptian to Cenomanian

An Aptian to Cenomanian (ca. 120 to 95 Ma) cooling phase is inferred by the inverse models from samples in the southern and central transect from the Araçuaí Orogen. Jelinek et al., (2014) also reported this phase in an adjacent area (Fig.1). The authors relate it with a denudational event triggered by the uplift of the rift shoulder, as the Atlantic opening occurred at this time. The role of the erosion is supported by the offshore syn-rift deposits in the offshore basins next to Araçuaí Orogen. The influence of the break-up is clearly relevant for the change of the base levels and drainage patterns (e.g. Gallagher et al., 1994; Van Ranst et al., 2020). The effect of the heat flow within the developing rift system cannot be ruled out (e.g. Brown et al., 1990; Gallagher et al., 1994; Morais Neto et al., 2009; Turner et al., 2008). The effects of the thermal influence decrease rapidly with the distance from the rift axes (Morgan, 1983; Gallagher et al., 1994; Cogné et al., 2011) and as our samples are from at least 150 km from the coast (Figure A.1 in Appendix A), its effect might have been minimal. Therefore, we support the Jelinek et al., (2014) hypothesis of a rift-shoulder-related denudation as the main cause of cooling during the syn-rift phase.

An estimation of the depth of exhumation is determined here based only on the effects of surface processes (i.e. erosion), since geothermal effects may have had little effect as mentioned. A direct constraint on paleo-geothermal gradients collected from vertical sections would improve

the calculation of denudational exhumation (Turner et al., 2008). As this data is hitherto not available, we adopt a simplified assumption of invariable thermal flux during the cooling, following the geothermal gradient estimates of Hamza et al., (2005) on the Brazilian continental margin (25 ± 5 °C/km). Within the constraints of this assumption and using the time–temperature paths predicted on the expected models, the Aptian to Cenomanian cooling corresponds to a removal of ~1.0 km of basement from the Araçuaí Orogen.

Late Cretaceous/Paleocene and Neogene

Our thermal history models display a possible post-rift rapid cooling phase during the Late Cretaceous to Paleocene (samples S13, C2, N3, N5, N11, Figure A.8-9 in Appendix A) or during the Neogene (samples N10, C18, C14, C16, Figure A.9-10 in Appendix A). This final cooling carried the samples from higher temperature conditions to below 65 °C, which is very close to the method's sensitivity. A "recent-cooling" artefact is well-known in numerical inversion of AFT data (e.g. Jonckheere, 2003) and this feature in the models should be rigorously tested against independent geological evidence.

Several previous thermochronological studies, in both the Araçuaí Orogen (Amaral-Santos et al. 2019, Carmo 2005; Jelinek et al. 2014; Van Ranst et al. 2020) and the SFC (Japsen et al., 2012; Jelinek et al., 2014), also revealed a Late Cretaceous to Paleocene cooling. Many samples from this published data present AFT central ages ranging from ca. 80 to 50 Ma with high MTL (> 13.5 μm) and showed narrow standard deviation for the track-length distribution, which means a fairly fast basement cooling between ca. 80 to 50 Ma. Thus, we consider that this cooling period may have taken place in some samples of our study area as well. The contemporaneous increase of sedimentary thickness recorded in the offshore basins (Milani et al., 2007), also corroborates increased sedimentary input and more widespread erosion during the Late Cretaceous to Paleocene (e.g. Jelinek et al., 2014). Based on this, a depth of exhumation of 1.3 to 2.0 km can be calculated considering an average geothermal gradient of 25 ± 5 °C/km (Hamza et al., 2005).

A Neogene cooling phase is discussed by some studies on the Brazilian margin (Japsen et al., 2012; Jelinek et al., 2014; Morais Neto et al., 2009), however it is solely inferred from thermal history models, since none of the samples showed Neogene AFT central ages. The authors highlight that a thick clastic wedge, built out in the offshore basins during this time, is evidence of some erosion and points to significant basement denudation in the source areas. In our data, the Neogene event is displayed by samples far from the coast, where only thin and small

sedimentary deposits are recorded. Therefore, this cooling is most likely a modelling artefact in our study area (e.g. Van Ranst et al., 2020; Dempster and Persano, 2006; Redfield, 2010).

5.3. Driving forces

Paleozoic

As discussed, a Paleozoic denudational cooling phase (Fig. 6) affected at least the SFC (Jelinek et al., 2014; Japsen et al., 2012 at the craton's continental margin) and Brasília Orogen (Fonseca et al., submitted). In the Matiqueira Province (Borba et al., 2002, 2003; Hueck et al., 2019; Machado et al., 2019; Oliveira et al., 2016; Riberio et al., 2005; Souza et al., 2014), Amazonian Craton (Harman et al., 1998) and ancient West Gondwana basement terrains in Africa (Kasanzu, 2017; Kasanzu et al., 2016), a Paleozoic cooling is also reported. The majority of the previous works argued for a far-field mechanism inducing widespread erosion and exhumation of the West Gondwana basement during this time (e.g. Fonseca et al., submitted). It is likely that other portions of the West Gondwana basement have also experienced this cooling phase but it is not recorded by low-temperature thermochronometers due to either posterior resetting by subsequent thermal events, or because more recent exhumation events have removed the overlying basement with this signal, exposing deeper sections of the crust. This may be the case in the Araçuaí Orogen, where the former cooling is not preserved for AFT detection. This hypothesis should be tested by applying other medium-T thermochronometers such as Zircon (U-Th)/He, Zircon Fission Track or apatite U-Pb dating. Among the processes supporting an increase of erosion rates, depocenter subsidence was widespread in West Gondwana during the Paleozoic, since several intracratonic basins (also called "interior cratonic basins" or "intracontinental sags") were generated during this time (Torsvik and Cocks, 2013), invoking base level drop and denudation of adjoining basement highs. For example, near the SFC and Brasília Orogen, the extensive Paraná Basin (Milani and De Wit, 2008; Linol et al., 2015; Zalán et al., 1990) shows high rates of episodic tectonic subsidence between the Ordovician (c.a. 450 Ma) and the Early Triassic (c.a. 240 Ma), which is coeval with the Paleozoic cooling period. As previously mentioned, (section 5.2), provenance studies on Paraná Basin sediments reveal that basement blocks of the SFC and the Brasília Orogen served as important source areas at that time (Alessandretti et al., 2016; Assine, 1999; Assine et al., 1998; Gesicki et al., 2002; Lobato and Borghi, 2005; Mottin et al., 2018; Scherer and Lavina, 2006). Therefore, the Paleozoic cooling of the analyzed basement rocks is likely associated with the basement erosion and sediment influx to the Paraná basin. Three thick sedimentary packages with a total thickness of 4500 m were deposited in the Paraná basin during this time (Milani et al., 2007). In addition,

significant Paleozoic sedimentary sequences are deposited in the Sanfranciscana Basin in the SFC interior as well (Fig. 6).

Although defining the subsidence mechanism of intracontinental sags remains challenging, Milani and Ramos, (1998) showed how the subsidence cycles of the Paraná Basin during the Paleozoic may be connected to the Gondwana geodynamic cycles; mainly to the Famatinian and Gondwanides orogeny (Fig. 6) (Pankhurst et al., 2006). Later, this was extended to the Congo and Cape-Karoo basins due to their similarities in their tectonic subsidence curve and stratigraphic correlation with the Paraná Basin (Milani and de Wit, 2008; Linol et al., 2015). Intraplate subsidence and Phanerozoic basement cooling of Precambrian stable areas (i.e. cratons and ancient orogenic belts) have been indeed linked to the effect of far-field tectonic stress variations (e.g. Kohn and Gleadow, 2019; Pinet, 2018).

The glacial nature of the erosional processes during the Ordovician (e.g. Le Heron et al., 2018; Torsvik and Cocks, 2013) and Carboniferous in West Gondwana may have contributed to increased denudation rates. According to Hallet et al. (1996), glacial erosion can increase the rate with one or two orders of magnitude compared to fluvial processes. A Carboniferous ice cap probably affected our study area, since it is close to the glacial deposits of the Sanfranciscana Basin and Paraná Basin and paleocurrent data indeed point to a northern source area (Eyles et al., 1993; Mottin et al., 2018). However, evidence of Ordovician ice caps is rare in Brazil, even though some authors describe glacial deposits in nearby basins, i.e. Parnaíba Basin.

The transition to the Mesozoic was accompanied by increasing arid conditions and a severe decrease in the tectonic subsidence rate in the Paraná Basin, coincident with the end of the orogenic cycle on the SW portion of Gondwana (Fig.6). The arid environment with shallow base level prevents further deep erosion and leads to very low denudation rates (Bishop, 2007).

Aptian to Cenomanian

The denudation inferred in the syn-rift stage (i.e. Aptian to Cenomanian) must be linked to the stretching and thinning processes in response to the extensional stress field that resulted in the opening of South Atlantic Ocean and subsequent formation of new oceanic basins. Models using kinematic constrains suggest that tectonic processes (e.g. flexure of the continental lithosphere followed by uplift) are the major driving forces on the early evolution of passive margins (Braun and Beaumont, 1989; Weissel and Karner, 1989; Watts, 2012). The uplift of the rift shoulders leads to drainage rearrangements and contribute to increase of the sediment

influx in the offshore basins (Watts, 2012). Thus, the destructive nature of erosion acting in the new structural architecture of the rifted continental margin generated the exhumation through denudational processes. According to Rouby et al. (2013) the flexural rift-shoulder is eroded away within 10 to 20 Myr, which is in agreement with our inferred cooling phase.

The driving mechanism that led to break-up remains controversial. A mantle plume is commonly invoked to explain the South Atlantic continental rupture (e.g. Quirk et al., 2013 and references therein), mainly because it was followed by huge magmatic events (e.g. Paraná-Etendeka L.I.P, with a volume of at least 1 700 000 km3; Frank et al., 2009). However, the original model proposed by Morgan (1971) predicted several phenomena (Campbell, 2007) that the South Atlantic margin fails to show (e.g. Foulger, 2018; Peace et al. 2019; Fromm et al., 2017). Our thermochronological data are insufficient to broadly contribute to this discussion, but brings more insights into the denudation history of the continent's interior. Nevertheless, there is no evidence for regional uplift followed by denudation in the Brasília Orogen preceding the emplacement of the Paraná L.I.P that occurred nearby our study area. A kilometer-scale domal surface uplift is predicted in response to plume-head emplacement at the base of the lithosphere (Campbell, 2007). Nor do we observe reheating effects of the Early Cretaceous volcanic activity in the SFC, i.e. Transminas mafic dike swarm, in our data.

Late Cretaceous - Paleocene

Our data combined with previous studies (e.g. Amaral-Santos, et al. 2019; Cogné et al., 2011, Hueck et al., 2019; Japsen et al., 2012; Jelinek et al., 2014; Krob et al., 2019; Oliveira et al., 2016; Machado et al., 2019; Van Ranst et al., 2020) show a widespread erosional denudation during the Late Cretaceous to Paleocene that is strongly imprinted in some of the segments of the Brazilian Atlantic margin, such as the Borborema Province (e.g. Morais Neto et al., 2009) and Mantiqueira Province (e.g. Van Ranst et al., 2020), but is also inferred in thermal history models for samples far away from the margin (e.g. Amaral-Santos et al., 2019; our results) and in the cratonic coastal region (e.g. Japsen et al., 2012). Thus, the Late Cretaceous to Paleocene cooling phase is widesread in the passive marginal domains as well as in the hinterland, which leads us to suggest that post-rift mechanisms with only local effects could not be the main root cause for the basement cooling.

Numerical modeling by Rouby et al., (2013) demonstrated that post-rift peaks of erosion and sediment accumulation should not be explained only by thermal relaxation and flexural isostasy. A major climate change would be one potential explanation for increasing erosion

rates, nonetheless, the currently available data point to stable climate conditions throughout that period (Bershaw et al, 2010; Garcia et al., 2005; Spier et al., 2006). A forced (tectonic) uplift and variations in drainage organization seems most likely in our case, as already stated by other authors (e.g. Van Ranst et al., 2020; Jelinek et al., 2014). Indeed, in SE Brazil, vertical motions along inherited Precambrian structures (crustal weak zones) are well documented (e.g. Cogné et al., 2012). However, the uplift/subsidence mechanisms that could trigger such rejuvenation of the topography remain poorly understood.

Paleostress analyses (Salomon et al., 2015; Ferrari, 2001) indicate a compressional NE–SW stress field operating in SE Brazil during the Late Cretaceous to Paleocene in a strike-slip regime. The stress system may be a result of the interplay between flexural bending of the margin and the intraplate compressive stress transmitted from the plate boundaries. Even though the former might not be the only cause of the uplift (Salomon et al., 2015), it may attribute to it (Van Ranst et al., 2020). The Atlantic spreading rate seems to have increased somewhat (4 to 5 cm/a) between 90 to 80 Ma to then decrease (5 to 3 cm/a) until 60 Ma (Clark, 2018). Thus, a ridge push force cannot be considered as the main cause of stress. At the convergent western boundary of the South American plate, the Peruvian tectono-orogenic cycle took place just before the denudational exhumation we observe (Fig. 6) and so could lead to the increase the intraplate stress, which could in turn trigger the reactivation of ancient structures resulting in differential uplift and denudation of certain fault blocks. This hypothesis is commonly proposed to explain the compressional events and cooling periods of the Brazilian passive margin (e.g. Cobbold et al., 2001; Cogné et al., 2011, 2012; Karl et al., 2013; Van Ranst et al. 2020) and our data can extend this interpretation to terrains more in the hinterland.

5.4. The influence of tectonic and lithospheric inheritance

The differential exhumation pattern revealed in our AFT analyses allows clustering the samples in two distinct main groups: (1) samples from the SFC and the Brasília Orogen that were exhumed mainly during the Paleozoic with slight exhumation in the Cenozoic; (2) Samples from the Araçuaí Orogen that were mainly exhumed during the Meso-Cenozoic.

A first discriminating characteristic is the distance to the coast. The Araçuaí Orogen is part of the Brazilian passive margin and thus closest to the rift axis and would have been more susceptible to heating and denudation processes caused by the rifting (e.g. rift shoulder uplift/ flexural isostasy). However, in the AFT central age vs. distance to coast plot (Figure A.1 in Appendix A), it is possible to see that between 200 to 300 km away from the margin, there are

several samples from both groups maintaining the characteristics that differentiate them (i.e. older ages in the SFC and Brasília Orogen). Besides, in the light of previous thermochronological data, the cratonic margin (Japsen et al., 2012; Jelinek et al.,2014; Harman et al., 1998) exhibits much more pre-rift AFT central ages than the orogenic margin (Fig.7.A), which seldomly preserves the former cooling but rather displays syn- and post-rift AFT ages. Therefore, we suggest that lithospheric features may be decisive in the manifestation of surface uplift and the denudation and cooling afterwards, at least during the Meso-Cenozoic events.
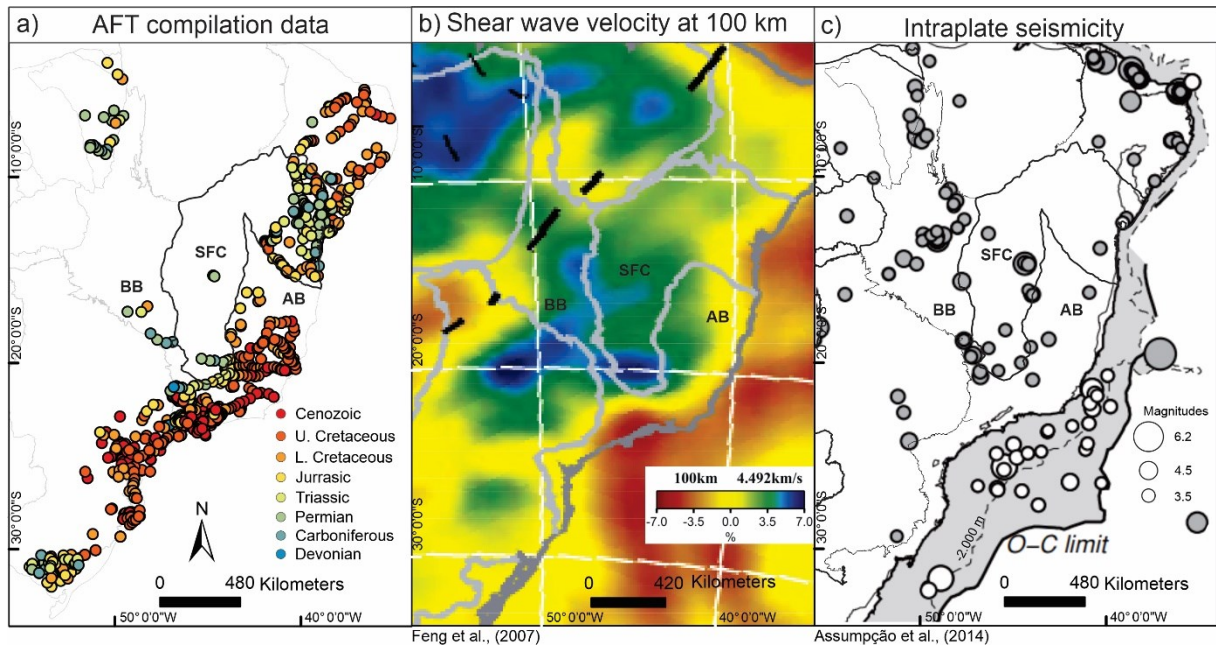
Fig.7 – Eastern Brazil maps. A) AFT ages from this and previous works (after Engelmann de Oliveira and Jelinek, 2017). B) Shear wave (s) velocity at 100 km depth (Feng et al., 2007). C) Intraplate seismicity onshore and offshore (Assumpção et al., 2014).

The Meso-Cenozoic tectonic activity should be mainly partitioned in pre-existing shear zones within the lithosphere, as shown by the parallelism between ancient structural lineaments of the Brasiliano belts and the younger rift systems, e.g. Atlantic Rift and Continental Rift of south-eastern Brazil (Ashby et al. 2010; Tommasi and Vauchez, 2001,2015; Reuber and Mann, 2019; Salomon et al., 2017; de Wit, et al., 2008; Nemcok, 2016). The mobile belts indeed possess several weak zones, such as faults, shear zones, and foliation planes, as well as a higher geothermal gradient (Misra and Mukherjee, 2015; Cloetingh et al., 1995; Rey et al., 2001; Corti et al., 2007). These features generate a warmer and weaker lithosphere compared to the cratonic one. Cratons are characterized by low heat flux, and a dehydrated mantle with refractory composition (e.g. Peslier et al., 2010; Sleep, 2003). Tommasi and Vauchez, (2001, 2015), taking into account these characteristics, suggest that the orogenic mantle provides deep pre-

existing weak zones as well, which play an important role in localizing strain during extension such as in the opening of the South Atlantic Ocean.

Hence, the South Atlantic margin gives a good example of how cratonic and orogenic lithospheres can create different features undergoing the same stress source (e.g. Brune et al., 2014; Buck, 1991; Huismans and Beaumont, 2005). The break-up of the cratonic Bahia bridge between the SFC and the Congo Craton resulted in deep narrow basins (marginal basins and the Recôncavo-Tucano-Jatobá aulacogen), while portions of extended orogenic belts (e.g. Araçuaí Orogen) generated a wider rifting zone (e.g. Mohriak et al., 2008). We earlier suggested the erosion of the rift shoulders as the main cause of the Aptian to Cenomanian cooling phase (section 5.3). It is absent in our in-land cratonic study area and also in some cratonic coastal portions (Jelinek et al., 2014) thus the driven deformation, i.e. flexural uplift, should not have regionally reached the cratonic strong lithosphere. Instead, and more likely, the deformation in the SFC was heterogeneously localized in narrow weak zones (e.g. Recôncavo–Tucano–Jatobá rift) and at the cratonic edges. In contrast, the mobile marginal belts (e.g. Araçuaí, Borborema and Ribeira belts) exhibit widespread Meso-Cenozoic denudational phases indicating far-reaching deformation. Distinct erosion patterns of cratonic rocks versus rocks from the boundary orogenic belts, are reported from the southern Africa Plateau as well, and is thought to stem from the same geodynamic driving force (Stanley et al., 2015).

Although the dichotomy cratonic vs. orogenic lithosphere works to understand the general context, it is too simplistic if we consider the several heterogeneities within one lithosphere or between two cases of the same lithospheric type. Figure 7.B is a tomographic image that displays the S-wave velocity model at 100 km depth (Feng et al., 2007). The higher S-wave velocity terrains are indeed underlain by old and stable cratonic lithosphere, however the tomography model shows that the thickness of the lithosphere is not homogeneous in the SFC and it is higher beneath its southern part (Feng et al., 2007). Surrounding the SFC, the Brasília and Araçuaí orogens present very different lithospheric architectures, which is also illustrated in Fig 7.B. The Brasília Orogen in our study area exhibits significantly faster S-wave velocities than the Araçuaí Orogen, which is interpreted as a deeper-seated extension of the SFC beneath the former orogen (Soares et al. 2006; Feng et al., 2007). In order to better understand the individuality of each region it is necessary to take into account the formation and evolution of the lithosphere over time.

Comparing our data in the SFC, samples nearby the cratonic boundary (samples C1, C22, S11, S13, S14) present the youngest AFT central ages, ranging from Triassic to Jurassic, along with

MTL values that are higher than 12.5 μm. Comparing to the intraplate seismicity analyses of Brazilian earthquakes (Fig.7.C) (compilation of Brazilian Seismic Bulletin and previous works), it is possible to note that the seismicity is more concentrated at the cratonic edges as compared to the inner craton (Assumpção et al., 2013), which is in agreement with observations by Mooney et al., (2012) on a global scale. The latter authors suggest that the increase in the seismic activity can be a consequence of stress concentration in areas with high lateral density variations. The stress concentration might result in more extensive reactivation of the basement, leading to faster exhumation, shorter APAZ residence time and thus the long MTL values observed for samples in the cratonic boundary as compared to the length distributions of the samples of the inner craton.

In the case of an orogenic lithosphere, factors that facilitate reworking or reactivation are well-understood, however many orogenic belts do not show evidence of later tectonic activity in extensive large-scale (Krabbendam, 2001). This could indeed be the case for the Brasília Orogen, since our data show little post-Paleozoic reactivation for samples from that domain. Krabbendam (2001) categorized the Brasília Orogen as "unlikely to be reworked", based on analyses of its stronger orogenic lithosphere. We suggest that the Brasília Orogen is a case of strong orogenic lithosphere capable to inhibit reactivation, at least compared to the weaker Araçuaí Orogen lithosphere. Processes that could lead to the relatively high lithospheric strength include the enrichment of radioactive isotopes in the shallow crust with depletion of the lower crust, dehydration metamorphism, and crustal thinning by erosion (Krabbendam, 2001). These processes are responsible to lower the geothermal gradient and consolidate a higher strength rheology to deeper-seated rocks.

The Brasília Orogen was formed by the closure of the wide Goiás ocean (Brito Neves, 1999; Pimentel, 2016) resulting in the incorporation of high amounts of mafic material and an island arc terrain (Valeriano, 2017 and references therein), which are depleted in radiogenic elements, in its structure. In addition, in our study area, there are many granulitic rocks including mafic granulites (e.g. Moraes et al., 2002; Piuzana et al., 2003) that indicate temperatures exceeding 1000 °C (Del Lama et al., 2000), and have resulted in a high strength dehydrated mineral assemblage. During the metamorphism, the partial melting also contributed to the depletion of incompatible radioactive elements in the lower crust. Finally, the orogenic collapse does not seem to have an evolved extensional phase, neither abundant magmatism (Carvalho et al., 2014), thus the erosion of the top crust may have been the main process of crustal thinning. The removal of the upper crust enriched in radiogenic elements produced an orogen depleted in

radiogenic heat and thereby led to a colder and stronger terrain. Another important feature revealed by the seismicic tomography (Feng et al., 2007) that points to an increased lithospheric stability is the above mentioned deep subcontinental lithospheric mantle in the south of the orogen.

In the Araçuaí Orogen, the samples from the northern transect yield AFT central ages ranging from the Late Cretaceous to the Jurassic and MTL values (11.5 µm) lower than in the central and southern transect (MTL > 12.2 µm). The thermal history models from samples N3 and N5 (Fig.6) reflect these data, showing a slow cooling since the Jurassic, in contrast to the other models from the Araçuaí Orogen that rather infer a fairly fast cooling just after the Early Cretaceous. This could be an effect of the distance to the coast or elevation (see Figure A.1 and A.2 in Appendix A), since these samples follow the normal trends defined by the dataset from this orogen. However, the crustal level exposed in the northern segment of the Araçuaí Orogen (north of 19 °S) is notable shallower than in the south (Alkmim et al., 2017; Pedrosa-Soares et al., 2011), which would mean that this sector was in general less deeply eroded, i.e. went through a slower denudational cooling. The evidence of the exposure of different crustal levels in the north of the orogen include the decrease in the metamorphic grade and the occurrence of shallower portions of the post-orogenic batholiths, i.e. much less mafic components (Almeida et al., 1978; Pedrosa-Soares et al., 1992, 2001,2011; Trompette, 1994; Pedrosa-Soares and Wiedemann-Leonardos).

A widespread sampling for thermochronological analysis in the northern sector of Araçuaí Orogen would cover samples closest to the margin and in a variety of elevations, therefore the influence of these variables could be checked. If a broad protracted cooling were to be revealed such as in our data, we would suggest that the degree of erosion contributes to the preservation of the upper crust in the northern sector. In this case the reactivations responsible to induce the denudational processes to the south would produce slower vertical motion to the north. The rigidity of the northern lithosphere is increased by the proximity to the more rigid cratonic bridge and a lesser amount of extension during the formation of precursor basin of the orogen. The analysis of the structural trend is also relevant, since it inflects to the NE in the north portion making it less parallel to the coastal margin and consequently less favorable to react to extensional forces inflicted by opening of the South Atlantic (e.g. Salomon et al., 2017). Ideally, the contribution of the lithospheric and structural inheritance in this segment of the belt should be clarified in future works.

7. Conclusion

We report the results of AFT thermochronology from forty-three new samples distributed in three transects that run across the São Francisco Craton (SFC) and two adjacent mobile orogenic belts, i.e. the Araçuaí and Brasília belts. Our analyses in combination with published data reveal three main phases of denudation during the Phanerozoic: (i) Paleozoic, recorded by samples from the SFC and Brasília Orogen; (ii) Aptian to Cenomanian, recorded by samples from the Araçuaí Orogen, and (iii) Late Cretaceous to Paleocene, inferred in samples from the SFC as well as from both the Brasília and Araçuaí orogens. We associated the Paleozoic phase with erosion induced by the effect of tectonic extension during the rifting of continental crust in the context of tectonic subsidence of the intracontinental basins, i.e. mainly the Paraná and Sanfranciscana basins. The Aptian to Cenomanian cooling was linked with the uplift induced denudation triggered by the opening of the South Atlantic Ocean during the syn-rift phase. Finally, the widespread post-rift erosional event, i.e. Late Cretaceous to Paleocene, was connected with reactivations prompted by the interplay between flexural bending of the margin and the intraplate compressive stress transmitted from the plate boundaries.

Differential uplift and exhumation in our study area are recorded in our AFT data. While the Araçuaí Orogen samples experienced fairly rapid cooling during Meso-Cenozoic times, the SFC and Brasília Orogen samples exhumed long before, more specifically during the Paleozoic, and remained in relative stable conditions near present outcrop position from the Mesozoic until the present day. We suggest that the lithospheric architecture of the tectonic provinces is deeply connected with deformational response to tectonic stresses. The strong, rigid and cold cratonic lithosphere likely partitioned and concentrated the Meso-Cenozoic reactivations in narrow weak zones (e.g. Recôncavo-Tucano-Jatobá rift) and at the cratonic borders as evidenced also by previous thermochronological studies in the cratonic basement of the Brazilian margin (Jelinek et al., 2014). In contrast, the Araçuaí Orogen displays a widespread Meso-Cenozoic denudational exhumation indicating far-reaching deformation. The Brasília Orogen seems to be an example of a strong orogenic lithosphere, since it remained stable from the early Mesozoic to the present. Therefore, we highlight the importance of inherited lithospheric structures in studies elucidating thermal histories.
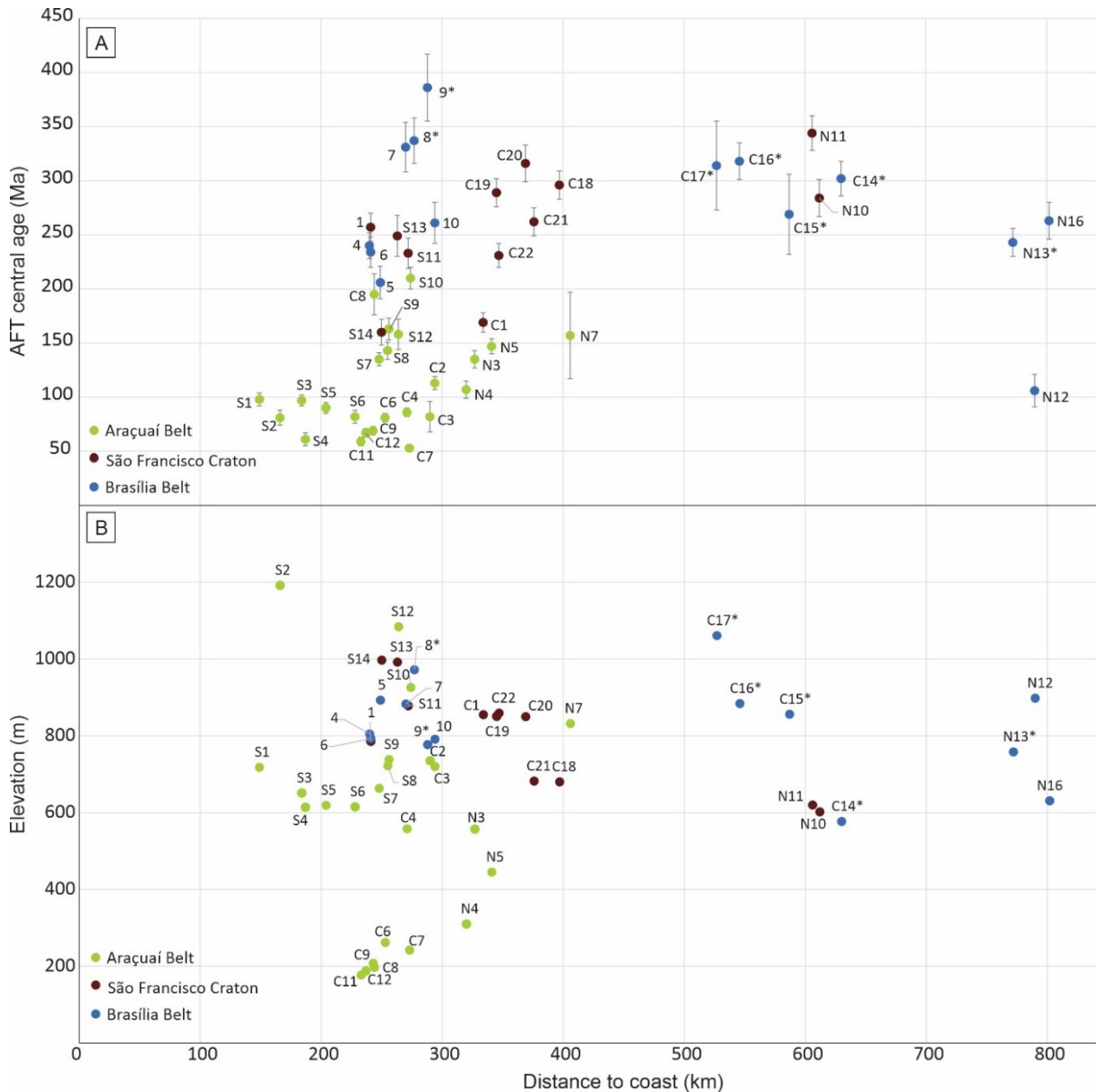
Appendix A supporting images and graphs

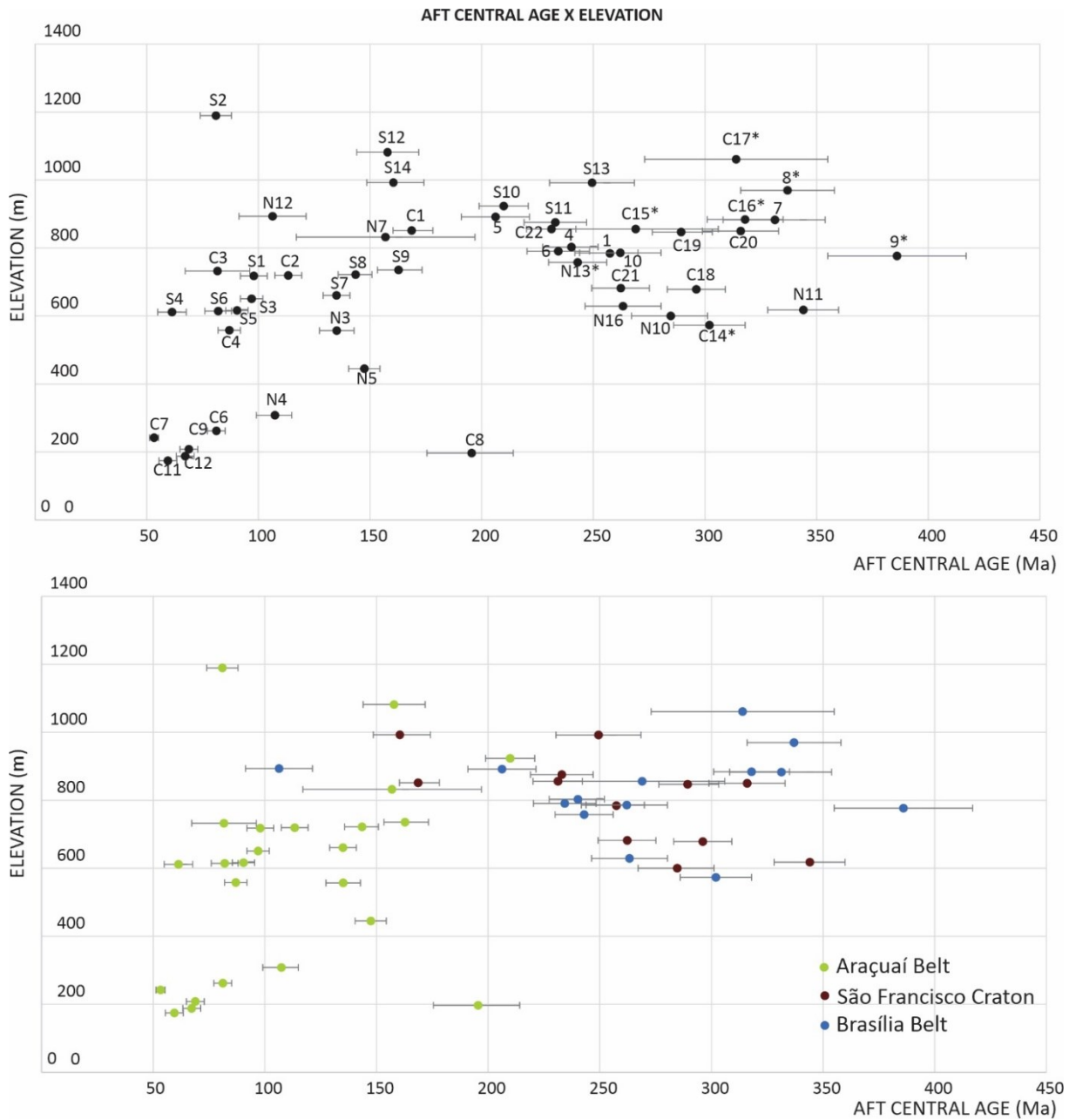Figure A.1. Distance to coast plots. A) vs. AFT central age. B) vs. Elevation.

Figure A.2. Plot of Apatite Fission Track (AFT) central age vs. elevation. A) per sample. B) per tectonic province.
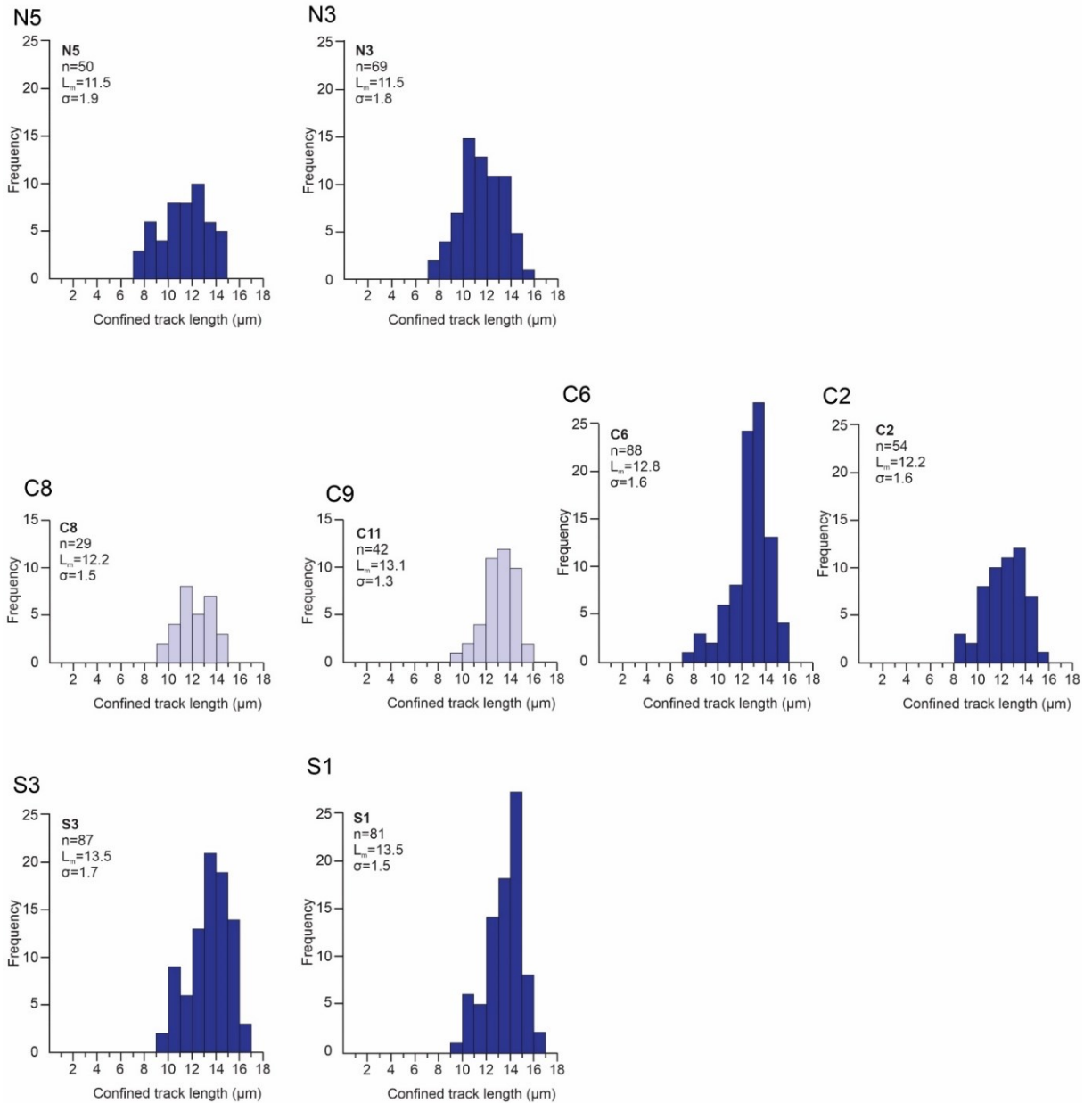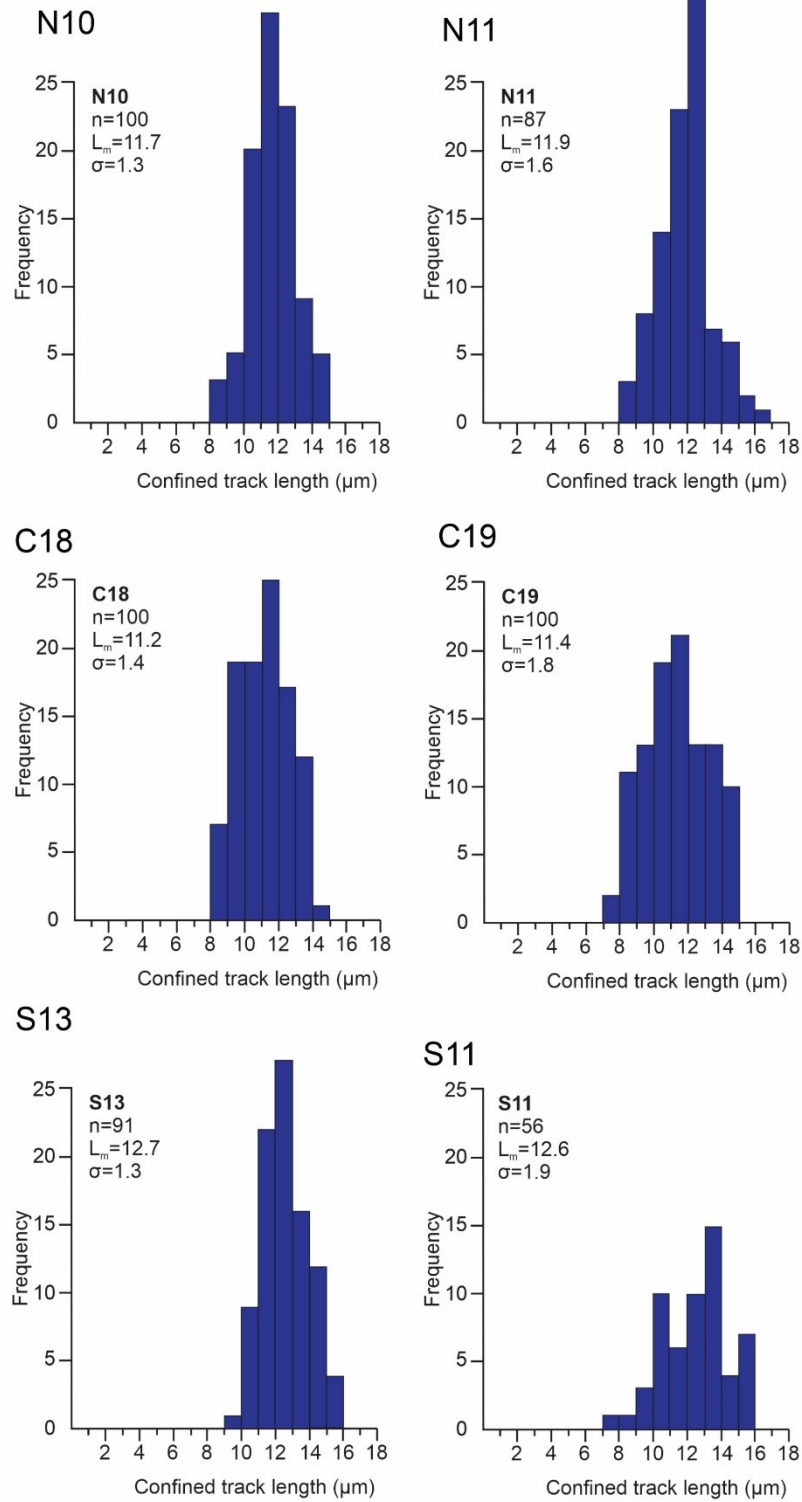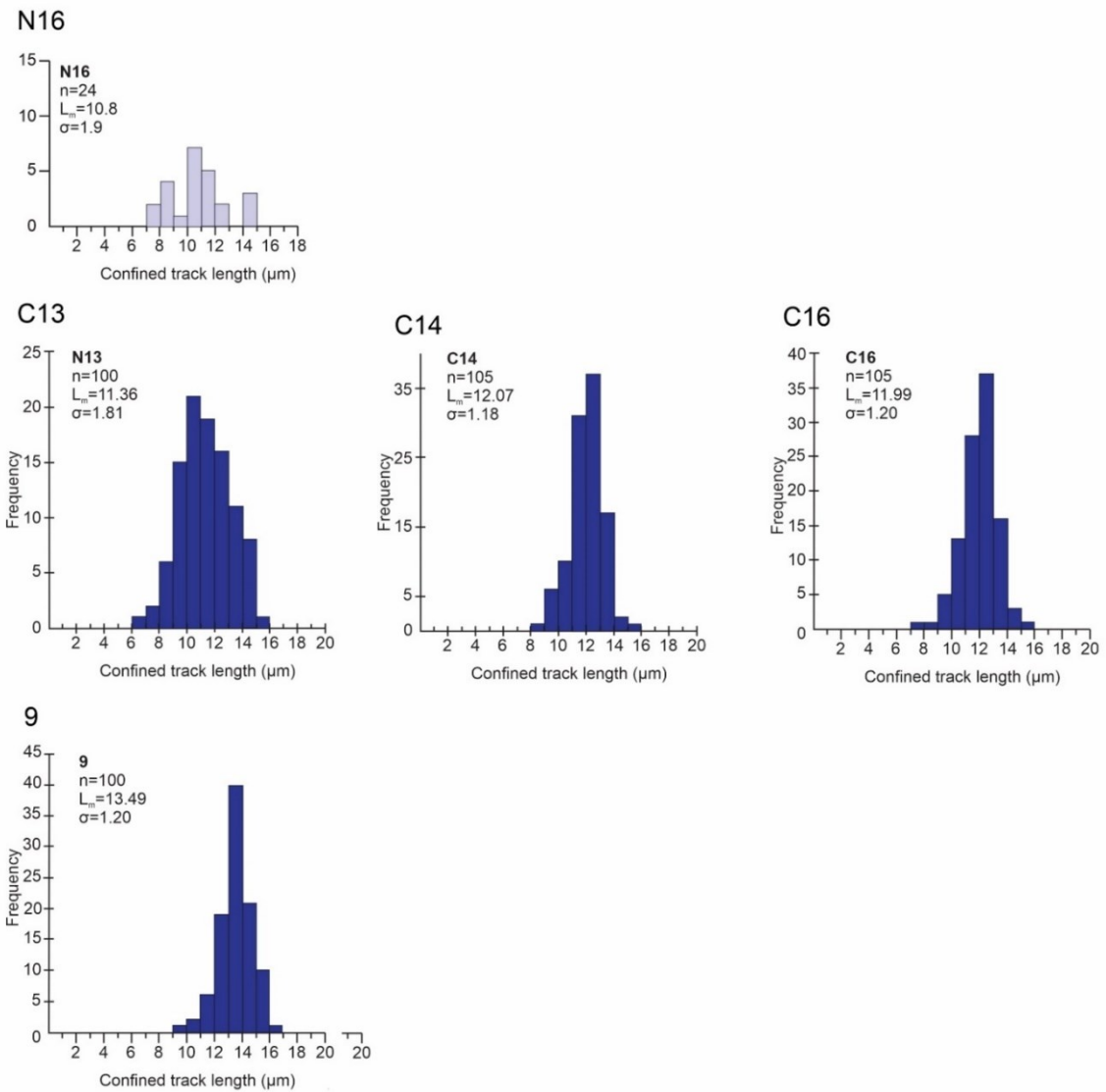
Araçuaí Orogen

Figure A.3. AFT confined track length-frequency distributions from samples of the Araçuaí Orogen (n= number of confined tracks counted; Lm = mean track length (in µm); σ= standard deviation (in µm); light blue histograms indicate insufficient measured lengths to produce a reliable data set).

Figure A.4. AFT confined track length-frequency distributions in samples from the São Francisco Craton (n= number of confined tracks counted; Lm= mean track length (in μm); σ= standard deviation, in μm).

Brasília Belt

Figure A.5. AFT confined track length-frequency distributions in samples from Brasília Belt (n= number of confined tracks counted; L= mean track length; σ= standard deviation; light blue histogram indicate insufficient measured lengths to produce a reliable data).
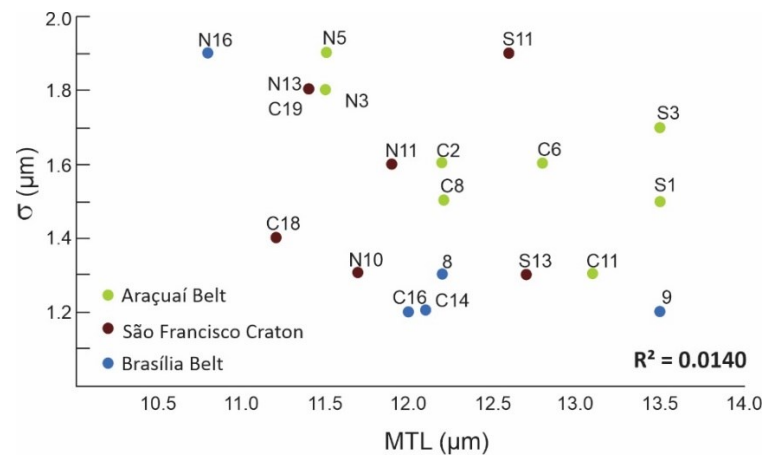
Figure A.6. Plot of mean track length (MTL, μm) vs. standard deviation (σ, in μm).
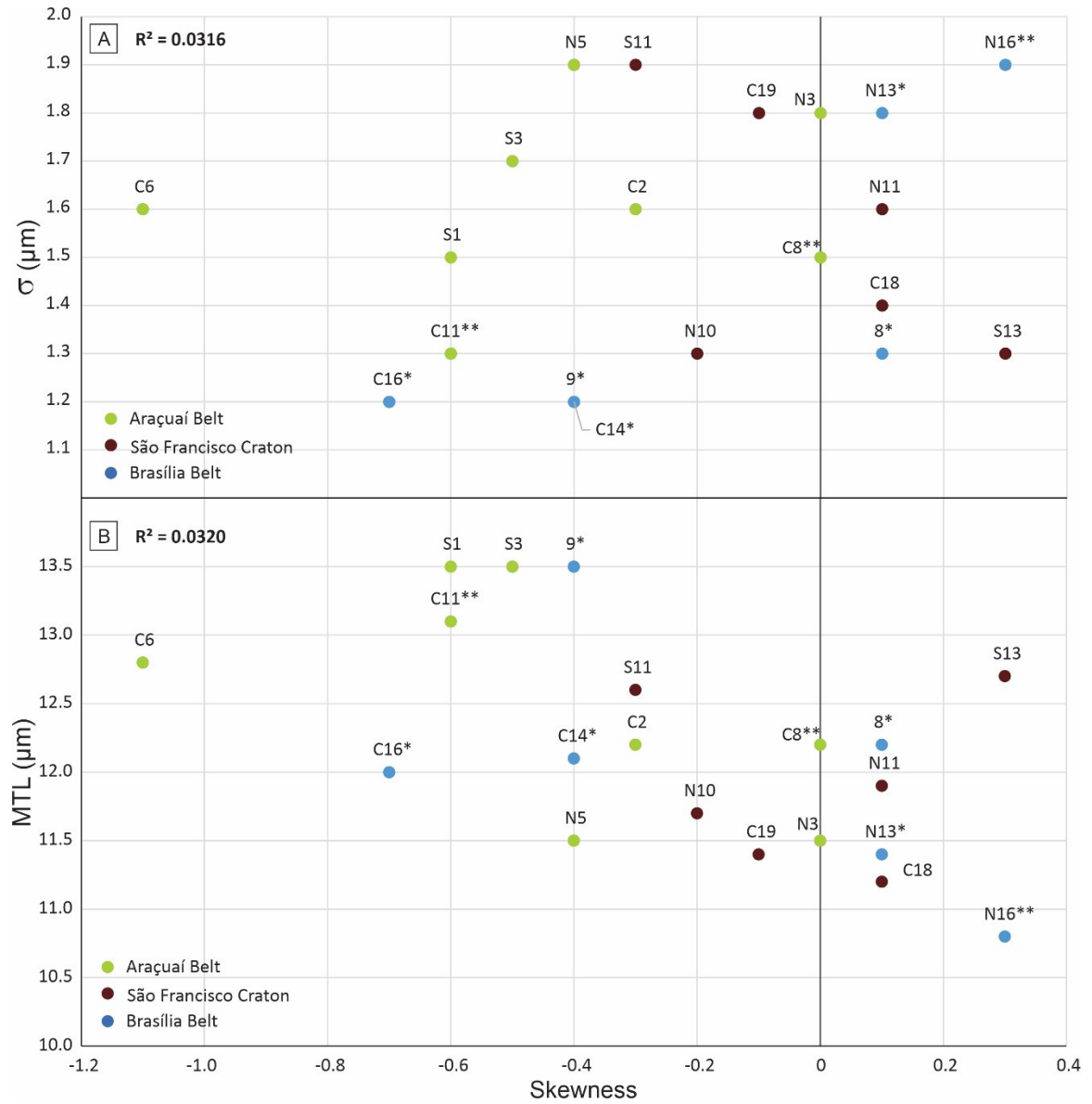
Figure A.7. Skewness plots. A) vs. □ (MTL, in μm). B) vs. MTL.

Araçuaí Orogen
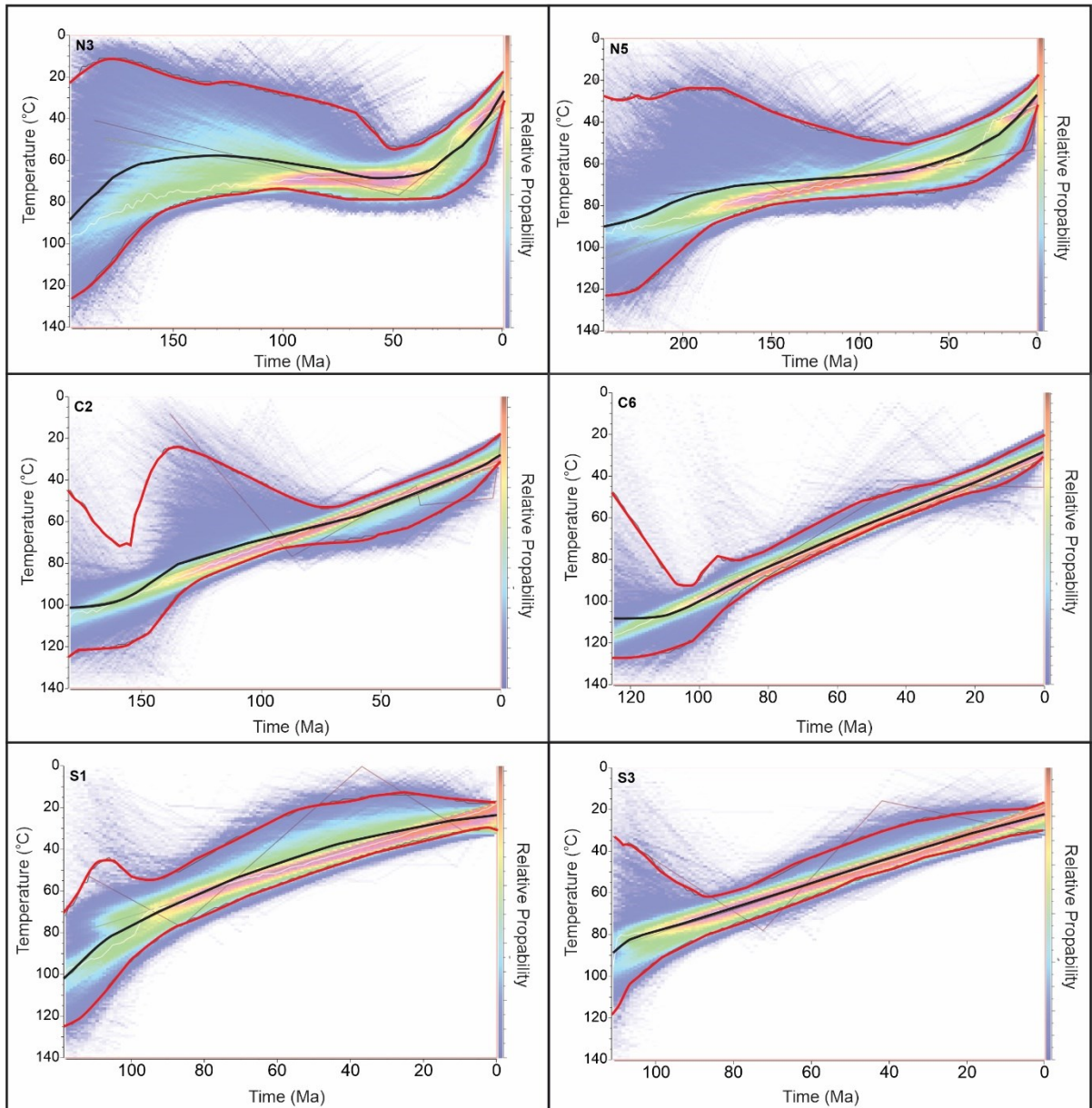
Figure A.8. Results of inverse MCMC modelling in QTQt (Gallagher, 2012) for samples from the Araçuaí Orogen. The expected model is displayed by the black curve, with the 90% credible interval in red for single samples.
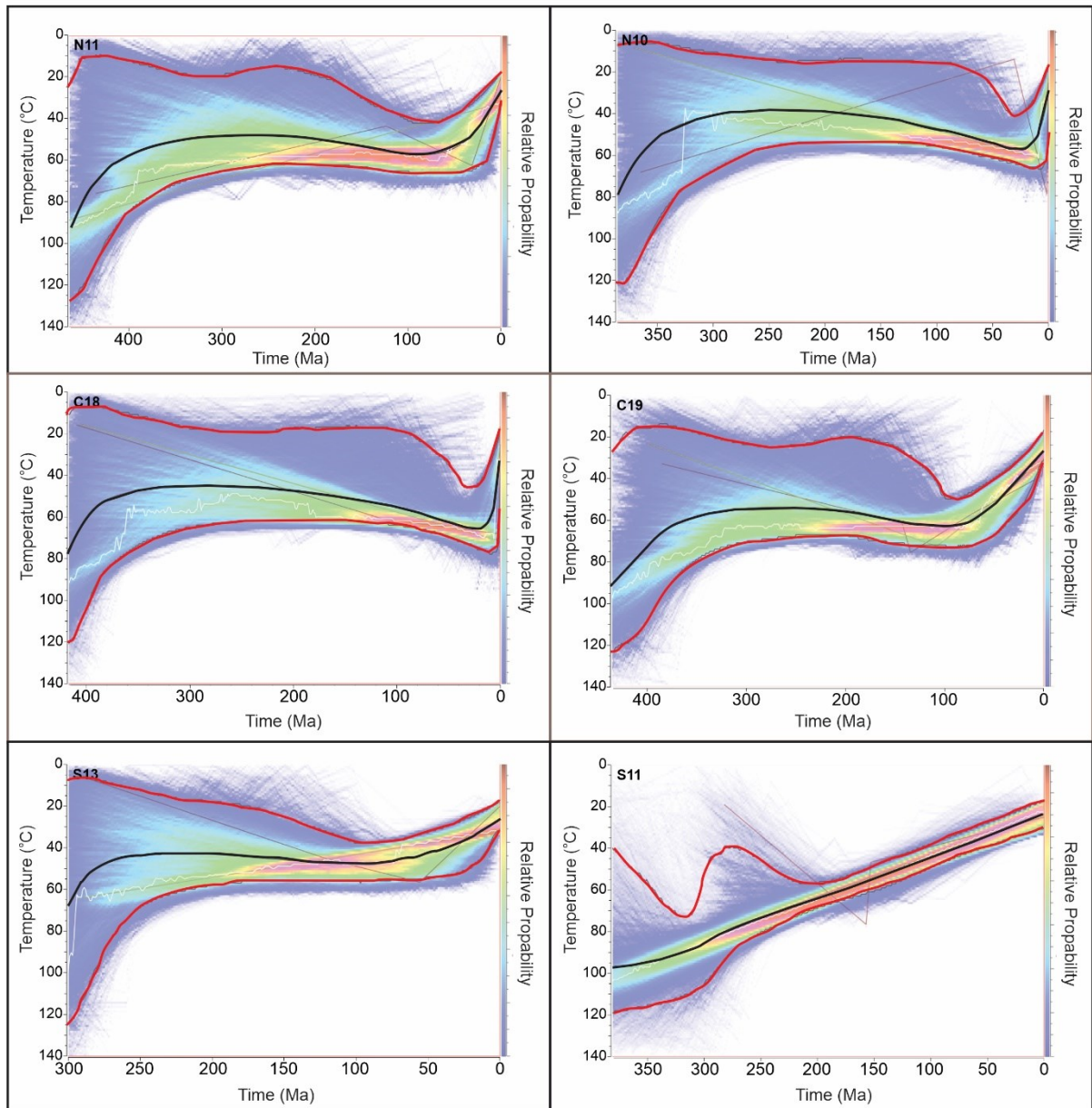
São Francisco Craton

Figure A.9. Results of inverse MCMC modelling in QTQt (Gallagher, 2012) for samples from the São Francisco Craton. The expected model is displayed by the black curve, with the 90% credible interval in red for single samples
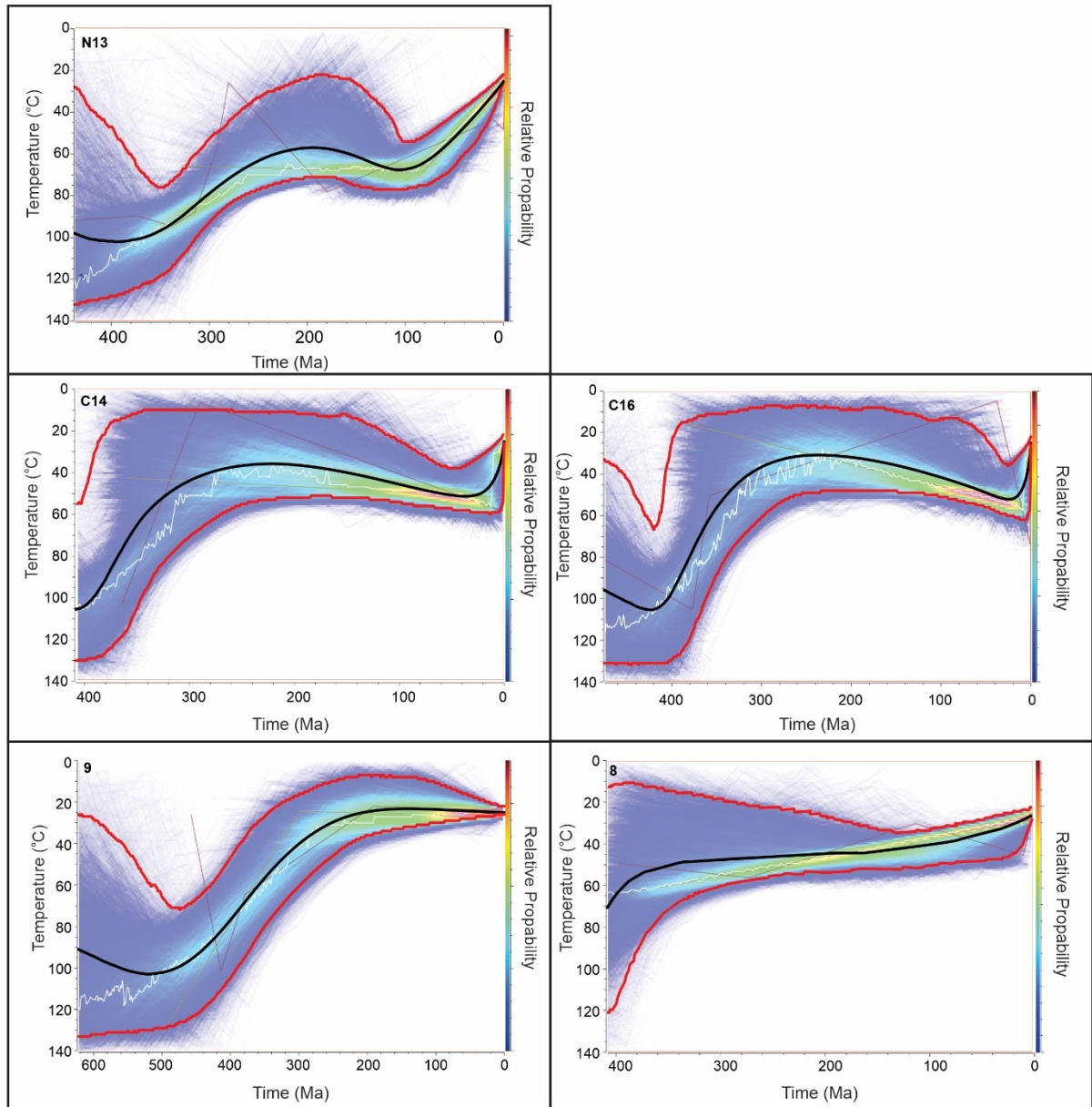
Brasília Belt

Figure A.10. Results of inverse MCMC modelling in QTQt (Gallagher, 2012) for samples from the Brasília Belt. The expected model is displayed by the black curve, with the 90% credible interval in red for single samples.

CHAPTER III

3.1 – Future work

The AFT analyses of 50 basement samples from São Francisco Craton, Araçuaí Belt, and Brasília Belt allowed to reconstruct the general picture on the differential cooling history of these terrains during the Phanerozoic. However, future investigations are necessary to better constrain and validate the conclusions and suggestions that are presented in Chapter II. Therefore, further research might:

1. apply multi-thermochronological approach to better constrain the time-temperature paths.

   - It would be possible to clarify if Araçuaí Belt was also strongly denudated during the Paleozoic, just like São Francisco Craton and Brasília Belt, using fission-track method but with higher-temperature thermochronometers, such as zircon grains, i.e. Zircon Fission-Track.

   - The Neogene cooling event suggested by some of the models presented in this work, can be better investigated using the (U-Th-Sm)/He approach in apatite grains. This method fundamentally constrains cooling events in even shallower portions of the crust.

2. perform more detailed sampling campaigns.

   - Other portions of the West Gondwana basement should also be investigated in order to evaluate the reach of the Paleozoic cooling phase and its connection with the West Gondwana orogenic cycles. Cratonic areas (e.g. São Francisco Craton) as well as orogenic belts trapped in the continental interior (e.g. Brasília Belt) could preserve the former cooling.

   - A broadly sampling in the northern portion of the Araçuaí Belt is necessary to check the influence of near-craton rheology and structural trend in its exhumation compared to the southern portion.

   - São Francisco Craton weak zones (e.g. Pirapora and Paramirim aulacogens) could be a locus of Meso-Cenozoic reactivations. This hypothesis warrants further investigation that could be achieved by AFT analyses of the basement crossing these structures. Boreholes may be required in cases where the Phanerozoic sediments fully covers the basement.

REFERENCES

Alessandretti, L., Machado, R., Warren, L.V., Assine, M.L., Lana, C., 2016. From source-to-sink: The Late Permian SW Gondwana paleogeography and sedimentary dispersion unraveled by a multi-proxy analysis. J. South Am. Earth Sci. 70, 368–382. https://doi.org/10.1016/j.jsames.2016.06.007

Alkmim, F.F., 2015. Geological Background: A Tectonic Panorama of Brazil, in: Vieira, B.C., Salgado, A.A.R., Santos, L.J.C. (Eds.), Landscapes and Landforms of Brazil. Springer, pp. 9–17. https://doi.org/10.1007/978-94-017-8023-0_2

Alkmim, F.F., 2004. O que faz de um cráton um cráton? O cratón São Francisco e as revelações almeidianas ao delimitá-lo, in: Mantesso-Neto, V., Bartorelli, A., Carneiro, C.D.R., Brito Neves, B.B. (Eds.), Geologia do Continente Sul-Americano: Evolução Da Obra de Fernando Flávio Marques de Almeida. Editora Beca, São Paulo, pp. 17–35.

Alkmim, F.F., Brito Neves, B.B., Alves, J.A.C., 1993. Arcabouço tectônico do Cráton do São Francisco - uma revisão, in: Dominguez, M.L., Misi, A. (Eds.), O Cratón Do São Francisco: Trabalhos Apresentados Na Reunião Preparatória Do II Simposio Sobre o Cráton Do São Francisco. SBG-SGM-CNPq, Salvador, pp. 45–62.

Alkmim, F.F., Kuchenbecker, M., Reis, H.L.S., Pedrosa-Soares, A.C., 2017. The Araçuaí Belt, in: Heilbron, M., Cordani, U.G., Alkmim, F.F. (Eds.), São Francisco Craton, Eastern Brazil. Springer, pp. 255–275. https://doi.org/10.1007/978-3-319-01715-0

Alkmim, F.F., Marshak, S., Pedrosa-Soares, A.C., Peres, G.G., Cruz, S.C.P., Whittington, A., 2006. Kinematic evolution of the Araçuaí-West Congo orogen in Brazil and Africa: Nutcracker tectonics during the Neoproterozoic assembly of Gondwana. Precambrian Res. 149, 43–64. https://doi.org/10.1016/j.precamres.2006.06.007

Alkmim, F.F., Martins-Neto, M.A., 2001. Bacia intracratônica do São Francisco: arcabouço estrutural e cenários evolutivos, in: Pinto, C.P., Martins-Neto, M.A. (Eds.), Bacia Do São Francisco: Geologia e Recursos Naturais. SBG/Núcleo MG, pp. 9–30.

Alkmim, F.F., Teixeira, W., 2017. The Paleoproterozoic Mineiro Belt and the Quadrilátero Ferrífero, in: Heilbron, M., Cordani, U.G., Alkmim, F.F. (Eds.), São Francisco Craton, Eastern Brazil. Springer, pp. 71–94. https://doi.org/10.1007/978-3-319-01715-0

Almeida, F.F.M. De, Brito Neves, B.B. De, Dal Ré Carneiro, C., 2000. The origin and evolution of the South American Platform. Earth-Science Rev. 50, 77–111. https://doi.org/10.1016/S0012-8252(99)00072-0

Almeida, F.F.M., 1977. O Craton do Säo Francisco. Rev. Barsileira Geociências 7, 349–364. https://doi.org/10.5327/rbg.v7i4.128

Almeida, F.F.M., 1969. Diferenciação tectônica da plataforma brasileira, in: Congresso Brasileiro de Geologia. SBG, Salvador, pp. 29–46.

Almeida, F.F.M., 1967. Origem e evolução da plataforma brasileira. Rio de Janeiro.

Almeida, F.F.M., Hasui, Y., Brito Neves, B.B., Fuck, R.A., 1981. Brazilian structural provinces: an introduction. Earth-Science Rev. 17, 1–29. https://doi.org/10.1016/0012-8252(81)90003-9

Amaral-Santos, E., Jelinek, A.R., Genezine, F.A., 2019. Phanerozoic cooling history of Archean/Paleoproterozoic basement in the southern Espinhaço Range, southeastern Brazil, through apatite fission-track analysis. J. South Am. Earth Sci. 102352. https://doi.org/10.1016/j.jsames.2019.102352

Amaral, G., Born, H., Hadler Neto, J.C., Iunes, P.J., Kawashita, K., Machado Jr., D.L., Oliveira, E.P., Paulo, S.R., Tello Saenz, C.A., 1997. Fission track analysis of apatites from São Francisco craton and Mesozoic alcaline-carbonatite complexes from central and southeastern Brazil. J. South Am. Earth Sci. 10, 285–294. https://doi.org/10.1016/S0895-9811(97)00020-5

Artemieva, I.M., 2006. Global $1° × 1°$ thermal model TC1 for the continental lithosphere: Implications for lithosphere secular evolution. Tectonophysics 416, 245–277. https://doi.org/10.1016/j.tecto.2005.11.022

Ashby, D., Mccaffrey, K., Holdsworth, B., Almeida, J., 2010. Structural Controls on the Evolution of the Southeastern Brazilian Continental Margin, in: Geophysical Research Abstracts. EGU General Assembly.

Asmus, H.E., 1982. Geotectonic significance of Mesozoic-Cenozoic magmatic rocks in the Brazilian continental margin and adjoining emerged area, in: Congresso Latino-Americano de Geologia. Servicio Geologico Nacional, Buenos Aires, pp. 761–779.

Assine, M.L., 1999. Fácies, icnofósseis, paleocorrentes e sistemas deposicionais da Formação Furnas no flanco sudeste da Bacia do Paraná. Rev. Bras. Geociências 29, 357–370.

Assine, M.L., Perinotto, J.A., Fulfaro, V.J., Petri, S., 1998. Progradação deltaica tibagi no devoniano médio da Bacia do Paraná. Rev. Bras. Geociências 28, 125–134. https://doi.org/10,1023 / A: 1014771612802

Assumpção, M., Feng, M., Tassara, A., Julià, J., 2013. Models of crustal thickness for South America from seismic refraction, receiver functions and surface wave tomography. Tectonophysics 609, 82–96. https://doi.org/10.1016/j.tecto.2012.11.014

Assumpção, M., Ferreira, J., Barros, L., Bezerra, H., França, G.S., Barbosa, J.R., Menezes, E., Carlos Ribotta, L., Pirchiner, M., Nascimento, A. do, Dourado, J.C., 2014. Intraplate seismicity in Brazil, in: Talwani, P. (Ed.), Intraplate Earthquakes. Cambridge University Press, Cambridge, pp. 50–71. https://doi.org/10.1017/CBO9781139628921.004

Autin, J., Bellahsen, N., Leroy, S., Husson, L., Beslier, M.O., d'Acremont, E., 2013. The role of structural inheritance in oblique rifting: Insights from analogue models and application to the Gulf of Aden. Tectonophysics 607, 51–64. https://doi.org/10.1016/j.tecto.2013.05.041

Babinski, M., Boggiani, P.C., Trindade, R.I.F., Fanning, C.M., 2013. Detrital zircon ages and geochronological constraints on the Neoproterozoic Puga diamictites and associated BIFs in the southern Paraguay Belt, Brazil. Gondwana Res. 23, 988–997. https://doi.org/10.1016/j.gr.2012.06.011

Barbarand, J., Carter, A., Wood, I., Hurford, T., 2003. Compositional and structural control of fission-track annealing in apatite. Chem. Geol. 198, 107–137. https://doi.org/10.1016/S0009-2541(02)00424-2

Barbosa, J.S.F., Barbosa, R.G., 2017. The Paleoproterozoic Eastern Bahia Orogenic Domain, in: Heilbron, M., Cordani, U.G., Alkmim, F.F. (Eds.), São Francisco Craton, Eastern Brazil. Springer, pp. 57–69. https://doi.org/10.1007/978-3-319-01715-0

Batezelli, A., 2017. Continental systems tracts of the Brazilian Cretaceous Bauru Basin and their relationship with the tectonic and climatic evolution of South America. Basin Res. 29, 1–25. https://doi.org/10.1111/bre.12128

Batezelli, A., Ladeira, F.S.B., 2016. Stratigraphic framework and evolution of the Cretaceous continental sequences of the Bauru, Sanfranciscana, and Parecis basins, Brazil. J. South Am. Earth Sci. 65, 1–24. https://doi.org/10.1016/j.jsames.2015.11.005

Bershaw, J., Garzione, C.N., Higgins, P., MacFadden, B.J., Anaya, F., Alvarenga, H., 2010. Spatial-temporal changes in Andean plateau climate and elevation from stable isotopes of mammal teeth. Earth Planet. Sci. Lett. 289, 530–538. https://doi.org/10.1016/j.epsl.2009.11.047

Bicca, M.M., Chemale Jr., F., Jelinek, A.R., Oliveira, C.H.E., Guadagnin, F., Armstrong, R., 2013. Tectonic evolution and provenance of the Santa Bárbara Group, Camaquã Mines region, Rio Grande do Sul, Brazil. J. South Am. Earth Sci. 48, 173–192. https://doi.org/10.1016/j.jsames.2013.09.006

Bigazzi, G., 1981. The problem of the decay constant λ_f of ^{238}U. Nucl. Tracks 5, 35–44. https://doi.org/10.1016/0191-278X(81)90024-X

Bishop, P., 2007. Long-term landscape evolution: linking tectonics and surface processes. Earth Surf. Process. Landforms 32, 329–365. https://doi.org/10.1002/esp

Borba, A.W., Lima, E.F., Vignol-Lelarge, M.L.M., Mizusaki, A.M.P., Sparrenberg, I., Barros, C.E., 2003. Significance of Late Paleozoic fission-track ages in volcanic rocks from the Lavras Do Sul region, Southernmost Brazil. Gondwana Res. 6, 79–88. https://doi.org/10.1016/S1342-937X(05)70645-6

Borba, A.W., Vignol-Lelarge, M.L.M., Mizusaki, A.M.P., 2002. Uplift and denudation of the Cacapava do Sul granitoids (southern Brazil) durning Late Paleozoic and Mesozoic: Constraints form apatite fission-track data. J. South Am. Earth Sci. 15, 683–692.

Boulton, G.S., 1990. Sedimentary and sea level changes during glacial cycles and their control on glacimarine facies architecture. Geol. Soc. London, Spec. Publ. 53, 15–52. https://doi.org/10.1144/gsl.sp.1990.053.01.02

Braun, J., Beaumont, C., 1989. Contrasting styles of lithospheric extension: implications for differences between Basin and Range province and rifted continental margins, in: Tankard, A.J., Balkwill, H.R. (Eds.), Extensional Tectonics and Stratigraphy of the North Atlantic Margins. American Association of Petroleum Geologists, pp. 53–79. https://doi.org/https://doi.org/10.1306/M46497 ISBN

Braun, J., Beek, P. Van der, Batt, G., 2006. Quantitative Thermochronology. Cambridge University Press, Cambridge. https://doi.org/10.1103/PhysRev.98.58

Braun, J., Robert, X., 2005. Constraints on the rate of post-orogenic erosional decay from low-temperature thermochronological data: Application to the Dabie Shan, China. Earth Surf. Process. Landforms 30, 1203–1225. https://doi.org/10.1002/esp.1271

Brito Neves, B.B., 2002. Main stages of the development of the sedimentary basins of South America and their relationship with the tectonics of supercontinents. Gondwana Res. 5, 175–196.

Brito Neves, B.B., 1999. América do Sul: quatro fusões, quatro fissões e o processo acrescionário andino. Rev. Bras. Geociências 29, 379–392.

Brito Neves, B.B., Fuck, R.A., Pimentel, M.M., 2014. The Brasiliano collage in South America: a review. Brazilian J. Geol. 44, 493–518. https://doi.org/10.5327/Z2317-4889201400030010

Brown, R.W., Rust, D.J., Summerfield, M.A., Gleadow, A.J.W., De Wit, M.C.J., 1990. An early cretaceous phase of accelerated erosion on the south-western margin of Africa: Evidence from apatite fission track analysis and the offshore sedimentary record. Nucl. Tracks Radiat. Meas. 17, 339–350. https://doi.org/10.1016/1359-0189(90)90056-4

Brune, S., Heine, C., Pérez-Gussinyé, M., Sobolev, S. V., 2014. Rift migration explains continental margin asymmetry and crustal hyper-extension. Nat. Commun. 5. https://doi.org/10.1038/ncomms5014

Buck, W.R., 1991. Modes of continental lithospheric extension. J. Geophys. Res. 96, 20161–20178. https://doi.org/10.1029/91jb01485

Buso, V.V., Aquino, C.D., Paim, P.S.G., Souza, P.A., Mori, A.L., Fallgatter, C., Milana, J.P., Kneller, B., 2017. Late Palaeozoic glacial cycles and subcycles in western Gondwana: Correlation of surface and subsurface data of the Paraná Basin, Brazil. Palaeogeogr. Palaeoclimatol. Palaeoecol. 531. https://doi.org/10.1016/j.palaeo.2017.09.004

Calegari, S.S., Neves, M.A., Guadagnin, F., França, G.S., Vincentelli, M.G.C., 2016. The Alegre Lineament and its role over the tectonic evolution of the Campos Basin and adjacent continental margin, Southeastern Brazil. J. South Am. Earth Sci. 69, 226–242. https://doi.org/10.1016/j.jsames.2016.04.005

Campbell, I.H., 2007. Testing the plume theory. Chem. Geol. 241, 153–176. https://doi.org/10.1016/j.chemgeo.2007.01.024

Campos, J.E.G., Dardenne, M.A., 1997. Origem e evolução tectônica da Bacia Sanfranciscana. Rev. Barsileira Geociências 27, 283–294. https://doi.org/10.5327/rbg.v27i3.596

Campos Neto, M.D.C., 2000. Orogenic systems from Southwestern Gondwana. An approach to Brasiliano-PanAfrican cycle and orogenic collage in Southeastern Brazil, in: Cordani, U.G., Milani, E.J., Thomaz, F.A., Campos, D.A. (Eds.), Tectonic Evolution of South America 31st International Geological Congress. Rio de Janeiro, pp. 335–365.

Canile, F.M., Babinski, M., Rocha-Campos, A.C., 2016. Evolution of the Carboniferous-Early Cretaceous units of Paraná Basin from provenance studies based on U-Pb, Hf and O isotopes from detrital zircons. Gondwana Res. 40, 142–169. https://doi.org/10.1016/j.gr.2016.08.008

Caputo, M.V., Crowell, J.C., 1985. Migration of glacial centers across Gondwana during Paleozoic Era. Geol. Soc. Am. Bull. 96, 1020–1036. https://doi.org/10.1130/0016-7606(1985)96<1020

Carlson, W.D., 1990. Mechanisms and kinetics of apatite fission-track annealing. Am. Mineral. 75, 1120–1139.

Carlson, W.D., Donelick, R.A., Ketcham, R.A., 1999. Variability of apatite fission-track annealing kinetics: I. Experimental results. Am. Mineral. 84, 1213–1223. https://doi.org/10.2138/am-1999-0901

Carmo, I.D.O., 2005. Geocronologia do Intemperismo Cenozóico no Sudeste do Brasil. PhD thesis. Universidade Federal do Rio de Janeiro.

Carneiro, Celso Dal Ré, Almeida, Fernando Flávio Marques, Hasui, Yociteru, Zalán, P.V., Teixeira, J.B.G., 2012. Estágios evolutivos do Brasil no Fanerozóico, in: Hasui, Y., Carneiro, C.D.R., Almeida, F.F.M., Bartorelli, A. (Eds.), Geologia do Brasil. Beca, pp. 131–136.

Carvalho, A.H., Vesely, F.F., 2017. Facies relationships recorded in a Late Paleozoic fluvio-deltaic system (Paraná Basin, Brazil): Insights into the timing and triggers of subaqueous sediment gravity flows. Sediment. Geol. 352, 45–62. https://doi.org/10.1016/j.sedgeo.2016.12.004

Carvalho, B.B., Janasi, V. de A., Henrique-Pinto, R., 2014. Geochemical and Sr-Nd-Pb isotope constraints on the petrogenesis of the K-rich Pedra Branca Syenite: Implications for the Neoproterozoic post-collisional magmatism in SE Brazil. Lithos 205, 39–59. https://doi.org/10.1016/j.lithos.2014.06.016

Cavalcante, C., Hollanda, M.H., Vauchez, A., Kawata, M., 2018. How long can the middle crust remain partially molten during orogeny? Geology 46, 839–842. https://doi.org/10.1130/G45126.1

Chadderton, L.T., 2003. Nuclear tracks in solids: registration physics and the compound spike. Radiat. Meas. 36, 13–34. https://doi.org/10.1016/S1350-4487(03)00094-5

Chaves, A.D.O., 2013. Enxames De Diques Máficos De Minas Gerais – O Estado Da Arte. Geonomos 21, 29–33. https://doi.org/http://dx.doi.org/10.18285/geonomos.v21i1.253

Clark, S.R., 2018. Uncertainty in the breakup, spreading history, and velocity variations of Gondwana. Gondwana Res. 53, 189–196. https://doi.org/10.1016/j.gr.2017.04.029

Cloetingh, S., van Wees, J.D., van der Beek, P.A., Spadini, G., 1995. Role of pre-rift rheology in kinematics of extensional basin formation: constraints from thermomechanical models of Mediterranean and intracratonic basins. Mar. Pet. Geol. 12, 793–807. https://doi.org/10.1016/0264-8172(95)98848-Y

Cobbold, P.R., Meisling, K.E., Mount, V.S., 2001. Reactivation of an obliquely rifted margin, Campos and Santos basins, southeastern Brazil. Am. Assoc. Pet. Geol. Bull. 85, 1925–1944. https://doi.org/10.1306/8626d0b3-173b-11d7-8645000102c1865d

Coelho, R.M., Chaves, A.O., 2017. Diques máficos de Minas Gerais do Cretáceo Inferior: Idades Ar-Ar e correlação com a Província Ígnea Paraná-Etendeka. Geociências 4, 613–622.

Cogné, N., Gallagher, K., Cobbold, P.R., 2011. Post-rift reactivation of the onshore margin of southeast Brazil: Evidence from apatite (U-Th)/He and fission-track data. Earth Planet. Sci. Lett. 309, 118–130. https://doi.org/10.1016/j.epsl.2011.06.025

Cogné, N., Gallagher, K., Cobbold, P.R., Riccomini, C., Gautheron, C., 2012. Post-breakup tectonics in southeast Brazil from thermochronological data and combined inverse-forward thermal history modeling. J. Geophys. Res. B Solid Earth 117, 1–16. https://doi.org/10.1029/2012JB009340

Cordani, U.G., 1973. Evolução geológica pré-cambriana da faixa costeira do Brasil entre Salvador e Vitória. Thesis. Universidade de São Paulo.

Cordani, U.G., Melcher, G.C., Almeida, F.F.M., 1968. Outline of Precambrian geochronology of South America. Can. J. Earth Sci. 5, 629–632.

Corti, G., van Wijk, J., Cloetingh, S., Morley, C.K., 2007. Tectonic inheritance and continental rift architecture: Numerical and analogue models of the East African Rift system. Tectonics 26, 1–13. https://doi.org/10.1029/2006TC002086

Cowan, G.A., Adler, H.H., 1976. The variability of the natural abundance of ^{235}U. Geochim. Cosmochim. Acta 40, 1487–1490. https://doi.org/10.1016/0016-7037(76)90087-9

Daemon, R.F., Quadros, L.P. de, 1970. Bioestratigrafia do Neopaleozóico da Bacia do Paraná. in: Congresso Brasileiro de Geologia. 24, 359-412.

D'Agrella-Filho, M.S., Trindade, R.I.F., Tohver, E., Janikian, L., Teixeira, W., Hall, C., 2011. Paleomagnetism and 40Ar/39Ar geochronology of the high-grade metamorphic rocks of the Jequié block, São Francisco Craton: Atlantica, Ur and beyond. Precambrian Res. 185, 183–201. https://doi.org/10.1016/j.precamres.2011.01.008

Danderfer, A., De Waele, B., Pedreira, A.J., Nalini, H.A., 2009. New geochronological constraints on the geological evolution of Espinhaço basin within the São Francisco Craton—Brazil. Precambrian Res. 170, 116–128. https://doi.org/10.1016/j.precamres.2009.01.002

De Corte, F., Bellemans, F., Van den haute, P., Ingelbrecht, C., Nicholl, C., 1998. A New U Doped Glass Certified By the European Commission for the Calibration of Fission-Track Dating, in: van den Haute, P., de Corte, F. (Eds.), Advances in Fission-Track Geochronology. Springer, Dordrecht.

De Grave, J., Glorie, S., Buslov, M.M., Izmer, A., Fournier-Carrie, A., Batalev, V.Y., Vanhaecke, F., Elburg, M., Van den haute, P., 2011. The thermo-tectonic history of the Song-Kul plateau, Kyrgyz Tien Shan: Constraints by apatite and titanite thermochronometry and zircon U/Pb dating. Gondwana Res. 20, 745–763. https://doi.org/10.1016/j.gr.2011.03.011

De Grave, J., Glorie, S., Vermaercke, P., Vittiglio, G., Van den haute, P., 2010. A " new " irradiation facility for FT applications at the Belgian Nuclear Research Centre: the BR1 reactor, in: Thermochronology,12th International Conference.

De Pelsmaeker, E., Glorie, S., Buslov, M.M., Zhimulev, F.I., Poujol, M., Korobkin, V. V., Vanhaecke, F., Vetrov, E. V., De Grave, J., 2015. Late-Paleozoic emplacement and Meso-Cenozoic reactivation of the southern Kazakhstan granitoid basement. Tectonophysics 662, 416–433. https://doi.org/10.1016/j.tecto.2015.06.014

de Wit, M.J., Brito Neves, B.B., Trouw, R.A.J., Pankhurst, R.J., 2008. Pre-Cenozoic correlations across the South Atlantic region: (the ties that bind), in: Pankhurst, R.J., Trouw, R.A.J., Brito Neves, B.B., de Wit, M.J. (Eds.), West Gondwana: Pre-Cenozoic Correlations Across the South Atlantic Region. Geological Society, London, pp. 1–8. https://doi.org/10.1144/SP294.1

Del Lama, E.A., Zanardo, A., Oliveira, M.A.F., Morales, N., 2000. Exhumation of high-pressure granulites of the Guaxupé Complex, southeastern Brazil. Geol. J. 35, 231–249. https://doi.org/10.1002/gj.859

Dempster, T.J., Persano, C., 2006. Low-temperature thermochronology: Resolving geotherm shapes or denudation histories? Geology 34, 73–76. https://doi.org/10.1130/G21980.1

Dodson, M.H., 1979. Theory of Cooling Ages, in: Jäger, E., Hunziker, J.C. (Eds.), Lectures in Isotope Geology. Springer, Berlin, Heidelberg.

Dodson, M.H., 1973. Closure temperature in cooling geochronological and petrological systems. Contrib. to Mineral. Petrol. 40, 259–274. https://doi.org/10.1007/BF00373790

Donelick, R.A., 2005. Apatite Fission-Track Analysis. Rev. Mineral. Geochemistry 58, 49–94. https://doi.org/10.2138/rmg.2005.58.3

Donelick, R.A., 1991. Crystallographic orientation dependence of mean etchable fission track length in apatite: an empirical model and experimental observations. Am. Mineral. 76, 83–91.

Donelick, R.A., Ketcham, R.A., Carlson, W.D., 1999. Variability of apatite fission-track annealing kinetics: II. Crystallographic orientation effects. Am. Mineral. 84, 1224–1234. https://doi.org/10.2138/am-1999-0902

Doranti-Tiritan, C., Hackspacher, P.C., Ribeiro, M.C.S., Glasmacher, U.A., Souza, D.H. De, 2014. Relief evolution of Poços de Caldas (SP/MG) Region based in thermochronology data and 3D thermokinematic modeling. Rev. Bras. Geomorfol. 15, 291–310. https://doi.org/10.20502/rbg.v15i2.491

Du Toit, A.L., 1937. Our wandering continents: an hypothesis of continental drifting. Oliver and Boyd, Edinburgh, UK.

Du Toit, A.L., 1927. A geological comparison of South America with South Africa. Washington Publications Carnegy Institution, Washington, DC.

Dunlap, W.J., 2000. Nature's diffusion experiment: The cooling-rate cooling-age correlation. Geology 28, 139–142.

Durrani, I.R., Bull, R.K., 1987. Solid State Nuclear Track Detection (Principles, Methods and Application). Pergamon Press, Oxford.

Ebert, H., 1968. Ocorrências de fácies granulítica no sul de Minas Gerais e em áreas adjacentes, em dependência da estrutura orogênica: hipóteses sobre sua origem, in: Anais Da Academia Brasileira de Ciências 40. Rio de Janeiro, pp. 215–219.

Engelmann de Oliveira, C.H., Jelinek, A.R., 2017. História termotectônica da margem continental Brasileira a partir de dados de traços de fissão em apatita. Pesqui. em Geociencias 44, 387–400. https://doi.org/10.22456/1807-9806.83263

Enkelmann, E., Garver, J.I., 2016. Low-temperature thermochronology applied to ancient settings. J. Geodyn. 93, 17–30. https://doi.org/10.1016/j.jog.2015.11.001

Enkelmann, E., Ridgway, K.D., Carignano, C., Linnemann, U., 2014. A thermochronometric view into an ancient landscape: Tectonic setting, development, and inversion of the Paleozoic eastern Paganzo basin, Argentina. Lithosphere 6, 93–107. https://doi.org/10.1130/l309.1

Ernesto, M., 2005. Paleomagnetism of the post-Paleozoic alkaline magmatism in the Brazilian platform: questioning the mantle plume model, in: Comin-Chiaramonti, P., Gomes, C.B. (Eds.), Mesozoic to Cenozoic Alkaline Magmatism in the Brazilian Platform. Editora da Universidade de São Paulo, São Paulo, pp. 689–705.

Ernesto, M., Marques, L.S., Piccirillo, E.M., Molina, E.C., Ussami, N., Comin-Chiaramonti, P., Bellieni, G., 2002. Paraná Magmatic Province-Tristan da Cunha plume system: Fixed versus mobile plume, petrogenetic considerations and alternative heat sources. J. Volcanol. Geotherm. Res. 118, 15–36. https://doi.org/10.1016/S0377-0273(02)00248-2

Eyles, C.H., Eyles, N., Franca, A.B., 1993. Glaciation and tectonics in an active intracratonic basin: the Late Palaeozoic Itararé Group, Paraná Basin, Brazil. Sedimentology 40, 1–25.

Fan, M., Carrapa, B., 2014. Late Cretaceous-early Eocene Laramide uplift, exhumation, and basin subsidence in Wyoming: Crustal responses to flat slab subduction. Tectonics 33, 509–529. https://doi.org/10.1002/2012TC003221

Feng, M., van der Lee, S., Assumpção, M., 2007. Upper mantle structure of South America from joint inversion of waveforms and fundamental mode group velocities of Rayleigh waves. J. Geophys. Res. Solid Earth 112, 1–16. https://doi.org/10.1029/2006JB004449

Fernie, N., Glorie, S., Jessell, M.W., Collins, A.S., 2018. Thermochronological insights into reactivation of a continental shear zone in response to Equatorial Atlantic rifting (northern Ghana). Sci. Rep. 8, 1–14. https://doi.org/10.1038/s41598-018-34769-x

Ferrari, A.L., 2001. Evolução Tectônica do Graben da Guanabara. PhD Thesis. Universidade de São Paulo.

Fitzgerald, P.G., Muñoz, J.A., Coney, P.J., Baldwin, S.L., 1999. Asymmetric exhumation across the Pyrenean orogen: Implications for the tectonic evolution of a collisional orogen. Earth Planet. Sci. Lett. 173, 157–170. https://doi.org/10.1016/S0012-821X(99)00225-3

Fleisher, R.L., Price, P.B., Walker, R.M., 1975. Nuclear tracks in solids: Principles and applications. University of California Press, Berkeley, Calif.

Fonseca, A.C., Piffer, G., Nachtergaele, S., Van Ranst, G., De Grave, J., Novo, T., n.d. Paleozoic post-orogenic denudation of the Brasília Belt of West Gondwana: insights from apatite fission track thermochronology.

Fossen, H., Cavalcante, G.C., Almeida, R.P., 2017. Hot Versus Cold Orogenic Behavior: Comparing the Araçuaí-West Congo and the Caledonian Orogens. Tectonics 36, 2159–2178. https://doi.org/10.1002/2017TC004743

Foulger, G.R., 2018. Origin of the South Atlantic igneous province. J. Volcanol. Geotherm. Res. 355, 2–20. https://doi.org/10.1016/j.jvolgeores.2017.09.004

Frank, H.T., Gomes, M.E.B., Formoso, M.L.L., 2009. Review of the areal extent and the volume of the Serra Geral Formation, Paraná Basin, South America. Pesqui. em Geociências 36, 49–57.

Fromm, T., Jokat, W., Ryberg, T., Behrmann, J.H., Haberland, C., Weber, M., 2017. The onset of Walvis Ridge: Plume influence at the continental margin. Tectonophysics 716, 90–107. https://doi.org/10.1016/j.tecto.2017.03.011

Galbraith, R.F., 2005. Statistics for fission track analysis. Chapman and Hall/CRC, New York.

Galbraith, R.F., 1981. On statistical models for fission track counts. Math. Geol. 13, 471–478. https://doi.org/10.1007/BF01034498

Galbraith, R.F., Laslett, G.M., 1993. Statistical models for mixed fission track ages. Nucl. Tracks Radiat. Meas. 21, 459–470. https://doi.org/10.1016/1359-0189(93)90185-C

Gallagher, K., 2012. Transdimensional inverse thermal history modeling for quantitative thermochronology. J. Geophys. Res. 117, 1–16. https://doi.org/10.1029/2011JB008825

Gallagher, K., Hawkersworth, C.J., Mantovani, M.S.M., 1995. Denudation, fission track analysis and the long-term evolution of passive margin topograpy: application to the southeastet Brazilian margin. Journ. South Am. Earth Sci. 8, 65–77. https://doi.org/0895-9811(94)00042-5

Gallagher, K., Hawkesworth, C.J., Mantovani, M.S.M., 1994. The denudation history of the onshore continental margin of SE Brazil inferred from apatite fission track data. J. Geophys. Res. 99, 18117–18145. https://doi.org/10.1029/94JB00661

Garcia, A.J.V., Rosa, Á.A.S., Goldberg, K., 2005. Paleoenvironmental and paleoclimatic control on early diagenetic processes and fossil record in Cretaceous continental sandstones of Brazil. J. South Am. Earth Sci. 19, 243–258. https://doi.org/10.1016/j.jsames.2005.01.008

Georgieva, V., Gallagher, K., Sobczyk, A., Sobel, E.R., Schildgen, T.F., Ehlers, T.A., Strecker, M.R., 2019. Effects of slab-window, alkaline volcanism, and glaciation on thermochronometer cooling histories, Patagonian Andes. Earth Planet. Sci. Lett. 511, 164–176. https://doi.org/10.1016/j.epsl.2019.01.030

Geraldes, M.C., Motoki, A., Costa, A., Mota, C.E., Mohriak, W.U., 2013. Geochronology (Ar/Ar and K-Ar) of the south Atlantic post-break-up magmatism. Geol. Soc. Spec. Publ. 369, 41–74. https://doi.org/10.1144/SP369.21

Gesicki, A.L.D., Riccomini, C., Boggiani, P.C., 2002. Ice flow direction during late Paleozoic glaciation in Western Paraná Basin, Brazil. J. South Am. Earth Sci. 14, 933–939. https://doi.org/10.1016/S0895-9811(01)00076-1

Gibson, S.A., Thompson, R.N., Leonardos, O.H., Dickin, A.P., Mitchell, J.G., 1995. The Late Cretaceous Impact of the Trindade Mantle Plume: Evidence from Large-volume, Mafic, Potassic Magmatism in SE Brazil. J. Petrol. 36, 189–229. https://doi.org/10.1093/petrology/36.1.189

Gillespie, J., Glorie, S., Xiao, W., Zhang, Z., Collins, A.S., Evans, N., McInnes, B., De Grave, J., 2017. Mesozoic reactivation of the Beishan, southern Central Asian Orogenic Belt: Insights

from low-temperature thermochronology. Gondwana Res. 43, 107–122. https://doi.org/10.1016/j.gr.2015.10.004

Gleadow, A.J.W., Belton, D.X., Kohn, B.P., Brown, R.W., 2002. Fission Track Dating of Phosphate Minerals and the Thermochronology of Apatite. Rev. Mineral. Geochemistry 48, 579–630. https://doi.org/10.2138/rmg.2002.48.16

Gleadow, A.J.W., Duddy, I.R., 1981. A natural long-term track annealing experiment for apatite. Nucl. Tracks 5, 169–174. https://doi.org/10.1016/0191-278X(81)90039-1

Gleadow, A.J.W., Duddy, I.R., Green, P.F., Lovering, J.F., 1986. Confined fission track lengths in apatite: a diagnostic tool for thermal history analysis. Contrib. to Mineral. Petrol. 94, 405–415. https://doi.org/10.1007/BF00376334

Glorie, S., De Grave, J., Buslov, M.M., Elburg, M.A., Stockli, D.F., Gerdes, A., Van den haute, P., 2010. Multi-method chronometric constraints on the evolution of the Northern Kyrgyz Tien Shan granitoids (Central Asian Orogenic Belt): From emplacement to exhumation. J. Asian Earth Sci. 38, 131–146. https://doi.org/10.1016/j.jseaes.2009.12.009

Glorie, S., De Grave, J., Buslov, M.M., Zhimulev, F.I., Elburg, M.A., Van den haute, P., 2012. Structural control on Meso-Cenozoic tectonic reactivation and denudation in the Siberian Altai: Insights from multi-method thermochronometry. Tectonophysics 544–545, 75–92. https://doi.org/10.1016/j.tecto.2012.03.035

Green, P.F., 1981. A new look at statistics in fission-track dating. Nucl. Tracks 5, 77–86. https://doi.org/10.1016/0191-278X(81)90029-9

Green, P.F., Duddy, I.R., Gleadow, A.J.W., Lovering, J.F., 1989. Apatite Fission-Track Analysis as a paleotemperature indicator for hydrocarbon exploration, in: Naeser, N.D., McCulloh, T.H. (Eds.), Thermal History of Sedimentary Basins. Springer-Verlag, New York, pp. 181–195. https://doi.org/10.1007/978-1-4612-3492-0_11

Green, P.F., Duddy, I.R., Gleadow, A.J.W., Tingate, P.R., Laslett, G.M., 1986. Thermal annealing of fission tracks in apatite. Chem. Geol. Isot. Geosci. Sect. 59, 237–253. https://doi.org/http://dx.doi.org/10.1016/0168-9622(86)90074-6

Green, P.F., Japsen, P., Chalmers, J.A., Bonow, J.M., Duddy, I.R., 2018. Post-breakup burial and exhumation of passive continental margins: Seven propositions to inform geodynamic models. Gondwana Res. 53, 58–81. https://doi.org/10.1016/j.gr.2017.03.007

Gresse, P.G., Scheepers, R., 1993. Neoproterozoic to Cambrian (Namibian) rocks of South Africa: a geochronological and geotectonic review. J. African Earth Sci. 16, 375–393. https://doi.org/10.1016/0899-5362(93)90097-A

Griffis, N.P., Montañez, I.P., Fedorchuk, N., Isbell, J., Mundil, R., Vesely, F., Weinshultz, L., Iannuzzi, R., Gulbranson, E., Taboada, A., Pagani, A., Sanborn, M.E., Huyskens, M., Wimpenny, J., Linol, B., Yin, Q.Z., 2018. Isotopes to ice: Constraining provenance of glacial deposits and ice centers in west-central Gondwana. Palaeogeogr. Palaeoclimatol. Palaeoecol. 1–14. https://doi.org/10.1016/j.palaeo.2018.04.020

Hackspacher, P.C., Godoy, D.F., Ribeiro, L.F.B., Neto, J.C.H., Franco, A.O.B., 2007. Modelagem térmica e geomorfologia da borda sul do Cráton do São Francisco: termocronologia por traços de fissão em apatita Peter 37, 76–86.

Hackspacher, P.C., Ribeiro, L.F.B., Ribeiro, M.C.S., Fetter, A.H., Hadler Neto, J.C., Tello, C.E.S., Dantas, E.L., 2004. Consolidation and break-up of the South American Platform in southeastern Brazil: Tectonothermal and denudation histories. Gondwana Res. 7, 91–101. https://doi.org/10.1016/S1342-937X(05)70308-7

Hallet, B., Hunter, L., Bogen, J., 1996. Rates of erosion and sediment evacuation by glaciers: A review of field data and their implications. Glob. Planet. Change 12, 213–235. https://doi.org/10.1029/2004JF000189

Hamza, V.M., Dias, F.J.S.S., Gomes, A.J.L., Terceros, Z.G.D., 2005. Numerical and functional representations of regional heat flow in South America. Phys. Earth Planet. Inter. 152, 223–256. https://doi.org/10.1016/j.pepi.2005.04.009

Harman, R., Gallagher, K., Brown, R., Raza, A., Bizzi, L., 1998. Accelerated denudation and tectonic/geomorphic reactivation of the cratons of northeastern Brazil during the Late Cretaceous. J. Geophys. Res. 103, 27091–27105. https://doi.org/10.1029/98JB02524

Hasebe, N., Barbarand, J., Jarvis, K., Carter, A., Hurford, A.J., 2004. Apatite fission-track chronometry using laser ablation ICP-MS. Chem. Geol. 207, 135–145. https://doi.org/10.1016/j.chemgeo.2004.01.007

Hasui, Y., Almeida, F.F.M., 1970. Geocronologia do centro-oeste brasileiro. Bol. da Soc. Bras. Geol. 19, 5–26.

Hasui, Y., Carneiro, C.D.R., Coimbra, A.M., 1975a. The Ribeira folded belt. Rev. Bras. Geociências 5, 257–266. https://doi.org/10.25249/0375-7536.1975257266

Hasui, Y., Sadowski, G.R., Suguio, K., Fuck, G.F., 1975b. The Phanerozoic tectonic evolution of the Western Minas Gerais State. Academia Brasileira Ciências, Anais, pp. 431–438.

Heilbron, M., Cordani, U.G., Alkmim, F.F., Reis, H.L.S., 2017. Tectonic Genealogy of a Miniature Continent, in: Heilbron, Mônica, Cordani, U.G., Alkmim, F.F. (Eds.), São Francisco Craton, Eastern Brazil. Springer, pp. 321–331. https://doi.org/10.1007/978-3-319-01715-0

Heilbron, M., Valeriano, C.M., Tassinari, C.C.G., Almeida, J., Tupinambá, M., Siga, O., Trouw, R., 2008. Correlation of Neoproterozoic terranes between the Ribeira Belt, SE Brazil and its African counterpart: comparative tectonic evolution and open questions, in: Geological Society, London, Special Publications. pp. 211–237. https://doi.org/10.1144/SP294.12

Heredia, N., García-Sansegundo, J., Gallastegui, G., Farias, P., Giacosa, R., Hongn, F., Tubía, J.M., Alonso, J.J., Busquets, P., Charrier, R., Clariana, P., Colombo, F., Cuesta, A., Gallastegui, J., Giambiagi, L., González-Menéndez, L., Limarino, O., Martín-González, F., Pedreira, D., Quintana, L., Rodríguez-Fernández, L.R., Rubio-Ordóñez, Á., Seggiaro, R., Serra-Varela, S., Spalletti, L., Cardó, R., Ramos, V.A., 2018. The Pre-Andean Phases of Construction of the Southern Andes Basement in Neoproterozoic–Paleozoic Times, in: Folguera, A., Contreras-Reyes, E., Heredia, N., Encinas, A., Iannelli, S.B., Oliveros, V., Dávila, F.M., Vanesa, G.C., Giambiagi, L., Maksymowicz, A., Llanos, M.P.I., Naipauer, M.T.M., Orts, D., Litvak, V.D.,

Álvarez, O., Arriagada, C. (Eds.), The Evolution of the Chilean-Argentinean Andes. Springer, pp. 111–131. https://doi.org/10.1007/978-3-319-67774-3_5

Hueck, M., Oriolo, S., Dunkl, I., Wemmer, K., Oyhantçabal, P., Schanofski, M., Basei, M.Â.S., Siegesmund, S., 2017. Phanerozoic low-temperature evolution of the Uruguayan Shield along the South American passive margin. J. Geol. Soc. London. 174, 609–626. https://doi.org/10.1144/jgs2016-101

Hueck, M., Dunkl, I., Heller, B., Basei, M.A.S., Siegesmund, S., 2018. (U-Th)/He Thermochronology and Zircon Radiation Damage in the South American Passive Margin: Thermal Overprint of the Paraná LIP? Tectonics 37, 4068–4085. https://doi.org/10.1029/2018TC005041

Hueck, M., Dunkl, I., Oriolo, S., Wemmer, K., Basei, M.A.S., Siegesmund, S., 2019. Comparing contiguous high- and low-elevation continental margins: New (U-Th)/He constraints from South Brazil and an integration of the thermochronological record of the southeastern passive margin of South America. Tectonophysics 770, 228222. https://doi.org/10.1016/j.tecto.2019.228222

Huismans, R.S., Beaumont, C., 2005. Effect of litospheric stratificationon extensional styles and rift basin geometry, in: Post, P. (Ed.), 25th Annual GCSSEPM Foundation Bob F. Perkins Research Conference Proceedings. Petroleum Systems of Divergent Continental Margin Basins, p. 2005.

Hurford, A.J., 2019. An Historical Perspective on Fission-Track Thermochronology, in: Malusà, M.G., Fitzgerald, P.G. (Eds.), Fission-Track Thermochronology and Its Application to Geology. Springer Textbooks in Earth Sciences, Geography and Environment, pp. 3–23. https://doi.org/10.1007/978-3-319-89421-8_1

Hurford, A.J., 1990. Standardization of fission track dating calibration: Recommendation by the Fission Track Working Group of the I.U.G.S. Subcommission on Geochronology. Chem. Geol. Isot. Geosci. Sect. 80, 171–178. https://doi.org/10.1016/0168-9622(90)90025-8

Hurford, A.J., Green, P.F., 1983. The zeta age calibration of fission-track dating. Isot. Geosci. 1, 285–317. https://doi.org/10.1016/S0009-2541(83)80026-6

Hurford, A.J., Green, P.F., 1982. A users' guide to fission track dating calibration. Earth Planet. Sci. Lett. 59, 343–354. https://doi.org/10.1016/0012-821X(82)90136-4

Jaffey, A.H., Flynn, K.F., Glendenin, L.E., Bentley, W.C., Essling, A.M., 1971. Precision measurement of half-lives and specific activities of U^{235} and U^{238}. Phys. Rev. C 4, 1889–1906. https://doi.org/10.1103/PhysRevC.4.1889

Japsen, P., Bonow, J.M., Green, P.F., Cobbold, P.R., Chiossi, D., Lilletveit, R., Magnavita, L.P., Pedreira, A., 2012. Episodic burial and exhumation in NE Brazil after opening of the South Atlantic. Bull. Geol. Soc. Am. 124, 800–816. https://doi.org/10.1130/B30515.1

Jelinek, A.R., Chemale, F., van der Beek, P.A., Guadagnin, F., Cupertino, J.A., Viana, A., 2014. Denudation history and landscape evolution of the northern East-Brazilian continental margin from apatite fission-track thermochronology. J. South Am. Earth Sci. 54, 158–181. https://doi.org/10.1016/j.jsames.2014.06.001

Jonckheere, R., 2003. On methical problems in estimating geological temperature and time from measurements of fission tracks in apatite. Radiat. Meas. 36, 43–55. https://doi.org/10.1016/S1350-4487(03)00096-9

Julià, J., Assumpção, M., Rocha, M.P., 2008. Deep crustal structure of the Paraná Basin from receiver functions and Rayleigh-wave dispersion: Evidence for a fragmented cratonic root. J. Geophys. Res. 113, 1–23. https://doi.org/10.1029/2007JB005374

Karl, M., Glasmacher, U.A., Kollenz, S., Franco-Magalhaes, A.O.B., Stockli, D.F., Hackspacher, P.C., 2013. Evolution of the South Atlantic passive continental margin in southern Brazil derived from zircon and apatite (U–Th–Sm)/He and fission-track data. Tectonophysics 604, 224–244. https://doi.org/10.1016/j.tecto.2013.06.017

Kasanzu, C.H., 2017. Apatite fission track and (U-Th)/He thermochronology from the Archean Tanzania Craton: Contributions to cooling histories of Tanzanian basement rocks. Geosci. Front. 8, 999–1007. https://doi.org/10.1016/j.gsf.2016.09.007

Kasanzu, C.H., Linol, B., de Wit, M.J., Brown, R., Persano, C., Stuart, F.M., 2016. From source to sink in central Gondwana: Exhumation of the Precambrian basement rocks of Tanzania and sediment accumulation in the adjacent Congo basin. Tectonics 35, 2034–2051. https://doi.org/10.1002/2016TC004147

Keidel, J., 1916. La geología de las sierras de la provincia de Buenos Aires y sus relaciones con las montañas de Sud Africa y los Andes, Anales. Buenos Aires.

Ketcham, R.A., 2005. Forward and inverse modeling of low-temperature thermochronometry data. Rev. Mineral. Geochemistry 58, 275–314. https://doi.org/10.2138/rmg.2005.58.11

Ketcham, R.A., Carter, A., Donelick, R.A., Barbarand, J., Hurford, A.J., 2007a. Improved modeling of fission-track annealing in apatite. Am. Mineral. 92, 799–810. https://doi.org/10.2138/am.2007.2281

Ketcham, R.A., Carter, A., Donelick, R.A., Barbarand, J., Hurford, A.J., 2007b. Improved measurement of fission-track annealing in apatite using c-axis projection. Am. Mineral. 92, 789–798. https://doi.org/10.2138/am.2007.2280

Ketcham, R.A., Donelick, R.A., Carlson, W.D., 1999. Variability of apatite fission-track annealing kinetics: III. Extrapolation to geological time scales. Am. Mineral. 84, 1235–1255. https://doi.org/10.2138/am-1999-0902

Kohn, B., Gleadow, A., 2019. Application of Low-Temperature Thermochronology to Craton Evolution, in: Malusà, M.G., Fitzgerald, P.G. (Eds.), Fission-Track Thermochronology and Its Application to Geology. Springer Textbooks in Earth Sciences, Geography and Environment, pp. 373–393. https://doi.org/10.1007/978-3-319-89421-8_21

Krabbendam, M., 2001. When the Wilson cycle breaks down: How orogens can produce strong lithosphere and inhibit their future reworking, in: Miller, J.A., Holdsworth, R.E., Buick, I.S., Hand, M. (Eds.), Continental Reactivation and Reworking. Geological Society, pp. 57–75.

Krob, F.C., Glasmacher, U.A., Karl, M., Perner, M., Hackspacher, P.C., Stockli, D.F., 2019. Multi-chronometer thermochronological modelling of the Late Neoproterozoic to recent t-T-

evolution of the SE coastal region of Brazil. J. South Am. Earth Sci. 92, 77–94. https://doi.org/10.1016/j.jsames.2019.02.012

Kusznir, N.J., Park, R.G., 1984. Intraplate lithosphere deformation and the strength of the lithosphere. Geophys. J. Int. 79, 513–538. https://doi.org/10.1111/j.1365-246X.1984.tb02238.x

Le Heron, D.P., 2018. An exhumed Paleozoic glacial landscape in Chad. Geology 46, 91–94. https://doi.org/10.1130/G39510.1

Limarino, C.O., Césari, S.N., Spalletti, L.A., Taboada, A.C., Isbell, J.L., Geuna, S., Gulbranson, E.L., 2014. A paleoclimatic review of southern South America during the late Paleozoic: A record from icehouse to extreme greenhouse conditions. Gondwana Res. 25, 1396–1421. https://doi.org/10.1016/j.gr.2012.12.022

Linol, B., Milani, E.J., François, G., Scherer, C.M. dos S., 2015. New Regional Correlations Between the Congo, Paraná and Cape-Karoo Basins of Southwest Gondwana, in: Oberhansli, R., de Wit, M.J., Roure, F.M. (Eds.), Geology and Resource Potential of the Congo Basin. Springer, Verlag Berlin Heidelberg, pp. 245–268. https://doi.org/10.1007/978-3-642-29482-2

Lobato, G., Borghi, L., 2005. Análise estratigráfica da Formação Furnas (Devoniano Inferior) em afloramentos da borda Leste da Bacia Do Paraná), in: 3° Congresso Brasileiro de P&D Em Petróleo e Gás.

Lourenço, F.S., Alkmim, F.F., Araújo, M.N.C., Romeiro, M.A.T., Matos, G.C., Crósta, A.P., 2016. The Piúma lineament, southern Espirito Santo: structural expression and tectonic significance. Brazilian J. Geol. 46, 531–546. https://doi.org/10.1590/2317-4889201620150038

Machado, J.P.S.L., Jelinek, A.R., Bicca, M.M., Stephenson, R., Genezini, F.A., 2019. West Gondwana orogenies and Pangaea break-up: thermotectonic effects on the southernmost Mantiqueira Province, Brazil. J. Geol. Soc. London. 176, 1056–1075. https://doi.org/10.1144/jgs2019-018

Mackintosh, V., Kohn, B., Gleadow, A., Gallagher, K., 2019. Long-term reactivation and morphotectonic history of the Zambezi Belt, northern Zimbabwe, revealed by multi-method thermochronometry. Tectonophysics 750, 117–136. https://doi.org/10.1016/j.tecto.2018.11.009

Manatschal, G., Lavier, L., Chenin, P., 2015. The role of inheritance in structuring hyperextended rift systems: Some considerations based on observations and numerical modeling. Gondwana Res. 27, 140–164. https://doi.org/10.1016/j.gr.2014.08.006

Manhica, A.D.S.T., Grantham, G.H., Armstrong, R.A., Guise, P.G., Kruger, F.J., 2001. Polyphase deformation and metamorphism at the Kalahari Craton - Mozambique Belt boundary, in: Miller, J.A., Holdsworth, R.E., Buick, I.S., Hand, M. (Eds.), Continental Reactivation and Reworking. Geological Society, London, pp. 303–322. https://doi.org/10.1144/gsl.sp.2001.184.01.15

Marshak, S., Alkmim, F.F., Whittington, A., Pedrosa-Soares, A.C., 2006. Extensional collapse in the Neoproterozoic Araçuaí orogen, eastern Brazil: a setting for reactivation of asymmetric crenulation cleavage. J. Struct. Geol. 28, 129–147. https://doi.org/10.1016/j.jsg.2005.09.006

Martins-Neto, M.A., Pedrosa-Soares, A.C., Lima, S.A.A., 2001. Tectono-sedimentary evolution of sedimentary basins from Late Paleoproterozoic to Late Neoproterozoic in the São Francisco craton and Araçuaí fold belt, eastern Brazil. Sediment. Geol. 141–142, 343–370. https://doi.org/10.1016/S0037-0738(01)00082-3

Mendes, R.S., 2017. Petrografia, geoquímica, geologia isotópica e geocronologia dos diques máficos do sul do estado do Espírito Santo, Orógeno Araçuaí. Master's thesis. Universidade Federal de Minas Gerais.

Menegazzo, M.C., Catuneanu, O., Chang, H.K., 2016. The South American retroarc foreland system: The development of the Bauru Basin in the back-bulge province. Mar. Pet. Geol. 73, 131–156. https://doi.org/10.1016/j.marpetgeo.2016.02.027

Milani, E.J., De Wit, M.J., 2008. Correlations between the classic Paraná and Cape–Karoo sequences of South America and southern Africa and their basin infills flanking the Gondwanides: du Toit revisited. Geol. Soc. London, Spec. Publ. 294, 319–342. https://doi.org/10.1144/SP294.17

Milani, E.J., França, A.B., Schneider, R.L., 1994. Bacia do Paraná. Bol. Geociências da Petrobras 8, 69–72.

Milani, E.J., Melo, J.H.G., Souza, P.A., Fernandes, L.A., França, A.B., 2007. Bacia do Paraná, in: Boletim de Geociências Da Petrobras. pp. 265–287.

Milani, E.J., Ramos, V.A., 1998. Paleozoic orogenies in southwestern domain of Gondwana and the subsidence cycles of the Paraná Basin. Rev. Bras. Geociências 28, 473–484. https://doi.org/10.5327/rbg.v28i4.651

Milani, E.J., Thomas, F.A., 2000. Sedimentary basins of South América, in: Cordani, U.G., Milani, E.J., Thomas Filho, A.T., Campos, D.A. (Eds.), Tectonic Evolution of South America. 31st International Geological Congress, Rio de Janeiro, pp. 389–449.

Misra, A.A., Mukherjee, S., 2015. Tectonic Inheritance in Continental Rifts and Passive Margins, Springer Briefs in Earth Sciences. Springer International Publishing. https://doi.org/10.1007/978-3-319-20576-2

Mizusaki, A.M.P., Thomaz, F.A., Cesero, P., 1998. Ages of the magmatism and the opening of the South Atlantic Ocean. Pesqui. em Geociências 25, 47–57.

Mohriak, W., Nemčok, M., Enciso, G., 2008. South Atlantic divergent margin evolution: rift-border uplift and salt tectonics in the basins of SE Brazil, in: Pankhurst;, R.J., Trouw, R.A.J., Neve, B.B. de B., Wit, M.J. de (Eds.), West Gondwana: Pre-Cenozoic Correlations Across the South Atlantic Region. Geological Society, London, pp. 365–398. https://doi.org/https://doi.org/10.1144/SP294

Mohriak, W.U., Fainstein, R., 2012. Phanerozoic regional geology of the eastern Brazilian margin, in: Roberts, D.G., Bally, A.W. (Eds.), Regional Geology and Tectonics: Phanerozoic Passive Margins, Cratonic Basins and Global Tectonic Maps. Elsevier, pp. 222–282. https://doi.org/10.1016/B978-0-444-56357-6.00006-8

Montañez, I.P., Poulsen, C.J., 2013. The Late Paleozoic Ice Age: An Evolving Paradigm. Annu. Rev. Earth Planet. Sci. 41, 629–656. https://doi.org/10.1146/annurev.earth.031208.100118

Mooney, W.D., Ritsema, J., Hwang, Y.K., 2012. Crustal seismicity and the earthquake catalog maximum moment magnitude (Mcmax) in stable continental regions (SCRs): Correlation with the seismic velocity of the lithosphere. Earth Planet. Sci. Lett. 357–358, 78–83. https://doi.org/10.1016/j.epsl.2012.08.032

Moraes, R., Brown, M., Fuck, R.A., Camargo, M.A., Lima, T.M., 2002. Characterization and P-T Evolution of Melt-bearing Ultrahigh-temperature Granulites: an Example from the Anapolis-Itaucu Complex of the Brasilia Fold Belt, Brazil. J. Petrol. 43, 1673–1705. https://doi.org/10.1093/petrology/43.9.1673

Morais Neto, J.M., Hegarty, K.A., Karner, G.D., Alkmim, F.F., 2009. Timing and mechanisms for the generation and modification of the anomalous topography of the Borborema Province, northeastern Brazil. Mar. Pet. Geol. 26, 1070–1086. https://doi.org/10.1016/j.marpetgeo.2008.07.002

Morgan, P., 1983. Constraints on Rift thermal processes from heat flow and uplift. Tectonophysics 94, 277–298. https://doi.org/10.1016/B978-0-444-42198-2.50023-7

Morgan W. J., 1971. Convection Plumes in the Lower Mantle. Nature 230, 42–43.

Mottin, T.E., Vesely, F.F., Rodrigues, M.C. de L.N., Kipper, F., Souza, P.A., 2018. The paths and timing of late Paleozoic ice revisited: New stratigraphic and paleo-ice flow interpretations from a glacial succession in the upper Itararé Group (Paraná Basin, Brazil). Palaeogeogr. Palaeoclimatol. Palaeoecol. 490, 488–504. https://doi.org/10.1016/j.palaeo.2017.11.031

Nachtergaele, S., Glorie, S., Morley, C., Charusiri, P., Kanjanapayont, P., Vermeesch, P., Carter, A., Van Ranst, G., De Grave, J., 2019. Cenozoic tectonic evolution of southeastern Thailand derived from low-temperature thermochronology. J. Geol. Soc. London. jgs2018-167. https://doi.org/10.1144/jgs2018-167

Naeser, C.W., Dodge, F.C., 1969. Fission-Track Ages of Accessory Minerals from Granitic Rocks of the Central Sierra Nevada Batholith, California. GSA Bull. 80, 2201–2212. https://doi.org/https://doi.org/10.1130/0016-7606(1969)80[2201:FAOAMF]2.0.CO;2

Nemčok, M., 2016. Rifts and passive margins: Structural architecture, thermal regimes, and petroleum systems. Cambridge University Press.

Nonnotte, P., Guillou, H., Le Gall, B., Benoit, M., Cotten, J., Scaillet, S., 2008. New K-Ar age determinations of Kilimanjaro volcano in the North Tanzanian diverging rift, East Africa. J. Volcanol. Geotherm. Res. 173, 99–112. https://doi.org/10.1016/j.jvolgeores.2007.12.042

Oliveira, C.H.E. de, Jelinek, A.R., Chemale, F., Bernet, M., 2016. Evidence of post-Gondwana breakup in Southern Brazilian Shield: Insights from apatite and zircon fission track thermochronology. Tectonophysics 666, 173–187. https://doi.org/10.1016/j.tecto.2015.11.005

Oliveira, E.P., Windley, B.F., Araújo, M.N.C., 2010. The Neoproterozoic Sergipano orogenic belt, NE Brazil: A complete plate tectonic cycle in western Gondwana. Precambrian Res. 181, 64–84. https://doi.org/10.1016/j.precamres.2010.05.014

Oliveira, L.O.A., 1989. Aspectos da evolução termomecânica da Bacia do Paraná no Brasil. Rev. Bras. Geociências. https://doi.org/10.25249/0375-7536.1989330342

Pankhurst, R.J., Rapela, C.W., Fanning, C.M., Márquez, M., 2006. Gondwanide continental collision and the origin of Patagonia. Earth-Science Rev. 76, 235–257. https://doi.org/10.1016/j.earscirev.2006.02.001

Pazzaglia, F., Kelley, S., 1998. Large-scale geomorphology and fission-track thermochronology in topographic and exhumation reconstructions of the Southern Rocky Mountains. Rocky Mt. Geol. 33, 229–257. https://doi.org/10.2113/33.2.229

Peace, A.L., Phethean, J.J.J., Franke, D., Foulger, G.R., Schiffer, C., Welford, J.K., McHone, G., Rocchi, S., Schnabel, M., Doré, A.G., 2019. Publisher's Note. Earth-Science Rev. 196, 102865. https://doi.org/10.1016/j.earscirev.2019.05.009

Pedrosa-Soares, A., Noce, C., Wiedemann, C.M., Pinto, C.P., 2001. The Araçuaí--West-Congo Orogen in Brazil: an overview of a confined orogen formed during Gondwanaland assembly. Precambrian Res. 110, 307–323. https://doi.org/10.1016/S0301-9268(01)00174-7

Pedrosa-Soares, A.C., Alkmim, F.F., Tack, L., Noce, C.M., Babinski, M., Silva, L.C., Martins-Neto, M.A., 2008. Similarities and differences between the Brazilian and African counterparts of the Neoproterozoic Araçuaí-West Congo orogen, in: Pankhurst, R.J., Trouw, R.A.J., Brito Neves, B.B., de Wit, M.J. (Eds.), . Geological Society, London, pp. 153–172. https://doi.org/10.1144/SP294.9

Pedrosa-Soares, A.C., De Campos, C.P., Noce, C., Silva, L.C., Novo, T., Roncato, J., Medeiros, S., Castañeda, C., Queiroga, G., Dantas, E., Dussin, I., Alkmim, F., 2011. Late Neoproterozoic-Cambrian granitic magmatism in the Araçuaí orogen (Brazil), the Eastern Brazilian Pegmatite Province and related mineral resources. Geol. Soc. London, Spec. Publ. 350, 25–51. https://doi.org/10.1144/SP350.3

Pedrosa-Soares, A.C., Noce, C.M., Alkmim, F.F., Silva, L.C., Babinski, M., Cordani, U., Castañeda, C., 2007. Orógeno Araçuaí: Síntese do conhecimento 30 anos após Almeida 1977. Geonomos 1–16.

Pedrosa-Soares, A.C., Noce, C.M., Vidal, P., Monteiro, R.L.B.P., Leonardos, O.H., 1992. Toward a new tectonic model for the Late Proterozoic Araçuaí (SE Brazil)-West Congolian (SW Africa) Belt. J. South Am. Earth Sci. 6, 33–47. https://doi.org/10.1016/0895-9811(92)90015-Q

Pedrosa-Soares, A.C., Wiedemann-Leonardos, C., 2000. Evolution of the Araçuaí belt and its connection to the Ribeira belt, eastern Brazil, in: Cordani, U.G., Milani, E.J., Thomaz, F.., Campos, D.A. (Eds.), Tectonic Evolution of South America, 31st International Geological Congress. Rio de Janeiro, pp. 265–285.

Pérez-Díaz, L., Eagles, G., 2014. Constraining South Atlantic growth with seafloor spreading data. Tectonics 33, 1848–1873. https://doi.org/10.1002/2014TC003644

Peslier, A.H., Woodland, A.B., Bell, D.R., Lazarov, M., 2010. Olivine water contents in the continental lithosphere and the longevity of cratons. Nature 467, 78–81. https://doi.org/10.1038/nature09317

Petersen, K.D., Schiffer, C., 2016. Wilson cycle passive margins: Control of orogenic inheritance on continental breakup. Gondwana Res. 39, 131–144. https://doi.org/10.1016/j.gr.2016.06.012

Pimentel, M., Fuck, R., Jost, H., Filho, C., Araújo, S., 2000. The Basement of the Brasília Fold Belt and the Goiás Magmatic Arc, in: Cordani, U.G., Milani, E.J., Thomaz Filho, A., Campos, D.A. (Eds.), Tectonic Evolution of South America. Rio de Janeiro, pp. 195–229. https://doi.org/10.1016/j.ijms.2013.07.006

Pimentel, M.M., 2016. The tectonic evolution of the Neoproterozoic Brasília Belt, central Brazil: a geochronological and isotopic approach. Brazilian J. Geol. 46, 67–82. https://doi.org/10.1590/2317-4889201620150004

Pimentel, M.M., Jost, H., Fuck, R.A., 2004. O embasamento da Faixa Brasília e o Arco Magmático de Goiás, in: Mantesso-Neto, V., Bartorelli, A., Carneiro, C.D.R., Brito Neves, B.B. (Eds.), Geologia Do Continente Sul-Americano: Evolução Da Obra de Fernando Flávio Marques de Almeida. Editora Beca, pp. 324–355.

Pinet, N., 2018. The ups and downs of the Canadian Shield: 2- preliminary results of apatite fission-track analysis from a 3.6 km vertical profile, LaRonde mine, Quebec. https://doi.org/10.4095/308067

Pires, G.L.C., Bongiolo, E.M., Geraldes, M.C., Renac, C., Santos, A.C., Jourdan, F., Neumann, R., 2016. New ^{40}Ar/ ^{39}Ar ages and revised ^{40}K/^{40}Ar* data from nephelinitic–phonolitic volcanic successions of the Trindade Island (South Atlantic Ocean). J. Volcanol. Geotherm. Res. 327, 531–538. https://doi.org/10.1016/j.jvolgeores.2016.09.020

Piuzana, D., 2003. Neoproterozoic granulite facies metamorphism and coeval granitic magmatism in the Brasilia Belt, Central Brazil: regional implications of new SHRIMP U–Pb and Sm–Nd data. Precambrian Res. 125, 245–273. https://doi.org/10.1016/S0301-9268(03)00108-6

Porada, H., 1989. Pan-African rifting and orogenesis in southern to Equatorial Africa and Eastern Brazil. Precambrian Res. 44, 103–136. https://doi.org/10.1016/0301-9268(89)90078-8

Powell, R.D., Cooper, J.M., 2002. A glacial sequence stratigraphic model for temperate, glaciated continental shelves, in: Dowdeswell, J.A., Ó Cofaigh, C. (Eds.), Glacier-Influenced Sedimentation on High-Latitude Continental Margins. Geological Society, London, pp. 215–244. https://doi.org/10.1144/gsl.sp.2002.203.01.12

Quintas, M.C.L., Mantovani, M.S.M., Zalán, P.V., 1999. Contribuição ao estudo da evolução mecânica da Bacia Do Paraná. Rev. Bras. Geociências 29, 217–226.

Quirk, D.G., Hertle, M., Jeppesen, J.W., Raven, M., Mohriak, Webster Ueipass, Kann, D.J., Nørgaard, M., Howe, M.J., Hsu, D., Coffey, B., Mendes, M.P., 2013. Rifting, subsidence and continental break-up above a mantle plume in the central South Atlantic, in: Mohriak, W. U., Danforth, A., Post, P.J., Brown, D.E., Tari, G.C., Nemčok, M., Sinha, S.T. (Eds.), Conjugate Divergent Margins. Geological Society, London, pp. 185–214. https://doi.org/10.1144/sp369.20

Redfield, T.F., 2010. On apatite fission track dating and the Tertiary evolution of West Greenland topography. J. Geol. Soc. London. 167, 261–271. https://doi.org/10.1144/0016-76492009-036

Reiners, P.W., Brandon, M.T., 2006. Using thermochronology to understand orogenic erosion. Annu. Rev. Earth Planet. Sci. 34, 419–466. https://doi.org/10.1146/annurev.earth.34.031405.125202

Reis, H.L.S., Alkmim, F. F., Fonseca, R.C.S., Nascimento, T.C., Suss, J.F., Prevatti, L.D., 2017. The São Francisco Basin, in: Heilbron, M., Cordani, U.G., Alkmim, Fernando F. (Eds.), São Francisco Craton, Eastern Brazil. Springer, pp. 117–143. https://doi.org/10.1007/978-3-319-01715-0

Renne, P.R., Ernesto, M., Pacca, I.G., Coe, R.S., Glen, J.M., Prevot, M., Perrin, M., 1992. The Age of Parana Flood Volcanism, Rifting of Gondwanaland, and the Jurassic-Cretaceous Boundary. Science. 258, 975–979. https://doi.org/10.1126/science.258.5084.975

Reno, B.L., Brown, M., Kobayashi, K., Nakamura, E., Piccoli, P.M., Trouw, R.A.J., 2009. Eclogite–high-pressure granulite metamorphism records early collision in West Gondwana: new data from the Southern Brasília Belt, Brazil. J. Geol. Soc. London. 166, 1013–1032. https://doi.org/10.1144/0016-76492008-140

Reuber, K., Mann, P., 2019. Control of Precambrian-to-Paleozoic orogenic trends on along-strike variations in Early Cretaceous continental rifts of the South Atlantic Ocean. Interpretation 7, SH45–SH69. https://doi.org/10.1190/INT-2018-0257.1

Rey, P., Vanderhaeghe, O., Teyssier, C., 2001. Gravitational collapse of the continental crust: definition, regimes and modes. Tectonophysics 342, 435–449. https://doi.org/10.1016/S0040-1951(01)00174-3

Ribeiro, L.F.B., Hackspacher, P.C., Ribeiro, M.C.S., Hadler Neto, J.C., Tello, S.C.A., Iunes, P.J., Franco, A.O.B., Godoy, D.F., 2005. Thermotectonic and fault dynamic analysis of Precambrian basement and tectonic constraints with the Parana basin. Radiat. Meas. 39, 669–673. https://doi.org/10.1016/j.radmeas.2004.09.007

Riccomini, C., Sant'Anna, L.G., Ferrari, A.L., 2004. Evolução geológica do rift continental do sudeste do Brasil, in: Mantesso-Neto, V., Bartorelli, A., Carneiro, C.D.R., Brito Neves, B.B. (Eds.), Geologia do Continente Sul-Americano: Evolução da Obra de Fernando Flávio de Almeida. Editora Beca, São Paulo, pp. 383–406.

Riccomini, C., Velázquez, V.F., Gomes, C.B., 2005. Tectonic controls of the Mesozoic and Cenozoic alkaline magmatism in the central- southeastern Brazilian Platform, in: Comin-Chiaramonti, P., Gomes, C.B. (Eds.), Mesozoic to Cenozoic Alkaline Magmatism in the Brazilian Platform. Editora da Universidade de São Paulo, São Paulo, pp. 31–57.

Richter, F., Lana, C., Stevens, G., Buick, I., Pedrosa-Soares, A.C., Alkmim, F.F., Cutts, K., 2016. Sedimentation, metamorphism and granite generation in a back-arc region: Records from the Ediacaran Nova Venécia Complex (Araçuaí Orogen, Southeastern Brazil). Precambrian Res. 272, 78–100. https://doi.org/10.1016/j.precamres.2015.10.012

Rosa, E.L.M., Vesely, F.F., Isbell, J.L., Kipper, F., Fedorchuk, N.D., Souza, P.A., 2019. Constraining the timing, kinematics and cyclicity of Mississippian-early Pennsylvanian glaciations in the Paraná Basin, Brazil. Sediment. Geol. 384, 29–49. https://doi.org/10.1016/j.sedgeo.2019.03.001

Rosset, A., De Min, A., Marques, L.S., Macambira, M.J.B., Ernesto, M., Renne, P.R., Piccirillo, E.M., 2007. Genesis and geodynamic significance of Mesoproterozoic and Early Cretaceous tholeiitic dyke swarms from the São Francisco craton (Brazil). J. South Am. Earth Sci. 24, 69–92. https://doi.org/10.1016/j.jsames.2007.02.002

Rouby, D., Braun, J., Robin, C., Dauteuil, O., Deschamps, F., 2013. Long-term stratigraphic evolution of Atlantic-type passive margins: A numerical approach of interactions between surface processes, flexural isostasy and 3D thermal subsidence. Tectonophysics 604, 83–103. https://doi.org/10.1016/j.tecto.2013.02.003

Salomon, E., Koehn, D., Passchier, C., Hackspacher, P.C., Glasmacher, U.A., 2015. Contrasting stress fields on correlating margins of the South Atlantic. Gondwana Res. 28, 1152–1167. https://doi.org/10.1016/j.gr.2014.09.006

Salomon, E., Passchier, C., Koehn, D., 2017. Asymmetric continental deformation during South Atlantic rifting along southern Brazil and Namibia. Gondwana Res. 51, 170–176. https://doi.org/10.1016/j.gr.2017.08.001

Santiago, R., Caxito, F. de A., Neves, M.A., Dantas, E.L., Medeiros Júnior, E.B., Queiroga, G.N., 2019. Two generations of mafic dyke swarms in the Southeastern Brazilian coast: reactivation of structural lineaments during the gravitational collapse of the Araçuaí-Ribeira Orogen (500 Ma) and West Gondwana breakup (140 Ma). Precambrian Res. 105344. https://doi.org/10.1016/j.precamres.2019.105344

Sawasato, E.Y., 1995. Estruturação da porção meridional da Bacia Alto-Sanfranciscana - Cretáceo do oeste de Minas Gerais. Master's thesis. Universidade Federal de Ouro Preto.

Scherer, C.M.S., Lavina, E.L.C., 2006. Stratigraphic evolution of a fluvial–eolian succession: The example of the Upper Jurassic—Lower Cretaceous Guará and Botucatu formations, Paraná Basin, Southernmost Brazil. Gondwana Res. 9, 475–484. https://doi.org/10.1016/j.gr.2005.12.002

Schiffer, C., Doré, A.G., Foulger, G.R., Franke, D., Geoffroy, L., Gernigon, L., Holdsworth, B., Kusznir, N., Lundin, E., McCaffrey, K., Peace, A.L., Petersen, K.D., Phillips, T.B., Stephenson, R., Stoker, M.S., Welford, J.K., 2019. Structural inheritance in the North Atlantic. Earth-Science Rev. 102975. https://doi.org/10.1016/j.earscirev.2019.102975

Sgarbi, G.N.C., Dardenne, M.A., 1996. Evolução climática do Gondwana nas regiões centro-sul do Brasil e seus registros geológicos continentais durante o Mesozóico, enfatizando o Arco do Alto Paranaíba, a borda NNE da Bacia do Paraná e a porção meridional da Bacia Sanfranciscana, no oeste do Estado de Minas Gerais. Geonomos 4, 21–49. https://doi.org/10.18285/geonomos.v4i1.193

Sgarbi, G.N.C., Sgarbi, P.B.A., Campos, J.E.G., Dardenne, M.A., Penha, U.C., 2001. Bacia Sanfranciscana: O registro Fanerozóico da Bacia do São Francisco, in: Pinto, C.P., Martins-Neto, M.A. (Eds.), Bacia Do São Francisco: Geologia e Recursos Naturais. Soc. Bras. Geol. (SBG) – Núcleo MG, Belo Horizonte.

Sims, J.P., Ireland, T.R., Camacho, A., Lyons, P., Pieters, P.E., Skirrow, R.G., Stuart-Smith, P.G., Miró, R., 1998. U-Pb, Th-Pb and Ar-Ar geochronology from the southern Sierras Pampeanas, Argentina: implications for the Palaeozoic tectonic evolution of the western

Gondwana margin, in: Pankhurst, R.J., Rapela, C.W. (Eds.), The Proto-Andean Margin of Gondwana. Geological Society, London, pp. 259–281. https://doi.org/10.1144/gsl.sp.1998.142.01.13

Sleep, N.H., 2003. Survival of Archean cratonal lithosphere. J. Geophys. Res. Solid Earth 108, 1–29. https://doi.org/10.1029/2001jb000169

Soares, C.J., Guedes, S., Jonckheere, R., Hadler, J.C., Passarella, S.M., Dias, A.N.C., 2016. Apatite fission-track analysis of Cretaceous alkaline rocks of Ponta Grossa and Alto Paranaíba Arches, Brazil. Geol. J. 51, 805–810. https://doi.org/10.1002/gj

Soares, J.E., Berrocal, J., Fuck, R.A., Mooney, W.D., Ventura, D.B.R., 2006. Seismic characteristics of central Brazil crust and upper mantle: A deep seismic refraction study. J. Geophys. Res. Solid Earth 111, 1–31. https://doi.org/10.1029/2005JB003769

Souza, D.H. de, Hackspacher, P.C., Doranti-Tiritan, C., Godoy, D.F., 2014. Comparison of long and short term evolutionary dynamics, between the Poços de Caldas plateau and the São Pedro de Caldas plateau. Rev. Bras. Geomorfol. 16, 251–272.

Spier, C.A., Vasconcelos, P.M., Oliviera, S.M.B., 2006. [40]Ar/[39]Ar geochronological constraints on the evolution of lateritic iron deposits in the Quadrilátero Ferrífero, Minas Gerais, Brazil. Chem. Geol. 234, 79–104. https://doi.org/10.1016/j.chemgeo.2006.04.006

Spotila, J.A., 2005. Applications of Low-Temperature Thermochronometry to Quantification of Recent Exhumation in Mountain Belts. Rev. Mineral. Geochemistry 58, 449–466. https://doi.org/10.2138/rmg.2005.58.17

Stanley, J.R., Flowers, R.M., Bell, D.R., 2015. Erosion patterns and mantle sources of topographic change across the southern African Plateau derived from the shallow and deep records of kimberlites. Geochemistry, Geophys. Geosystems 16, 3235–3256. https://doi.org/10.1002/2015GC005969

Steiger, R.H., Jager, E., 1977. Subcommission on geochronology: convention on the use of decay constants in geo- and cosmochronology. Earth Planet. Sctence Lett. 36, 359–362.

Stüwe, K., White, L., Brown, R., 1994. The influence of eroding topography on steady-state isotherms. Application to fission track analysis. Earth Planet. Sci. Lett. 124, 63–74. https://doi.org/10.1016/0012-821X(94)00068-9

Tagami, T., Galbraith, R.F., Yamada, R., Laslett, G.M., 1998. Revised annealing kinetics offission tracks in zircon and geological implications, in: Van den haute, P., de Corte, F. (Eds.), Advances in Fission-Track Geochronology. Springer, pp. 99–114. https://doi.org/10.l007/978-94-015-9133-1

Tankard, A.J., Ultiana, M.A., Welsink, H.A., Ramos, V.A., Turic, M., Franca, A.B., Milani, E.J., Brito Neves, B.B., Eyles, N., Skarmeta, J., Santa Ana et al., H., 1995. Structural and tectonic controls of basin evolution in southwestern Gondwana during the Phanerozoic, in: Tankard, A.J.S., Suárez, R., Welsink, H.J. (Eds.), Tectonic Controls of Basin Evolution in Southwestern Gondwana. AAPG Memoir, pp. 5–52. https://doi.org/10.1002/dc

Thiede, D.S., Vasconcelos, P.M., 2010. Paraná flood basalts: Rapid extrusion hypothesis confirmed by new [40]Ar/[39]Ar results. Geology 38, 747–750. https://doi.org/10.1130/G30919.1

Thompson, R.N., Gibson, S.A., Mitchell, J.G., Dickin, A.P., Leonardos, O.H., Brod, J.A., Greenwood, J.C., 1998. Migrating Cretaceous-Eocene Magmatismin the Serra do Mar Alkaline Province, SE Brazil: Melts from the Deflected Trindade Mantle Plume? J. Petrol. 39, 1493–1526. https://doi.org/10.1093/petroj/39.8.1493

Tinker, J., de Wit, M., Brown, R., 2008. Mesozoic exhumation of the southern Cape, South Africa, quantified using apatite fission track thermochronology. Tectonophysics 455, 77–93. https://doi.org/10.1016/j.tecto.2007.10.009

Tohver, E., D'Agrella-Filho, M.S., Trindade, R.I.F., 2006. Paleomagnetic record of Africa and South America for the 1200-500 Ma interval, and evaluation of Rodinia and Gondwana assemblies. Precambrian Res. 147, 193–222. https://doi.org/10.1016/j.precamres.2006.01.015

Tohver, E., Trindade, R.I.F., Solum, J.G., Hall, C.M., Riccomini, C., Nogueira, A.C., 2010. Closing the Clymene ocean and bending a Brasiliano belt: Evidence for the Cambrian formation of Gondwana, southeast Amazon Craton. Geology 38, 267–270. https://doi.org/10.1130/G30510.1

Tommasi, A., Vauchez, A., 2015. Heterogeneity and anisotropy in the lithospheric mantle. Tectonophysics 661, 11–37. https://doi.org/10.1016/j.tecto.2015.07.026

Tommasi, A., Vauchez, A., 2001. Continental rifting parallel to ancient collisional belts: an effect of the mechanical anisotropy of the lithospheric mantle. Earth Planet. Sci. Lett. 185, 199–210. https://doi.org/10.1016/S0012-821X(00)00350-2

Tommasi, A., Vauchez, A., 1997. Continental-scale rheological heterogeneities and complex intraplate tectono-metamorphic patterns: Insights from a case-study and numerical models. Tectonophysics 279, 327–350. https://doi.org/10.1016/S0040-1951(97)00117-0

Torsvik, T.H., Cocks, L.R.M., 2013. Gondwana from top to base in space and time. Gondwana Res. 24, 999–1030. https://doi.org/10.1016/j.gr.2013.06.012

Torsvik, T.H., Rousse, S., Labails, C., Smethurst, M.A., 2009. A new scheme for the opening of the South Atlantic Ocean and the dissection of an Aptian salt basin. Geophys. J. Int. 177, 1315–1333. https://doi.org/10.1111/j.1365-246X.2009.04137.x

Trompette, R., 1994. Geology of Western Gondwana (2000-500 Ma): Pan-African-Brasiliano aggregation of South America and Africa. Rotterdam.

Trompette, R.R., Uhlein, A., Silva, M.E., Karmann, I., 1992. O Cráton Brasiliano Do São Francisco - Uma Revisão. Rev. Bras. Geociências 22, 481–486. https://doi.org/10.25249/0375-7536.1991481486

Turner, J.P., Green, P.F., Holford, S.P., Lawrence, S.R., 2008. Thermal history of the Rio Muni (West Africa)-NE Brazil margins during continental breakup. Earth Planet. Sci. Lett. 270, 354–367. https://doi.org/10.1016/j.epsl.2008.04.002

Uhlein, A., Freitas, A. de M., Cruz, A.B. da, Silva, W.F. da, Caxito, F. de A., Moreira, G. de C., 2011. Projeto Alto Paranaíba - Folha Carmo do Paranaíba. Belo Horizonte.

Valeriano, C. de M., 2017. The Southern Brasília Belt, in: Heilbron, M., Cordani, U.G., Alkmim, F.F. (Eds.), São Francisco Craton, Eastern Brazil. Springer, pp. 189–203. https://doi.org/10.1007/978-3-319-01715-0_10

Valeriano, C. de M., Dardenne, M.A., Fonseca, M.A., Simões, L.S.A., Seer, H.J., 2004. A evolução tectônica da Faixa Brasília, in: Mantesso-Neto, V., Bartorelli, A., Carneiro, C.D.R., Brito Neves, B.B. (Eds.), Geologia Do Continente Sul-Americano: Evolução Da Obra de Fernando Flávio de Almeida. Editora Beca, São Paulo, pp. 575–592.

Valeriano, C. de M., Teixeira, W., Heilbron, M., Sergio, L., Simões, A., 2000. Southern Brasília Belt (SE Brazil): Tectonic Discontinuities, K-Ar Data and Evolution During the Neoproterozoic Brasiliano Orogeny. Rev. Bras. Geociências 30, 195–199.

Valeriano, C.M., Pimentel, M.M., Heilbron, M., Almeida, J.C.H., Trouw, R.A.J., 2008. Tectonic evolution of the Brasília Belt, Central Brazil, and early assembly of Gondwana, in: Pankhurst, R.J., Trouw, R.A.J., Brito Neves, B.B., de Wit, M.J. (Eds.), West Gondwana: Pre-Cenozoic Correlations Across the South Atlantic Region. Geological Society, London, pp. 197–210. https://doi.org/10.1144/SP294.11

Van den haute, P., De Corte, F., Jonckheere, R., Bellemans, F., 1998. The parameters that govern the accuracy of fission-track age determinations: a re-appraisal, in: Van den haute, P., De Corte, F. (Eds.), Advances in Fission-Track Geochronology. Kluwer Academic Publishers, Dordrecht, pp. 33–46.

Van Ranst, G., Baert, P., Fernandes, A.C., De Grave, J., n.d. Technical Note: TRACKFlow, a new versatile microscope system for fission track analysis. Geochronology. https://doi.org/https://doi.org/10.5194/gchron-2019-13

Van Ranst, G., Pedrosa-Soares, A.C., Novo, T., Vermeesch, P., De Grave, J., 2020. New insights from low-temperature thermochronology into the tectonic and geomorphologic evolution of the south-eastern Brazilian highlands and passive margin. Geosci. Front. 11, 303–324. https://doi.org/10.1016/j.gsf.2019.05.011

Vauchez, A., Barruol, G., Tommasi, A., 1997. Why do continents break-up parallel to ancient orogenic belts? Terra Nov. 9, 62–66. https://doi.org/10.1111/j.1365-3121.1997.tb00003.x

Vauchez, A., Egydio-Silva, M., Babinski, M., Tommasi, A., Uhlein, A., Liu, D., 2007. Deformation of a pervasively molten middle crust: Insights from the neoproterozoic Ribeira-Araçuaí orogen (SE Brazil). Terra Nov. 19, 278–286. https://doi.org/10.1111/j.1365-3121.2007.00747.x

Vauchez, A., Hollanda, M.H.B.M., Monié, P., Mondou, M., Egydio-Silva, M., 2019. Slow cooling and crystallization of the roots of the Neoproterozoic Araçuaí hot orogen (SE Brazil): Implications for rheology, strain distribution, and deformation analysis. Tectonophysics 766, 500–518. https://doi.org/10.1016/j.tecto.2019.05.013

Vaughan, A.P.M., Pankhurst, R.J., 2008. Tectonic overview of the West Gondwana margin. Gondwana Res. 13, 150–162. https://doi.org/10.1016/j.gr.2007.07.004

Vermeesch, P., 2018. IsoplotR: A free and open toolbox for geochronology. Geosci. Front. 9, 1479–1493. https://doi.org/10.1016/j.gsf.2018.04.001

Vesely, F.F., Assine, M.L., 2014. Ice-keel scour marks in the geological record: evidence from Carboniferous soft-sediment striated surfaces in the Paraná Basin, Southern Brazil. J. Sediment. Res. 84, 26–39. https://doi.org/10.2110/jsr.2014.4

Vesely, F.F., Assine, M.L., 2006. Deglaciation sequences in the Permo-Carboniferous Itararé Group, Paraná Basin, southern Brazil. J. South Am. Earth Sci. 22, 156–168. https://doi.org/10.1016/j.jsames.2006.09.006

Vesely, F.F., Trzaskos, B., Kipper, F., Assine, M.L., Souza, P.A., 2015. Sedimentary record of a fluctuating ice margin from the Pennsylvanian of western Gondwana: Paraná Basin, southern Brazil. Sediment. Geol. 326, 45–63. https://doi.org/10.1016/j.sedgeo.2015.06.012

Visser, J.N.J., 1987. The palaeogeography of part of southwestern Gondwana during the Permo-Carboniferous glaciation. Palaeogeogr. Palaeoclimatol. Palaeoecol. 61, 205–219. https://doi.org/10.1016/0031-0182(87)90050-2

Vitorello, I., Hamza, V.M., Pollack, H.N., 1980. Terrestrial heat flow in the Brazilian highlands. J. Geophys. Res. 85, 3778–3788. https://doi.org/10.1029/JB085iB07p03778

Wagner, G., Van den haute, P., 1992. Fission Tracks dating. Kluwer Academic Publishers, Dordrecht. https://doi.org/http://dx.doi.org/10.1016/B0-44-452747-8/00052-1

Watts, A.B., 2012. Models for the evolution of passive margins. Reg. Geol. Tectonics Phaneroz. Rift Syst. Sediment. Basins 32–57. https://doi.org/10.1016/B978-0-444-56356-9.00002-X

Weber, U.D., Hill, K.C., Brown, R.W., Gallagher, K., Kohn, B.P., Gleadow, A.J.W., Foster, D.A., 2004. Sediment supply to the Gippsland Basin from thermal history analysis: constraints on Emperor—Golden Beach reservoir composition. APPEA J. 44, 397–416. https://doi.org/10.1071/aj03015

Weissel, J.K., Karner, G.D., 1989. Flexural uplift of rift flanks due to mechanical unloading of the lithosphere during extension. J. Geophys. Res. Solid Earth 94, 13919–13950. https://doi.org/10.1029/JB094iB10p13919

Whipple, K.X., Meade, B.J., 2006. Orogen response to changes in climatic and tectonic forcing. Earth Planet. Sci. Lett. 243, 218–228. https://doi.org/10.1016/j.epsl.2005.12.022

Wildman, M., Brown, R., Watkins, R., Carter, A., Gleadow, A., Summerfield, M., 2015. Post break-up tectonic inversion across the southwestern cape of South Africa: New insights from apatite and zircon fission track thermochronometry. Tectonophysics 654, 30–55. https://doi.org/10.1016/j.tecto.2015.04.012

Will, T.M., Frimmel, H.E., 2018. Where does a continent prefer to break up? Some lessons from the South Atlantic margins. Gondwana Res. 53, 9–19. https://doi.org/10.1016/j.gr.2017.04.014

Zalán, P.V., Wolff, S., Astolfi, M.A.M., Vieira, I.S., Concelção, J.C.J., Appi, V.T., Neto, E.V.S., Cerqueira, J.R., Marques, A., 1990. The Paraná Basin, Brazil, in: Leighton, M.W., Kolata, D.R., Oltz, D.F., Eidel, J.J. (Eds.), Interior Cratonic Basins. Memoir of the American Association of Petroleum Geologists, pp. 681–708.

Zalán, P. V, 2004. Evolução Fanerozóica das Bacias Sedimentares Brasileiras, in: Mantesso-Neto, V., Bartorelli, A., Carneiro, C.D.R., Brito Neves, B.B. (Eds.), Geologia Do Continente Sul-Americano: Evolução Da Obra de Fernando Flávio Marques de Almeida. Beca, São Paulo, pp. 595–613.

Zerfass, H., Lavina, E.L., Schultz, C.L., Garcia, A.J.V., Faccini, U.F., Chemale, F., 2003. Sequence stratigraphy of continental Triassic strata of Southernmost Brazil: a contribution to Southwestern Gondwana palaeogeography and palaeoclimate. Sediment. Geol. 161, 85–105. https://doi.org/10.1016/s0037-0738(02)00397-4

Zhang, P., Molnar, P., Downs, W.R., 2001. Increased sedimentation rates and grain sizes 2-4Myr ago due to the influence of climate change on erosion rates. Nature 410, 891–897.